

Digitale fotonica op basis van laserdiodes  
voor optische netwerkknoppen

Digital Photonics Using Single Laser Diodes  
for All-Optical Network Nodes

Koen Huybrechts

Promotoren: prof. dr. ir. G. Morthier, prof. dr. ir. R. Baets  
Proefschrift ingediend tot het behalen van de graad van  
Doctor in de Ingenieurswetenschappen: Fotonica

Vakgroep Informatietechnologie  
Voorzitter: prof. dr. ir. D. De Zutter  
Faculteit Ingenieurswetenschappen  
Academiejaar 2009 - 2010



ISBN 978-90-8578-374-9  
NUR 959, 926  
Wettelijk depot: D/2010/10.500/50

Promotoren:

Prof. Dr. Ir. Geert Morthier  
Prof. Dr. Ir. Roel Baets

Examencommissie:

Prof. Dr. Ir. Daniël De Zutter (voorzitter)	Universiteit Gent, INTEC
Prof. Dr. Ir. Geert Morthier (promotor)	Universiteit Gent, INTEC
Prof. Dr. Ir. Christophe Peucheret	Technical University Denmark
Dr. Ir. Guang-Hua Duan	Alcatel-Thales, III-V lab
Prof. Dr. Ir. Jeroen Beeckman	Universiteit Gent, ELIS
Prof. Dr. Ir. Dries Van Thourhout (secretaris)	Universiteit Gent, INTEC
Prof. Dr. Ir. Mario Pickavet	Universiteit Gent, INTEC
Prof. Dr. Ir. Roel Baets (promotor)	Universiteit Gent, INTEC

Universiteit Gent  
Faculteit Ingenieurswetenschappen

Vakgroep Informatietechnologie  
Sint-Pietersnieuwstraat 41, B-9000 Gent, België

Tel.: +32-9-264.33.39  
Fax.: +32-9-331.35.93



Dit werk kwam tot stand in het kader van een  
specialisatiebeurs van het Instituut voor de aanmoediging  
van Innovatie door Wetenschap en Technologie in  
Vlaanderen (IWT)



# Dankwoord

Een doctoraat is niet iets wat je op je eentje bereikt. De unieke momenten die ik met enkele uitzonderlijke mensen heb mogen delen zijn voor mij dan ook zonder twijfel de bijzonderste resultaten uit dit doctoraat. Dit dankwoord omvat misschien niet veel pagina's, het zijn zonder twijfel wel de belangrijkste uit dit hele boek.

Eerst en vooral wil ik mijn promotoren Geert en Roel bedanken om een omgeving te creëren die dit werk mogelijk heeft gemaakt. De sterke ambitie van Roel om steeds opnieuw tot het uiterste te willen gaan heeft ervoor gezorgd dat onze onderzoeksgroep wereldwijd heel wat erkenning geniet. Dat Geert het woord procrastinatie niet in zijn woordenboek heeft staan, heeft ertoe geleid dat hij me van bij de start gestimuleerd heeft om efficiënt en resultaatgericht te werken. Het werk dat hier gepresenteerd wordt is dan ook voor een belangrijk deel zijn verdienste.

Toen ik aan mijn doctoraat begon, had ik nog nooit een optische vezel van dichtbij gezien. Ik ben dan ook heel wat dank verschuldigd aan Wouter D om me wegwijs te maken in het labo en me te begeleiden bij de eerste metingen die steevast wilden mislukken. Een typische werkdag werd om elf uur even onderbroken wanneer de laarzen van Lieven door de gang weergalmden om de koffiepauze aan te kondigen die Dave en Peter B vervolgens voorzagen van de nodige humor. Als we op vrijdag dan de werkweek doorspoelden waren Peter VDS, Wouter VP, Katrien, Shankar, ... (en vele anderen) steevast van de partij wat al wel eens durfde uitmonden in een typische '5-to-(almost)-5'. Joris voorzag de groep dan weer van een nieuwe traditie door elke namiddag voor een ruim publiek zijn kiwi te ontmantelen.

It was a privilege to visit other renowned research groups around the world. My time in Japan was a very interesting and pleasant period. Nakano-sensei and his secretaries did the utmost to make me feel welcome at the University of Tokyo. Special thanks to Takuo and Koji, not only to help me tackle the many technical obstacles, but - even more - for the nice conversations during our many evenings together. I owe Murat endless gratitude for introducing me the

concept of 'izakaya' and climbing mount Fuji with me. Christophe and Jorge were very helpful during the experiments at DTU in Denmark. I also want to acknowledge the many people who collaborated within the European Historic project.

De organisatie van het Photonics Event - waarmee we de band tussen de industrie en universiteit wilden versterken - beschouw ik als een van mijn belangrijkste realisaties. Bedankt aan i'Bram en vele anderen om me te helpen hierbij. Ik ben er zeker van dat Marie dit evenement op gepaste wijze zal voortzetten en ik hoop dat toekomstige edities nog succesvoller mogen zijn.

De voorbije jaren zijn zeer snel voorbijgegaan, maar elk jaar kwamen er nieuwe, interessante mensen bij. Ik denk dan vooral aan Peter DH ('is dat hier een feestje?'), Thijs ('vijs? je bedoelt een schroef?'), Diedrik (*gecensureerd*), Bart ('ik ben echt gestopt met cola'), Martin ('een stoel dient toch niet om gewoon op te zitten'), spraakwaterval Tom en Eva ('echt of wa? da's keigoe'), maar zeker ook Cristina ('come on') en Pauline ('girls just wanna have fun'). Yannick verdient zonder twijfel een prijs voor de meest enthousiaste thesisstudent, maar is zelfs nog fijner als collega. Björn was dan weer altijd bereid om samen in lastige wiskundige vergelijkingen te duiken en Wim ('ik heb geen ukelele') was vaak van de partij als we met de groep iets organiseerden. Waarschijnlijk vergeet ik hier nog een heleboel mensen, maar de groep is met de jaren veel te groot geworden om ze hier allemaal te kunnen vermelden.

Het zijn echter niet enkel collega's die hier een plaatsje verdienen. Deborah en Stijn terugzien is altijd leuk, ook al wonen jullie nu wat verder af. The many reunions with my friends from my time in Stockholm were always great and I hope we can keep the tradition of meeting each other once or twice a year. Linda en Marleen verdienen hier ook een plaatsje, al was het maar omdat het zo'n fijne mensen zijn. Ook bedankt aan Tom voor de vele filmavondjes samen.

Mijn bureaugenoten ga ik waarschijnlijk het meest missen. Joost die - terwijl hij bijna naar zijn trein moet spurten - voor de laatste keer die avond 'nog eentje hé, gastjes' zegt. Elewout die met zijn stem het poolijs kan laten smelten en zelfs bij Karel ('tjah') al eens een emotie weet los te weken. Wout en Kristof, echte vriendschap heeft niet veel woorden nodig: jullie weten wel wat jullie voor me betekenen. Dankzij jullie straalde ons bureautje een enorme gezelligheid uit en de vele avonden die we samen hebben doorgebracht (al dan niet gedrenkt in Talisker) zullen me zeker bijblijven.

Tot slot wil ik ook graag mijn familie bedanken. Arno om me als peter te kiezen. Mijn ouders om me onvoorwaardelijk te steunen en om me gewoon te laten zijn wie ik ben.

*Gent, september 2010*  
*Koen Huybrechts*





# Table of Contents

<b>Dankwoord</b>	<b>i</b>
<b>Nederlandse samenvatting</b>	<b>xiii</b>
<b>English summary</b>	<b>xxi</b>
<b>1 Introduction</b>	<b>1</b>
1.1 Optical fiber networks . . . . .	3
1.2 All-optical signal processing . . . . .	6
1.2.1 All-optical network nodes . . . . .	6
1.2.2 Regeneration . . . . .	11
1.3 Outline . . . . .	12
1.4 Publications . . . . .	12
References . . . . .	16
<b>2 DFB laser all-optical flip-flop</b>	<b>21</b>
2.1 Semiconductor DFB laser diodes . . . . .	22
2.1.1 Introduction . . . . .	22
2.1.2 Rate equations . . . . .	24
2.1.3 Coupled mode theory for DFB lasers . . . . .	26
2.2 Concept of the all-optical flip-flop . . . . .	29
2.3 Simulations . . . . .	34
2.4 Experimental results . . . . .	42
2.5 Discussion and conclusions . . . . .	51
References . . . . .	52
<b>3 DBR laser all-optical flip-flop</b>	<b>57</b>
3.1 Introduction . . . . .	57
3.2 Nonlinear effects . . . . .	59
3.3 Concept . . . . .	60
3.4 Simulation results . . . . .	62
3.5 Experimental results . . . . .	63
3.6 Conclusion . . . . .	68

---

References . . . . .	70
<b>4 Microdisk laser all-optical flip-flop</b>	<b>73</b>
4.1 Introduction . . . . .	74
4.2 Theoretical background . . . . .	75
4.3 Device structure . . . . .	79
4.4 Measurement results . . . . .	79
4.5 Conclusions . . . . .	84
References . . . . .	86
<b>5 Network motifs of coupled nonlinear cavities</b>	<b>91</b>
5.1 Introduction . . . . .	92
5.2 Three coupled cavities . . . . .	93
5.2.1 Symmetry breaking condition . . . . .	93
5.2.2 Static solutions . . . . .	95
5.2.3 Dynamic behaviour . . . . .	98
5.3 Four coupled cavities . . . . .	101
5.3.1 Symmetry breaking conditions . . . . .	101
5.3.2 Static solutions . . . . .	104
5.3.3 Dynamic behaviour . . . . .	104
5.4 Conclusion . . . . .	105
References . . . . .	107
<b>6 All-optical packet switching</b>	<b>109</b>
6.1 Introduction . . . . .	110
6.2 Experiment . . . . .	113
6.3 Conclusion . . . . .	120
References . . . . .	122
<b>7 Regeneration</b>	<b>125</b>
7.1 Introduction . . . . .	126
7.2 Theoretical approach . . . . .	130
7.3 Experiment . . . . .	136
7.3.1 Results at 10 Gbit/s . . . . .	136
7.3.2 Results at 25 Gbit/s . . . . .	140
7.4 Conclusion . . . . .	146
References . . . . .	147
<b>8 Conclusions and perspectives</b>	<b>151</b>
8.1 Conclusions . . . . .	151
8.2 Perspectives . . . . .	153





# List of Acronyms

## **A**

AOFF	All-optical flip-flop
APC	Angled physical contact
AR	Anti-reflection
ASE	Amplified spontaneous emission
ATT	Attenuator
AWG	Arrayed waveguide grating

## **B**

BER	Bit error rate
-----	----------------

## **C**

CW	Clockwise
CCW	Counter-clockwise
CMOS	Complimentary metal-oxide-semiconductor

## **D**

DFB	Distributed feedback
DBR	Distributed Bragg reflector

**E**

EDFA                      Erbium-doped fiber amplifier

**F**

FDL                      Fiber delay line  
FP                        Fabry P erot  
FTTH                     Fiber-to-the-home

**L**

LD                        Laser diode  
LN                        Lithium Niobate

**M**

MZI                      Mach-Zehnder interferometer  
MMI                      Multi-mode interferometer  
MQW                     Multi-quantum well

**N**

NRZ                      Non-return-to-zero

**O**

OBPF                     Optical band-pass filter  
ODL                      Optical delay line  
OSNR                     Optical signal-to-noise ratio

**P**

PCW	Polarization controlling wheels
PPG	Pulse pattern generation

**R**

RZ	Return-to-zero
----	----------------

**S**

SA	Saturable absorber
SOA	Semiconductor optical amplifier
SOI	Silicon-on-Insulator

**T**

TE	Transverse electric
TLLM	Transmission line laser model
TM	Transverse magnetic

**V**

VCSEL	Vertical-cavity surface-emitting lasers
-------	---

**W**

WDM	Wavelength-division multiplexing
-----	----------------------------------



# Nederlandse samenvatting

## –Summary in Dutch–

De bijna gelijktijdige uitvinding van de laser en de optische vezel heeft de telecommunicatiewereld drastisch veranderd gedurende de voorbije decennia. De transmissie van lichtsignalen door optische vezels heeft geleid tot een enorme capaciteit om informatie te verzenden met bitsnelheden die de snelheid van de conventionele elektronica ruim overschreiden. Door de toenemende, publieke belangstelling voor nieuwe internet gebaseerde diensten (zoals bv. video-on-demand, VoIP, ...) kan verwacht worden dat de vraag naar meer bandbreedte nog verder zal toenemen in de toekomst.

Het grote verschil tussen de enorme bandbreedte die we terugvinden in optische systemen en de beperkte snelheid van de elektronica, stelt een belangrijk probleem in de knooppunten van een optisch netwerk. Om lichtsignalen te verwerken in dergelijke netwerkknopen, worden ze namelijk eerst omgezet naar elektrische signalen. Nadat de elektronische verwerking is gebeurd, worden ze opnieuw naar het optisch domein gebracht en verzonden naar de volgende netwerkknoop. Deze opto-elektrische en elektro-optische omzettingen verbruiken niet alleen veel energie, maar bovendien is ook de elektronica die dergelijk hoge bitsnelheden moet aankunnen zeer duur. Deze moeilijkheden tonen duidelijk aan dat er nood is aan manieren om de signaalverwerking gedeeltelijk of volledig binnen de optische laag uit te voeren.

Optische geheugenelementen (of flip-flops) zijn de belangrijkste bouwstenen die vandaag nog ontbreken om signalen binnen het optisch domein te kunnen verwerken. Dergelijke optische geheugenelementen zijn essentieel aangezien ze de routeringsinformatie van een data-pakket optisch kunnen bijhouden terwijl het pakket naar de gewenste uitgangspoort wordt geleid. Bestaande concepten voor dergelijke flip-flops uit de vakliteratuur zijn vaak gebaseerd op complexe structuren opgebouwd uit meerdere lasersecties. Dergelijke concepten verbruiken daardoor niet alleen veel energie, maar bovendien zijn ze ook moeilijk te fabriceren en bieden ze beperkte schakelsnelheden. In dit werk bestuderen we een aantal nieuwe concepten waarbij het optisch geheugenelement slechts bestaat uit één enkele laser diode. Deze laser diodes zijn boven-

dien reeds standaardcomponenten in de huidige telecommunicatienetwerken waardoor ze een haalbaar alternatief vormen om op korte termijn in optische netwerkknoppen geïmplementeerd te worden. We tonen hun toepasbaarheid ook aan in een optische pakketschakelaar die uitsluitend met optische signalen werkt en data met bitsnelheden van 40 Gb/s naar de gewenste uitgangspoort brengt.

Wanneer er verschillende optische knooppunten met elkaar worden verbonden, kan er zich ruis op het signaal vormen door het gebruik van optische versterkers. In de traditionele routers wordt deze ruis onderdrukt omdat het signaal bij de omzetting naar het elektrisch domein opnieuw gedigitaliseerd wordt. Dit probleem vergt een optische component die het signaal optisch regeneert door de ruis te onderdrukken. We stellen in dit werk dan ook een nieuw regeneratieschema voor dat gebaseerd is op een enkele laser diode.

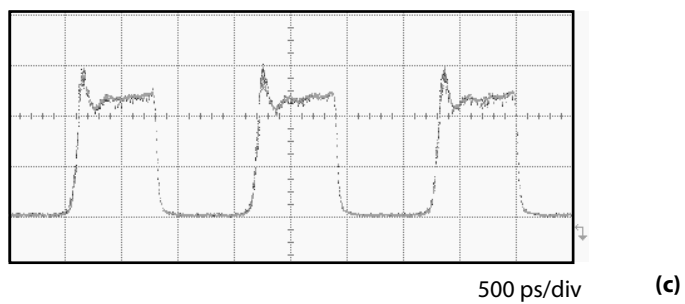
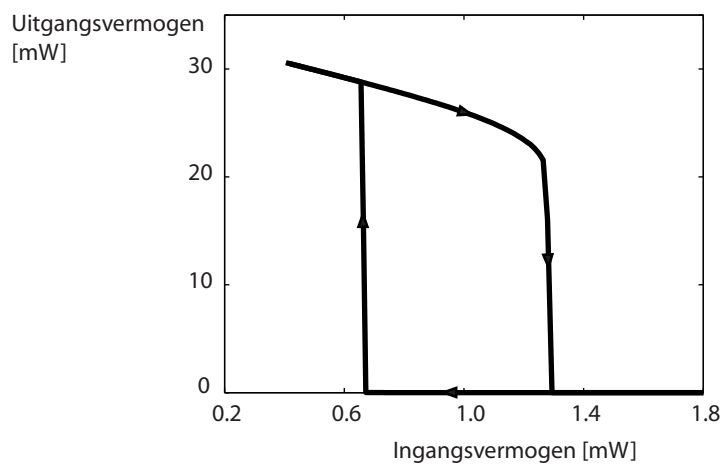
In wat volgt, bespreken we deze concepten in wat meer detail.

## **Optische geheugenelementen**

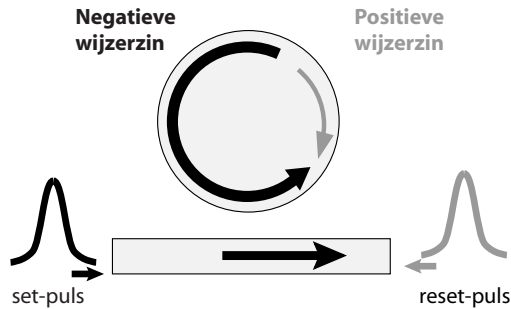
Onder optische geheugenelementen verstaan we een component die tussen twee of meerdere toestanden kan schakelen door het injecteren van optische pulsen. Algemeen genomen zijn geheugenelementen gebaseerd op een hysteresis effect.

### **DFB lasers**

DFB laserdiodes zijn de standaard transmitters in de meeste geavanceerde communicatiesystemen. In tegenstelling tot andere lasertypes, gebeurt de feedback niet door reflectie aan de facetten, maar is deze verdeeld over de lasercaviteit door diffractie aan een Bragg rooster (zie Figuur 1a). Wanneer we licht injecteren (met een golflengte die verschilt van de lasergolflengte), zal de longitudinale verdeling van de ladingsdragers wijzigen. Doordat veranderingen in de ladingsdragersdensiteit ook de brekingsindex van het materiaal wijzigen, zal de uniformiteit van de Bragg-reflectie verstoord worden en uiteindelijk houdt de laserwerking op. In dit werk tonen we aan dat er op die manier een hysteresis-effect in het uitgangsvermogen van de laser bekomen kan worden (zie Figuur 1b). Om in het bistabiele gebied te werken zorgen we voor een continue lichtstroom aan één zijde van de DFB laser. Wanneer er dan een puls geïnjecteerd wordt aan die zijde, zal de laser uitgeschakeld worden. Een puls die van de andere kant geïnjecteerd wordt zal daarentegen de uniformiteit van de ladingsdragers weer herstellen waardoor de laser terug aanschakelt. Op deze manier kunnen we de laser zeer snel aan- en uitschakelen (tot 45 ps) zoals getoond wordt in Figuur 1c.



**Figuur 1:** De DFB laser als optisch geheugenelement: (a) Illustratie van de component; (b) Hysteresis in het uitgangsvermogen van de laser bij externe lichtinjectie; (c) Experimenteel bekomen resultaat van het schakelgedrag.



**Figuur 2:** Flip-flopwerking in schijflasers.

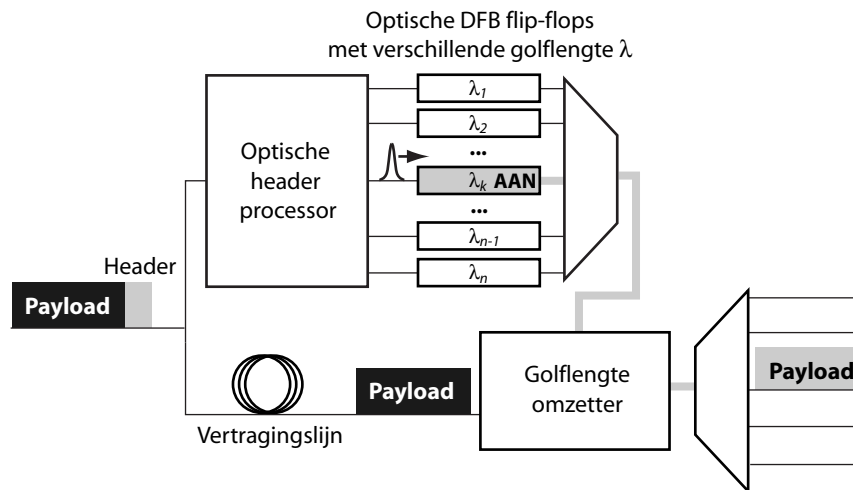
### DBR laser

Een DBR laser heeft aan één zijde van de caviteit een Bragg-rooster dat het licht bij een specifieke golflengte weerkaatst. Door een kleine stroom op dit rooster aan te brengen zal deze golflengte verschuiven en gaat de laser naar een andere longitudinale mode verspringen. Als de laser op deze manier wordt afgestemd, veroorzaakt een niet-lineaire winstonderdrukking een hysteresis in de golflengte van het laserlicht. Wanneer een stroom wordt aangebracht die overeenkomt met de hysteresis, kan de laser tussen twee verschillende golflengtes geschakeld worden door het injecteren van optische pulsen.

### Microschijf lasers

Laserwerking kan ook verkregen worden in componenten met een circulaire caviteit zoals ringen of schijven. Het licht is dan geconcentreerd aan de buitenste rand in de zogenaamde 'fluistergallerijmode'. Twee verschillende richtingen zijn dan mogelijk: laserwerking kan zowel in positieve als negatieve wijzerzin optreden. Een niet-lineaire winstonderdrukking kan ervoor zorgen dat een van de twee richtingen dominant wordt en er een unidirectioneel regime ontstaat. Door een puls in de ring of schijf te sturen kan men tussen de twee toestanden schakelen. Dit is geïllustreerd in Figuur 2 waarbij het licht wordt uitgekoppeld door een naburige golfgeleider. Wanneer de mode met negatieve wijzerzin dominant is, zal het licht naar de rechterkant propageren. De richting kan vervolgens omgekeerd worden door een puls in de tegenovergestelde richting aan te brengen.

In dit werk tonen we dit effect aan in een zeer kleine microschijflaser ( $7.5 \mu\text{m}$  diameter) die geïntegreerd is op silicon. Silicon is het standaardmateriaal om elektronische chips te maken. We kunnen met deze techniek schakeltijden van



**Figuur 3:** Optische pakketschakelaar met DFB lasers als geheugenelementen.

60 ps bekomen met zeer lage pulsenergieën (1.8 fJ).

### Gekoppelde niet-lineaire caviteiten

Door niet-lineaire (passieve) caviteiten met elkaar te koppelen in een symmetrische structuur, kunnen er interessante fenomenen optreden waarbij de symmetrie verbroken wordt. Zelfs wanneer we de structuur volledig symmetrisch exciteren, kunnen de uitgangen verschillen. We bestuderen deze asymmetrieën theoretisch in kleine netwerkmotieven bestaande uit drie en vier caviteiten. Bovendien tonen we met numerieke simulaties aan dat flip-flopwerking tussen meerdere toestanden mogelijk is.

### Optische pakketschakelaar

De reeds vermelde DFB laser kan als geheugenelement gebruikt worden in een optische pakketschakelaar (zie Figuur 3). Een optisch data-pakket bestaat in het algemeen uit een 'header' (die de routeringsinformatie bevat) en de 'payload' (met de eigenlijke data). De optische header processor zal een optische puls genereren als de header overeenkomt met een vooraf bepaalde bitsequentie. Deze optische puls wordt dan vervolgens gebruikt om de DFB laser flip-flop die correspondeert met de routeringsinformatie aan te schakelen. De uitgang van de DFB flip-flop kan vervolgens gebruikt worden als pomp voor een golflengte

omzetter. De payload wordt vervolgens omgezet naar de golflengte van de DFB flip-flop. Door gebruik te maken van een AWG kan men de verschillende golflengtekanalen opsplitsen in verschillende uitgangspoorten. Dit schema toont duidelijk aan dat de flip-flop essentieel is om de (verwerkte) header informatie bij te houden terwijl de payload naar zijn bestemming wordt gebracht.

Deze pakketschakelaar wordt experimenteel aangetoond voor bitsnelheden tot 40 Gb/s. Het voordeel van deze aanpak is dat de reeks DFB lasers eenvoudig kunnen worden afgestemd op de verschillende golflengtekanalen van het optische netwerk. Bovendien kunnen de DFB flip-flops ook zeer snel schakelen.

### **Regeneratie**

Wanneer er meerdere optische knooppunten met elkaar worden verbonden, zal de ruis en overspraak (veroorzaakt door optische versterkers) de prestaties van het netwerk beperken. Daardoor is er nood aan een zogenaamde optische regenerator die deze distorties kan wegwerken. Een regenerator heeft typisch een zeer uitgesproken stapfunctie in zijn transmissiekarakteristiek. Deze stapfunctie laat toe om het onderscheid tussen de twee logische niveau's te vergroten en de positie van de stap noemt men het decisieniveau.

De hiervoor vermelde hysteresis in de DFB laser is niet alleen aanwezig in het uitgangsvermogen van de laser, maar ook in de versterkingskarakteristiek van het geïnjecteerde licht. De zeer steile stapkarakteristiek van de hysteresis blijkt zeer effectief voor de regeneratie van een optisch signaal met veel ruis. Bovendien vermindert het niet enkel de ruis, maar is het ook in staat om het aantal foute bits te reduceren met verschillende grootte-orde. Dit komt doordat de hysteresis een decisieniveau oplevert dat meebeweegt met het datasignaal. We tonen dit effect aan voor bitsnelheden tot 25 Gb/s.





## English summary

The almost simultaneous invention of the laser and the optical fiber has drastically changed the landscape of telecommunication during the past decades. The transmission of light signals through optical fibers results today in an enormous capacity for the transportation of information with bitrates that largely exceed the speed at which conventional electronics can handle such signals. The growing popular attention for new internet-based services (such as video-on-demand, voice-over-IP, video conferencing, ...), suggests that the demand for even higher bandwidths can be expected to increase in the near future.

The mismatch between the huge bandwidth offered by optical systems and the limited speed available for the electronic processing is becoming a major bottleneck in optical network nodes. In order to process light signals in such optical network nodes, they are first converted to electrical signals by a photodiode. After the electronic processing is done, they are converted again to the optical domain and transmitted through an optical fiber to the next network node. These opto-electronic and electro-optic conversions are not only power consuming, but also the electronics required to process these signals at such high bitrates are very expensive. These difficulties clearly indicate that there is a need for devices that can do the processing partly or completely within the optical layer.

Optical memory elements (flip-flops) are the most important missing links to realize the all-optical processing of signals in optical network nodes. Such all-optical flip-flops are essential in all-optical packet switches as they store the routing information while an optical data packet is directed towards the correct output port. All-optical flip-flop concepts previously reported in literature are often based on rather complex structures consisting of multiple laser sections which are difficult to integrate and offer limited switching speeds. In this work, we demonstrate multiple novel concepts to create all-optical flip-flops based on single laser diodes. These laser diodes are already standard devices in today's telecommunication industry and offer therefore a viable alternative to implement all-optical network nodes. In order to illustrate the applicability of all-optical flip-flops, their use is also experimentally demonstrated by the implementation of an all-optical packet switch where different data packets are

routed to their desired output using only optical signals.

By cascading multiple optical network nodes, there can be an accumulation of noise that severely limits the performance of optical networks. Indeed, the conversion to the electrical domain (as in traditional network nodes), will re-digitalize the original signal and will, therefore, remove all the noise. We present a novel scheme, based on a single laser diode, to regenerate the signals within the optical domain.

### **All-optical flip-flops**

All-optical flip-flops are devices that can switch between two (or more) different states by injecting optical pulses. In general, all-optical flip-flops are based on some sort of hysteresis effect which means that different output states are possible under the same input conditions.

### **Distributed feedback lasers**

Distributed feedback (DFB) laser diodes are the standard transmitters in most advanced optical communication systems. In contrary to other types of lasers, the feedback is distributed along the laser cavity by diffraction on a Bragg grating (see Figure 1a). The injection of external light (with a wavelength outside the stop-band of the grating), will adjust the distribution of the carriers along the laser cavity. Because the differences in carrier density will affect the refractive index, the Bragg-reflections will become distorted and the laser will eventually stop lasing. In this work, we show that there can be a hysteresis effect in the laser output power under the injection of external light (see Figure 1b). We apply a holding beam at one side of the DFB laser in order to work within the bistable domain. A light pulse injected on the same side will switch off the laser diode. Injecting a pulse from the opposite side will restore the uniformity of the carriers and the laser will switch on again. This results in very fast flip-flop operation (with switching times as low as 45 ps) as shown in Figure 1c.

### **Distributed Bragg reflector lasers**

A distributed Bragg reflector laser has a wavelength selective mirror at one side of the cavity consisting of a grating. By applying a current to the grating section, the wavelength selectivity of the grating will shift and the laser will hop to a different longitudinal mode. In the resulting tuning characteristic, a non-linear gain suppression effect will create a spectral hysteresis around the mode hops. By applying a current that corresponds to the hysteresis, the laser can operate at two distinct wavelengths. We use pulses with a different duration to switch between these two wavelengths.

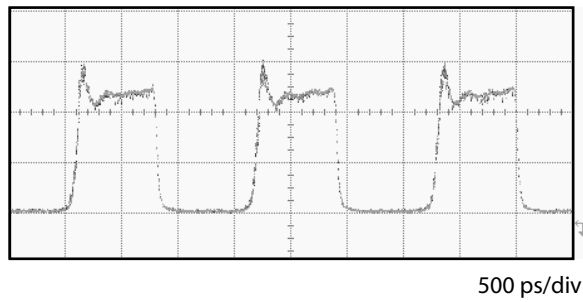
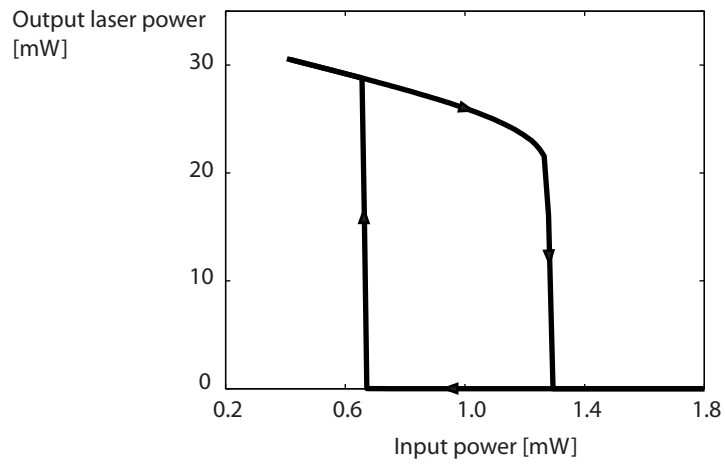


**Figure 1:** Distributed feedback laser as all-optical flip-flop: (a) Schematic of the device; (b) Hysteresis in laser output power under injection of light; (c) experimental demonstration of flip-flop operation.

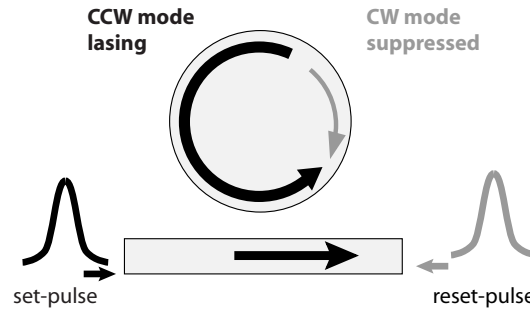


**Figure 2:** Flip-flop operation in disk lasers.

### Microdisk lasers

Lasing operation can also be obtained in devices with a circular cavity such as disk or ring lasers. The light is then concentrated at the edge of the laser in the so-called ‘whispering gallery mode’ and two different lasing directions are possible (clockwise and counterclockwise). Non-linear gain suppression can result in unidirectional operation of the microdisk laser with either the clockwise or the counterclockwise mode being dominant. The injection of an optical pulse allows to switch between these two states resulting in flip-flop operation. This is illustrated in Figure 2 where the light is coupled out of the laser by a neighbouring waveguide. When the counterclockwise mode is lasing, the light will propagate to the right output port. When we inject a pulse in the opposite direction, the clock-wise mode will become excited and the light will propagate to the left.

In this work, we demonstrate this effect in an ultra-small disk laser ( $7.5 \mu\text{m}$  diameter) which is bonded on silicon. Silicon is the standard material to manufacture electronic chips. We obtain switching times of 60 ps with very low pulse energies (1.8 fJ)

### Coupled non-linear cavities

By coupling non-linear (passive) cavities in a symmetric structure, interesting phenomena of symmetry breaking arise. Even when these structures are excited symmetrically, the output powers can differ. These asymmetries are studied theoretically in small network motifs of three and four cavities. Using numerical simulations, it is demonstrated that multi-state flip-flop operation can be achieved.

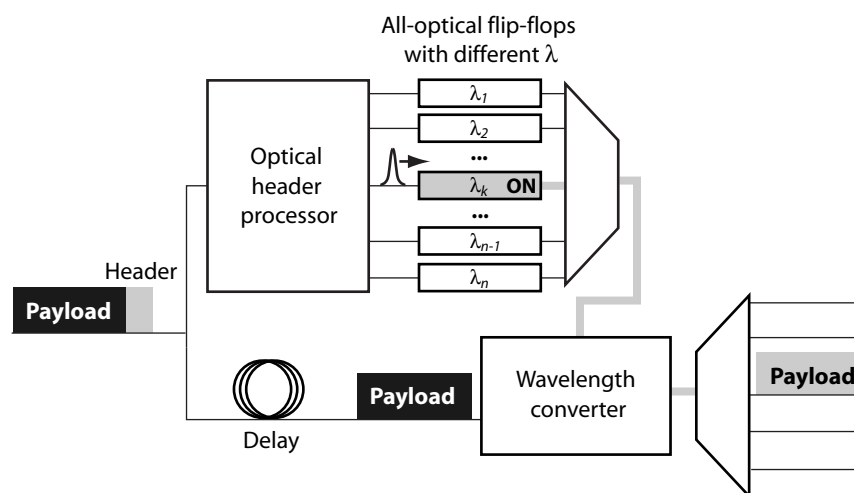


**Figure 3:** All-optical packet switching scheme using DFB lasers as all-optical flip-flop.

### All-optical packet switch

The previously mentioned distributed feedback (DFB) laser flip-flop is also applied in an all-optical packet switch (see Figure 3). An optical data-packet consists in general of a header (containing the routing information) and a payload (the actual data). The optical header processor will generate an optical pulse if the header matches with a predefined bit-sequence. This optical pulse is used to switch on the DFB laser flip-flop that has a wavelength which corresponds to the destination port. The output of the DFB flip-flop is used as the pump signal for a wavelength converter. The payload is then converted to the wavelength of the DFB flip-flop and with an arrayed waveguide grating (AWG) we can spatially divide the different output wavelengths. It is clear from this scheme that the flip-flop acts as an optical memory element by storing the header information while the payload is directed to its destination.

We demonstrate this packet switching scheme experimentally for bit-rates up to 40 Gb/s. The advantage of this approach is that the array of DFB laser diodes can be matched easily with the wavelength-division multiplexed (WDM) grid. Moreover, the DFB flip-flops allow for very fast switching speeds.

## **Regeneration**

When multiple all-optical nodes are cascaded, the noise and crosstalk effects from optical amplifiers and switches will limit the performance of the system. Therefore, there is a clear need for optical regenerators which can reduce these distortions. Such a regenerator has typically a very steep threshold in its transmission characteristic which will act as the decision level.

The hysteresis in the DFB laser is not only present in the laser output power but also in the amplification of the externally injected light. The steep threshold characteristic of the hysteresis is very effective in regenerating a noisy optical signal. It does not only reduce the noise, but can also improve the bit error rate of the signal with several orders of magnitude. This is because the hysteresis effect will introduce a decision level that is dynamically changing with the input signal. We demonstrate this technique for bit-rates up to 25 Gb/s.





# 1

## Introduction

Looking back on the twentieth century, the influence of microelectronics on our society can hardly be overestimated. The deployment and wide-spread use of radio, television, mobile phones and computer networks has drastically changed our everyday lives and will continue to do so as new internet-based services are being implemented. Never in history has distance constituted such a small obstacle and access to information been so close at hand.

If microelectronics was so influential for the twentieth century, one could wonder if nanophotonics will have a similar importance on our future lives. Indeed, when we look at this technological revolution from a physics point of view, we can ask ourselves if electrons are the best way to process huge amounts of information. Light - in its elementary form described by photons - could be considered as a valuable alternative for many applications. The main advantage of photons compared to electrons is their tremendous speed due to a lack of mass, a property which makes them very interesting for the transport of information. However, it also has the adverse effect that they are very difficult to trap for a long period of time in order to construct an optical memory element. Such an optical memory element that could replace the functionality of the electronic transistor remains one of the most important missing links in the development of photonics as a mature technology.

The almost simultaneous invention of the laser [1, 2] and the optical fiber [3] in the 1960's initiated the research towards optical communication systems. In

such systems we use modulated light from a laser source to transport information at extremely high bitrates over very long distances by sending the light through thin fibers made of glass. Intensive research has focused on the increase of the bitrates in such optical fibers. Today, this results in an enormous capacity for transport of information through optical fibers with bitrates (up to 640 Gb/s) that largely exceed the speed at which conventional electronics can handle such signals (typically 40 Gb/s).

The mismatch between the high optical bandwidth and the limited speed available for the electronic processing is becoming a major bottleneck in optical network nodes. In order to process light signals in such a network node, they are first converted to electrical signals by a photodiode. After the electronic processing is done, they are converted again to the optical domain and sent through an optical fiber to the next network node. These opto-electronic and electro-optic conversions are not only power and time consuming, but also the electronics needed to process these signals at such high bitrates is very expensive. These difficulties clearly indicate that there is a need for devices that can do the processing partly or completely within the optical layer, leading to the notion of 'all-optical networks' or 'transparent networks' where not only the transport of signals is done optically, but also their processing.

We see that optical telecommunication is not only progressing in long-haul optical networks, but also on a much smaller scale in intra-chip or on-chip interconnects. The high data rates in current information processing machines require connections that can contain much higher densities of information which can only be provided by optical links. Optics can also reduce the energy consumption as there is no need to charge the lines to the signal voltage: we only need to provide enough energy to charge a photodetector at the receiving end. The first commercial products, based on optical interconnects for application in large data-centers and computer clusters, have recently been introduced [5, 6]. Optical interconnects on a chip-scale level are still in their infancy, but their performance can surpass that of electronic interconnects and could allow for future demands to be met [7].

The evolution of optical interconnects brings forth the idea to implement a transparent computer where all the processing and logic are implemented solely within the optical domain. The construction of complete photonic processors working at the speed of light is still far beyond our reach and should be considered science fiction for now [8]. However, efforts oriented towards ultra-small optic devices with very fast dynamics are promising as they may offer the building blocks for future chip-scale optical logic: from micro-scale disk lasers [9] to nano-scale surface plasmons [10, 11] and even up to transistors on a (sub-)molecular level [12, 13]. However, for applications with extensive use of photonics such as the above-mentioned optical networks, there will be a clear

need to process light signals directly in the optical domain as the demand for higher bitrates increases. Therefore, the focus of this work will rather be on solutions that have significant impact on the processing of high bitrate signals in optical network nodes than on the construction of all-optical logic devices for optical computing. Although, it should be mentioned that the application of photonic components should also be seen in a much broader perspective than simply telecommunication and computing: other application areas, such as biophotonics, are becoming mature technologies which can also benefit from advanced optical signal processing devices.

Recent studies have shown that the impact of global information and communication technology (ICT) is becoming environmentally significant [14]. The estimated impact in terms of CO<sub>2</sub> emissions accounts now for 2%, a number that is equivalent to that of aviation. Therefore, the emphasis on the introduction of novel implementations for optical network nodes is done with respect to their power consumption. The question whether all-optical approaches reduce the power consumption is still part of an on-going and active debate [15–18] within the scientific world, but the possible advantages of optics over electronics at much higher bitrates are clear.

In this work, we will demonstrate novel techniques to construct optical memory elements (flip-flops) and their application in an all-optical packet switching scheme. Further on in this chapter, it will be shown that most of the concepts for all-optical flip-flops require multiple active elements which are difficult to integrate and have in general a large footprint and high power consumption. We will demonstrate that flip-flop operation is possible in various types of single laser diodes. Moreover, most of our work is concentrated on devices that are already standard components in today's telecommunication systems which facilitates their short-term implementation. Besides the experimental demonstration of flip-flops in an all-optical packet switch, we will also show how the noise accumulation in optical networks can be reduced by the use of a single DFB laser diode.

In order to understand the background and context of the obtained results, this introductory chapter will start off by giving an overview of the basic technology in optical fiber networks. Afterwards, an overview is given of the state of the art in all-optical flip-flops.

## 1.1 Optical fiber networks

Telecommunication commences with the introduction of the telegraph in the 19th century and the invention of the telephone in 1876. This initiated an era of electrical communication where the signals are being sent through twisted copper pairs and - later on - through coaxial cables. Coaxial cables only allow

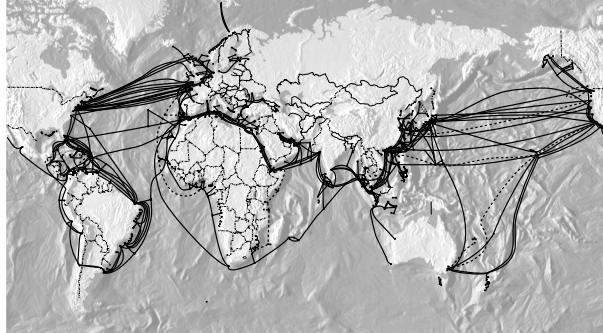


**Figure 1.1:** The state of the submarine optical fiber network in 2007.  
(Source: Alcatel-Lucent ©)

bandwidths up to 100 Mb/s on relatively short distances (1 km). During the past two decades, such electrical communication networks were superseded by optical fiber networks. In the beginning, this was done only for the very core of the communication networks with a.o. the introduction of fiber-optic submarine cables connecting the different continents (Figure 1.1). However, because of the growing public interest in the internet since the mid '90s (Figure 1.2), more and more electrical cables were replaced by optical fiber connections in order to meet the increasing demand for more bandwidth. Indeed, contrary to the limitations of coaxial cables, optical fibers can provide an almost unlimited capacity with bandwidths reaching up to 10 THz over very long distances. Recently, new internet-based services such as video-on-demand (YouTube, digital TV), voice-over-IP (Skype), video conferencing, ... are gaining more public attention and it can be expected that the demand for more data-traffic will continue to increase. In highly industrialized countries such as Japan, the shift towards optical fibers is much more visible: not only the core of the network is being implemented with optical fibers but also the whole access network. This results in the concept of fiber-to-the-home (FTTH) where optical fiber connections go all the way to the internet subscribers' premises. Already in 2008, the number of internet subscribers for FTTH in Japan superseded that of ADSL (transmission over standard copper telephone lines).

An optical fiber consists of a long wire of glass in which the light is concentrated. The core of the fiber is surrounded by a cladding layer which has a slightly lower refractive index. The underlying physical principle of an optical fiber can be understood from total internal reflection: when light that is travelling in a dense medium hits a boundary at a steep angle, the light will be completely reflected without loss. The glass used for the fabrication of optical fibers is called silica ( $\text{SiO}_2$ ) and has a very low loss (0.1-0.2 dB/km) around

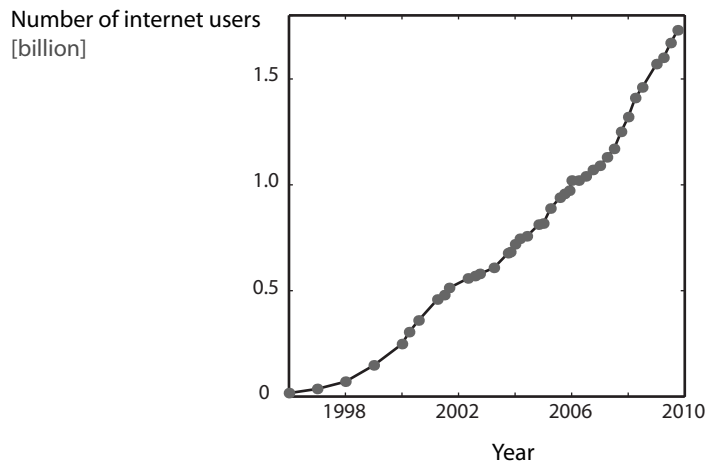


**Figure 1.2:** The number of internet users has drastically increased in the past decade. (Source: [www.internetworldstats.com](http://www.internetworldstats.com))

the telecommunication wavelengths of  $1.3 \mu\text{m}$  and  $1.55 \mu\text{m}$ . This very low attenuation allows the propagation of light over very long distances (e.g. 100 km without amplification). Besides attenuation in optical fibers, the light can get distorted by dispersion effects: light at slightly different wavelengths can experience small differences in refractive index which affects their speed and results in pulses that are being spread out. Most optical communication systems use standard single-mode fibers (core diameters of  $8\text{-}10 \mu\text{m}$ ) with a dispersion-compensating system afterwards.

The semiconductor laser proved to be a reliable and relatively cheap solution to act as the light source for optical fiber communication. A laser consists of a gain medium that is placed within a cavity in order to send the light several times through this gain medium before it is emitted by the laser. The acronym 'laser' stands for light amplification by stimulated emission of radiation which means that the amplified light has exactly the same physical properties (eg. direction, wavelength, polarization, phase, ...) as the light that is already present in the gain medium. When the amplification by stimulated emission is combined with the feedback mechanism and wavelength selectivity of the cavity, we generate a narrow beam of photons which are all nearly identical.

The capacity of optical fibers was further improved by sending light at different wavelengths through the same optical fiber. This technique is known as wavelength division multiplexing (WDM). At the transmitter side, multiple optical signals, each at a separate carrier wavelength, are joined together and sent

through a single optical fiber. These systems allow for a multiplication in capacity: modern systems can handle up to 80 signals at a bitrate of 100 Gb/s resulting in a transmission of 8 Tb/s through a single fiber [19].

In the implementation of WDM systems, it is important to have laser diodes that support a single wavelength with a narrow spectral width. Edge-emitting semiconductor lasers with a Bragg grating (eg. distributed feedback lasers or distributed Bragg reflector lasers) offer single-mode operation and are tunable by changing the temperature and/or current. The requirement of single-mode operation with a very narrow spectral width is not only necessary to multiplex signals with different wavelengths, but also to avoid dispersion-related effects.

To overcome the fiber loss, the optical signal needs to be amplified in long-haul systems. Erbium-doped fiber amplifiers (EDFA) can amplify the complete WDM signal at once. This limits the use of power consuming electrical repeaters which convert each WDM signal separately to the electrical domain to perform a regeneration (amplification, reshaping, retiming) before retransmitting it again through the optical fiber.

Recently, advanced modulation techniques based on multilevel phase modulation and/or coherent detection allow to go to even much higher bitrates by using the wave properties of light. These modulation formats do not only use the amplitude but also the phase and polarization of the light. With a combination of these techniques, the information of multiple bits can be stored together within a so-called symbol. Combining the different techniques it is possible to go up to 69.1 Tb/s [4].

## 1.2 All-optical signal processing

### 1.2.1 All-optical network nodes

The major bottleneck for the further evolution of optical communication systems is the routing of high-speed signals at the network nodes. As discussed in the previous section, the use of optical fibers has led to an enormous increase in bandwidth for the transmission of signals. However, in the nodes of the network this information needs to be processed in order to be routed to the correct output port and then retransmitted to the next network node. The electronic processing of these high-speed signals requires expensive and power consuming electronics. The solution for the mismatch between the high bandwidth offered by optical transmission systems and the limited capabilities of electronics, requires that we look into the possibility of processing the light signals completely within the optical domain without making use of electronics. When we can avoid the electrical processing of signals, we also eliminate the power consuming opto-electronic (O/E) and electro-optic (E/O) conversions.

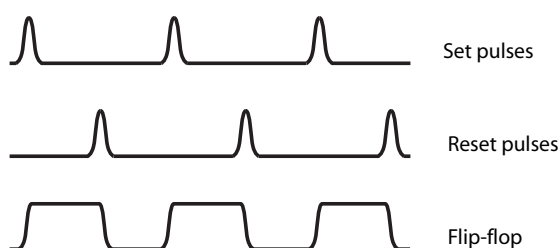


**Figure 1.3:** A schematic illustration of flip-flop operation: the output switches when the set and reset pulses are injected.

One of the most important elements in the engineering of such optical network nodes, is the all-optical flip-flop element. This is a device that can switch between two (or more) different states by the injection of optical pulses. The basic principle is depicted in Figure 1.3 showing how set and reset pulses are used to switch the device on and off. The all-optical flip-flop operation can be used as a one-bit optical memory because it allows us to store the set pulse for a longer period of time.

The underlying physical mechanism is always based on some sort of hysteresis effect [20]. Hysteresis (or bistability) refers to a system which can have multiple states under the same input conditions and where its current state is determined by the history of the input. In general, hysteresis can be achieved by a combination of a feedback mechanism and a nonlinear effect.

The application of all-optical flip-flops as optical memory elements is especially interesting when we want to temporarily store the routing information of a data packet while it is directed to the correct output port. A simplified schematic for all-optical switching of packets using wavelength routing [21] is shown in Figure 1.4. The first part of the data packet consists of a header which contains the information needed to route the packet through the network. After the header, there is the actual data which is called the payload. The signal is split and one part is sent through a delay line, while, in the other arm, the header information is extracted and processed. The header processor will compare the bits of the header with a pre-defined bit sequence and it will send a pulse to the optical flip-flop when there is a correlation. This pulse will change the output state of the flip-flop to light with a different wavelength. We can use the output light of the flip-flop as the pump power of a wavelength converter. The original signal that has been delayed, will then be converted to the wavelength provided by the flip-flop. This means that the resulting signal wavelength matches the routing information contained in the header. Finally, we can spa-

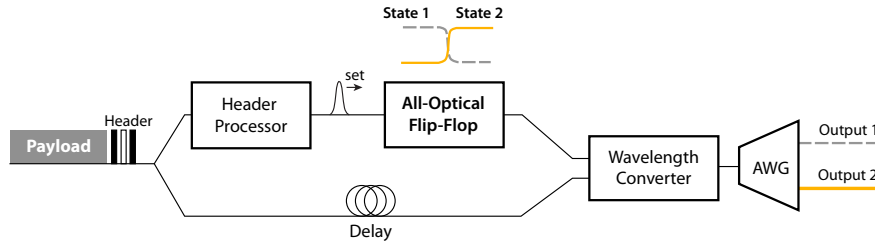


**Figure 1.4:** Schematic of an all-optical packet switch: the all-optical flip-flop is necessary to store the processed header information while the signal is routed to the output. [21, 22]

tially divide the two output wavelengths by using an arrayed waveguide grating (AWG). Other methods for optical packet switching will be further discussed in Chapter 6, but we can already conclude from this analysis that the optical flip-flop is necessary to store the processed header information while the signal is being routed to the output port.

Many designs for all-optical flip-flop operation have been proposed in the past. Most of them require the combination of multiple active sections that are combined with each other by passive waveguides. This means that they are not only very complex, but also require a difficult fabrication due to the on-chip integration of active and passive sections. Because of their high footprint, they also suffer from rather slow switching speeds and high power consumption. In this work, several concepts will be presented for all-optical flip-flops that are based on single laser diodes. Not only do they outperform most of the existing schemes, some of them are also very easy to implement due to the already widespread use of these laser diodes in today's telecommunication industry. We will here give a short overview of the prevalent concepts in literature.

### Coupled laser diodes

By coupling two laser diodes with separate cavities both lasing at a different wavelength, it is possible to obtain all-optical flip-flop operation [23–26]. The coupling of the lasers causes one of the lasers to act as a master laser and to quench lasing action in the other (see Figure 1.5). The flip-flop will therefore switch between two wavelengths as the flip-flop state is determined by the laser that is currently lasing. By injecting external light (at a different wavelength) in the master laser, its output power can be reduced or stopped which allows the other laser to start lasing and become the master laser.

The implementation of this concept with two coupled microring lasers

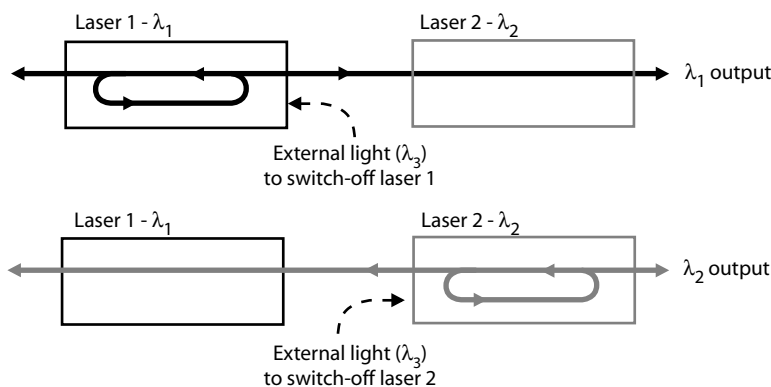


**Figure 1.5:** A bistability originating from a coupled laser structure where one laser quenches lasing in the other. [25]

(each  $16 \mu\text{m}$  diameter) allows for very fast flip-flop operation (20 ps switching time) with low pulse energy (5.5 fJ) [27]. Two circular laser sections connected with each other by a waveguide allow to switch between a clockwise and counter-clockwise lasing mode. However, the concept was only demonstrated for pulsed operation. As will be explained in chapter 4, it is possible to exploit certain gain nonlinearities to establish flip-flop operation in a single disk or ring laser [9].

Instead of coupling two laser diodes, it is also possible to combine a distributed feedback laser diode and a semiconductor optical amplifier (SOA) [28–30]. Switching times of 50 ps were demonstrated in this manner and such structures allow the integration of multiple laser diodes operating at different wavelengths.

### Bistable laser diodes

One of the most well-known concepts for flip-flop operation consists of an active multi-mode interference 2x2 coupler inside a laser cavity [31, 32] (see Figure 1.6). Saturable absorber sections on the sides provide the necessary non-linearity to provide bistable operation. Due to the large footprint of the device ( $595 \mu\text{m} \times 12 \mu\text{m}$  without SA), the switching times are limited and the pulse energies rather high: the best reported rise time is 280 ps [33] and pulse energies are typically 40 pJ. Several improvements have been made to this device such as (tunable) wavelength selective mirrors [33, 34] and polarization insensitive operation [35]. To overcome the need for saturable absorbers, an active Mach-Zehnder structure has been proposed in order to have a perfect overlap of the two lasing modes [36].

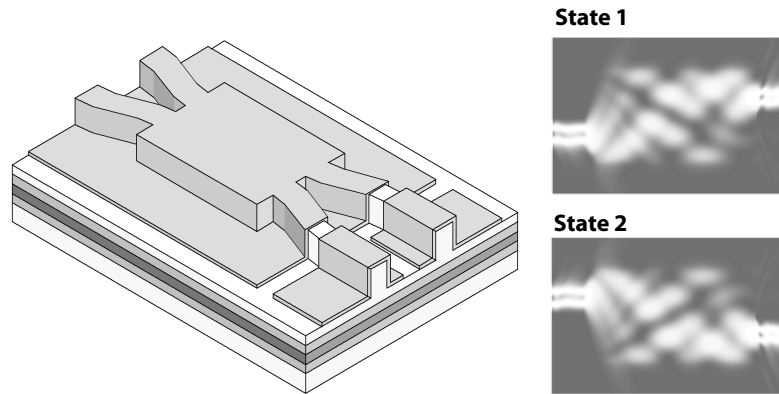


**Figure 1.6:** Two separate states in an active multi-mode interference coupler (Courtesy of K. Takeda).

Much of the early work on optical flip-flops was based on bistabilities in standard laser diodes [20, 37]. They can be based, for example, on a multi-segment DFB laser with one segment acting as a saturable absorber [38]. The carrier recovery time in the saturable absorber (SA) is the main limiting factor in obtaining high switching speeds for these devices. Saturable absorber sections are also used for flip-flop operation in nonlinear directionally coupled laser diodes [39]. Dispersive bistabilities in DFB amplifiers (biased under lasing threshold) offer an alternative [40] but require a tight wavelength control.

#### Active Mach-Zehnder interferometers

Using interference effects, optical flip-flop operation has been demonstrated in Mach-Zehnder interferometer (MZI) structures with SOAs in the arms. The effect is based on phase changes in the SOAs. This has been demonstrated first in two coupled Mach-Zehnder structures [41, 42], but afterwards also for a single MZI with a feedback loop [43, 44].

#### Polarization bistable

Two orthogonal polarizations of light can be used to implement a bistability useful for flip-flop operation. By injecting set and reset pulses with a different polarization, some devices can switch between two polarization states. The most successful results were obtained in vertical cavity surface emitting lasers (VCSELs) [45, 46]. Flip-flop operation with very low-energy pulses can be obtained using such devices: record low switching energies of 0.3 fJ [47] are pos-

sible. Using higher pulse energies, the switching speed can be as fast as 7 ps. These first results account for flip-flop operation in a VCSEL with an operating wavelength at 980 nm, but recently it was also demonstrated in devices with a wavelength of 1.55  $\mu\text{m}$  [48]. The pulse energies in such devices are 10 fJ for a repetition rate of 3.1 GHz ( $\sim 300$  ps). The VCSEL flip-flop is promising, but difficult to integrate on-chip. The use of polarization states for flip-flop operation was also exploited in structures consisting of two semiconductor optical amplifiers (SOAs) [49].

### **Multistate flip-flop operation**

For some signal processing applications it can be an advantage to switch between multiple different states instead of only two. Different concepts have been proposed to achieve multistate flip-flop operation by combining multiple active elements with wavelength selective mirrors [50–52] or ring laser cavities [53]. In chapter 5, we will discuss a novel concept for multistate flip-flop operation in more detail.

### **1.2.2 Regeneration**

When several all-optical nodes are cascaded, there will be an accumulation of noise, distortion and cross-talk which severely limits the performance of the optical network. Indeed, non-transparent network nodes which convert the signals to the electrical domain, also act as repeaters because the O/E/O conversion removes the noise when retransmitting the signal. An alternative approach is to regenerate the signal using all-optical techniques. The noise on such signals comes in general from amplifiers (eg. EDFAs) that are needed in order to overcome the attenuation losses. Therefore, we use regenerators that can perform pulse reshaping. Typically, they have a very steep nonlinear transmission curve in order to increase the extinction ratio of the signal. More advanced regenerators also do the retiming of a signal, however this is not strictly necessary for certain practical applications [54].

Several concepts for all-optical regeneration have been proposed and will be discussed further in chapter 7. In this work, a novel type of 2R regeneration will be demonstrated based on the use of a single DFB laser diode. When a hysteresis is used instead of a nonlinear power transfer function, we can not only reduce the noise but even recover bits that would otherwise have been detected wrong.

### 1.3 Outline

It was demonstrated that the evolution of optical networks will require the implementation of all-optical network nodes because the electronic processing of high-speed signals is power consuming and expensive. This requires a whole range of new functionalities that will be explored in subsequent chapters.

In the first chapters, several new concepts for all-optical flip-flop operation will be introduced. We start with all-optical flip-flops based on edge-emitting laser diodes. The first being the distributed feedback (DFB) laser where a non-linear effect based on the distribution of carriers is used to switch the laser on and off with light pulses. The second is the distributed Bragg reflector (DBR) laser which shows flip-flop operation because of a hysteresis in its tuning characteristic. Both lasers are already widely used as light sources in today's telecommunication industry. In chapter four, an overview will be given of results obtained on flip-flop operation in microdisk lasers. The part on all-optical flip-flops will be concluded by a more theoretical chapter explaining how structures consisting of passive coupled cavities can exhibit multistable behaviour.

In chapter six, experimental results of all-optical packet switching using a distributed feedback laser as all-optical flip-flop will be discussed.

A novel concept for all-optical regeneration using a single laser diode at bit-rates up to 25 Gb/s is proposed in the last chapter: a theoretical analysis on the use of hysteresis for regeneration is given together with experimental results that demonstrate an improvement in the bit-error rate.

### 1.4 Publications

The results obtained within this work have been published in several papers and were presented at various conferences. The results on 2R regeneration have led to a patent application. The following list gives an overview.

#### Publications in international journals

1. K. Huybrechts, T. Tanemura, K. Takeda, Y. Nakano, R. Baets, G. Morthier, "All-optical 2R regeneration using the hysteresis in a distributed feedback laser diode," *IEEE Journal of Selected Topics in Quantum Electronics*, accepted for publication.
2. K. Huybrechts, B. Maes, G. Morthier, "Symmetry breaking in networks of coupled cavities" *Journal of the Optical Society of America-B*, 27(4), p.708-713 (2010).

3. L. Liu, R. Kumar, K. Huybrechts, T. Spuesens, G. Roelkens, E.-J. Geluk, T. de Vries, P. Regreny, D. Van Thourhout, R. Baets, G. Morthier, "An ultra-small, low-power, all-optical flip-flop memory on a silicon chip," *Nature Photonics*, 4(3), p.182-187 (2010).
4. K. Huybrechts, R. Baets, G. Morthier, "All-optical flip-flop operation in a standard tunable DBR laser diode," *IEEE Photonics Technology Letters*, 21(11), p.703-705 (2009).
5. K. Huybrechts, T. Tanemura, Y. Nakano, R. Baets, G. Morthier, "40 Gb/s all-optical packet switching with a distributed feedback laser as all-optical flip-flop," *IEEE Photonics Technology Letters*, 21(11), p.703-705 (2009).
6. G. Morthier, W. D'Oosterlinck, K. Huybrechts, "All-optical flip-flops based on DFB laser diodes and DFB-arrays," *Journal of Materials Science - Materials in Electronics*, 20(Suppl. 1), p.385-389 (2009)
7. K. Huybrechts, G. Morthier, R. Baets, "Fast all-optical flip-flop based on a single distributed feedback laser diode," *Optics Express*, 16(15), p.11405-11410 (2008).
8. K. Huybrechts, W. D'Oosterlinck, G. Morthier, R. Baets, "Proposal for an all-optical flip-flop using a single distributed feedback laser diode," *IEEE Photonics Technology Letters*, 20(1), p.18 - 20 (2008)

### Publications in international conferences

9. K. Huybrechts, T. Tanemura, K. Takeda, Y. Nakano, R. Baets, G. Morthier, "All-Optical 2R Regeneration and BER Improvement using Hysteresis in a DFB Laser Diode," *Photonics in Switching*, United States (2010).
10. G. Morthier, L. Liu, R. Kumar, P. Mechet, K. Huybrechts, G. Roelkens, T. Spuesens, E.-J. Geluk, T. de Vries, P. Regreny, R. Baets, D. Van Thourhout, "Heterogeneous InP on SOI Integration for the Realization of All-Optical Logic Devices," *Conference on Integrated Photonics Research (IPR'10)*, **invited**, United States (2010).
11. K. Huybrechts, L. Liu, R. Kumar, T. Spuesens, G. Roelkens, E.-J. Geluk, T. de Vries, M.K. Smit, P. Regreny, P. Rojo-Romeo D. Van Thourhout, R. Baets, G. Morthier, "Digital photonics using microdisk lasers heterogeneously integrated in SOI," *15th European Conference on Integrated Optics (ECIO 2010)*, **invited**, p.WeF1, United Kingdom (2010).
12. R. Kumar, K. Huybrechts, L. Liu, G. Roelkens, T. Spuesens, E.-J. Geluk, T. De Vries, D. Van Thourhout, R. Baets, G. Morthier, "An ultra-small,

- low-power all-optical flip-flop memory on a silicon chip, *Optical Fiber Communication Conference (OFC/NFOEC 2010)*, p.OTuN7, United States (2010).
13. K. Huybrechts, R. Baets, G. Morthier, "All-optical signal processing with standard edge-emitting laser diodes," *14th Annual Symposium of the IEEE Photonics Society Benelux Chapter*, Belgium, p.25-28 (2009).
  14. K. Huybrechts, A. Ali, R. Baets, G. Morthier, "Novel concept for all-optical flip-flop operation in a single DBR laser diode," *22nd Annual Meeting of the IEEE Photonics Society*, Turkey, ThF2 (2009).
  15. Y. De Koninck, K. Huybrechts, G. Van der Sande, J. Danckaert, R. Baets, G. Morthier, "Nonlinear dynamics of asymmetrically coupled microdisk lasers," *22nd Annual Meeting of the IEEE Photonics Society*, Turkey, WN4 (2009).
  16. K. Huybrechts, A. Ali, T. Tanemura, Y. Nakano, G. Morthier, "Numerical and experimental study of the switching times and energies of DFB laser based all-optical flip-flops," *Photonics in Switching*, Italy, p.We12-6 (2009).
  17. K. Huybrechts, A. Ali, G. Morthier, "All-optical 2R regeneration and wavelength conversion at 10 Gb/s using a single bistable DFB laser diode," *Photonics in Switching*, Italy, FrII2-6 (2009).
  18. B. Maes, M. Fiers, K. Huybrechts, G. Morthier, P. Bienstman, "Dynamics and Instabilities in Series of Coupled Nonlinear Resonators," *ICTON 2009*, **invited**, Portugal, p.We.C4.3 (2009).
  19. K. Huybrechts, T. Tanemura, Y. Nakano, R. Baets, G. Morthier, "Fast 40 Gb/s optical packet switching using an all-optical flip-flop based on a single distributed feedback laser," *Optical Fiber Communication Conference (OFC/NFOEC 2009)*, p. OMU4, United States, (2009).
  20. K. Huybrechts, G. Morthier, R. Baets, "Fast operation of a broadband all-optical flip-flop based on a single DFB-laser diode," *European Conference on Optical Communication (ECOC 2008)*, We.2.C.4, Belgium, (2008).
  21. K. Huybrechts, G. Morthier, R. Baets, "Experimental demonstration of all-optical flip-flop operation in a single distributed feedback laser diode," *Photonics in Switching*, Japan, (2008).
  22. B. Maes, K. Huybrechts, G. Morthier, P. Bienstman, R. Baets, "Switching with Coupled Photonic Crystal Cavities," *SIAM Conference on Nonlinear Waves and Coherent Structures*, **invited**, Italy, (2008).

23. B. Maes, K. Huybrechts, G. Morthier, P. Bienstman, R. Baets, "Nonlinear Switching Effects in Coupled Micro-photonic Cavities," *Progress In Electromagnetics Research (PIERS)*, **invited**, United States, p.187 (2008).
24. G. Morthier, K. Huybrechts, "Optical bistability and flip-flop operation in DFB laser diodes injected with a CW signal," *SPIE Photonics Europe conference*, France, p.138 (2008).
25. K. Huybrechts, B. Maes, G. Morthier, R. Baets, "Tristable all-optical flip-flop using coupled nonlinear cavities," *IEEE/LEOS Winter topicals*, TuA1.2, Italy, p.16-17 (2008).
26. K. Huybrechts, W. D'Oosterlinck, G. Morthier, R. Baets, "All-optical Flip-flop based on a single Distributed Feedback Laser Diode," *12th Annual Symposium of the IEEE/LEOS Benelux Chapter*, Belgium, p.47 (2007).
27. G. Morthier, W. D'Oosterlinck, K. Huybrechts, "All-optical flip-flops based on DFB laser diodes and DFB-arrays," *International Conference on Optical, Optoelectronic and Photonic Materials and Applications (ICOOPMA07)* (**invited**), United Kingdom, (2007).
28. K. Huybrechts, W. D'Oosterlinck, G. Morthier, R. Baets, "Optical flip-flop operation using an AR-coated distributed feedback laser diode," *Conference on Lasers and Electro-optics (CLEO)*, JWA36, United States, (2007).
29. K. Huybrechts, W. D'Oosterlinck, G. Morthier, R. Baets, "All-optical flip-flop operation using an AR-coated distributed feedback laser diode," *ePIXnet Winter School*, poster nr. 21, Switzerland, (2007)

### **Publications in national conferences**

30. K. Huybrechts, Digital photonics for optical network nodes, FIRW PhD symposium, p.282, Belgium, (2009)
31. K. Huybrechts, A single laser diode for all-optical flip-flop operation, FIRW PhD symposium, p.35, Belgium, (2007)

## References

- [1] A. L. Schawlow and C. H. Townes. *Infrared and Optical Masers*. Physical Review, 112(6):1940–1949, 1958.
- [2] T. H. Maiman. *Stimulated optical radiation in ruby*. Nature, 187(4736):493–494, 1960.
- [3] K. C. Kao and G. A. Hockham. *Dielectric-fibre surface waveguides for optical frequencies*. Proceedings of the Institution of Electrical Engineers-London, 113(7):1151–1158, 1966.
- [4] A. Sano, H. Masuda, T. Kobayashi, M. Fujiwara, K. Horikoshi, E. Yoshida, Y. Miyamoto, M. Matsui, M. Mizoguchi, H. Yamazaki, Y. Sakamaki, and H. Ishii. *69.1-Tb/s (432 x 171-Gb/s) C- and extended L-band transmission over 240 km Using PDM-16-QAM modulation and digital coherent detection*. In Conference on Optical Fiber Communication (OFC), 2010.
- [5] C. Gunn. *CMOS Photonics for High-Speed Interconnects*. IEEE Micro, 26(2):58–66, 2006.
- [6] A. Narasimha, B. Analui, Y. Liang, T. J. Sleboda, S. Abdalla, E. Balmater, S. Gloeckner, D. Guckenberger, M. Harrison, Rgmp Koumans, D. Kucharski, A. Mekis, S. Mirsaidi, D. Song, and T. Pinguet. *A fully integrated 4x 10-Gb/s DWDM optoelectronic transceiver implemented in a standard 0.13  $\mu\text{m}$  CMOS SOI technology*. IEEE Journal of Solid-State Circuits, 42(12):2736–2744, 2007.
- [7] D. A. B. Miller. *Device Requirements for Optical Interconnects to Silicon Chips*. Proceedings of the IEEE, 97(7):1166–1185, 2009.
- [8] D. A. B. Miller. *Are optical transistors the logical next step?* Nature Photonics, 4(1):3–5, 2010.
- [9] L. Liu, R. Kumar, K. Huybrechts, T. Spuesens, G. Roelkens, E. J. Geluk, T. de Vries, P. Regreny, D. Van Thourhout, R. Baets, and G. Morthier. *An ultra-small, low-power, all-optical flip-flop memory on a silicon chip*. Nature Photonics, 4(3):182–187, 2010.
- [10] D. K. Gramotnev and S. I. Bozhevolnyi. *Plasmonics beyond the diffraction limit*. Nature Photonics, 4(2):83–91, 2010.
- [11] D. E. Chang, A. S. Sorensen, E. A. Demler, and M. D. Lukin. *A single-photon transistor using nanoscale surface plasmons*. Nature Physics, 3(11):807–812, 2007.

- [12] J. Hwang, M. Pototschnig, R. Lettow, G. Zumofen, A. Renn, S. Gotzinger, and V. Sandoghdar. *A single-molecule optical transistor*. *Nature*, 460(7251):76–80, 2009.
- [13] Hideo Mabuchi. *Cavity-QED models of switches for attojoule-scale nanophotonic logic*. *Physical Review A*, 80(4):045802, Oct 2009.
- [14] *Gartner Estimates ICT Industry Accounts for 2 Percent of Global CO2 Emissions*. <http://www.gartner.com/it/page.jsp?id=503867>, April 2007.
- [15] R.S. Tucker, K. Hinton, and G. Raskutti. *Energy consumption limits in high-speed optical and electronic signal processing*. *Electronics Letters*, 43(17):906–908, august 2007.
- [16] R. S. Tucker. *Optical packet switching: A reality check*. *Optical Switching and Networking*, 5(1):2–9, 2008.
- [17] S. J. B. Yoo. *Optical Packet and Burst Switching Technologies for the Future Photonic Internet*. *Journal of Lightwave Technology*, 24(12):4468–4492, 2006.
- [18] R. Van Caenegem, J. A. Martinez, D. Colle, M. Pickavet, P. Demeester, F. Ramos, and J. Marti. *From IP over WDM to all-optical packet switching: Economical view*. *Journal of Lightwave Technology*, 24(4):1638–1645, 2006.
- [19] *Infinera launches new line system, sets new standard for capacity*. <http://www.infinera.com/pdfs/news/2008/pr20080609a.pdf>, 2008.
- [20] H.M. Gibbs. *Optical bistability: controlling light with light*. Academic Press, 1985.
- [21] M. T. Hill, A. Srivatsa, N. Calabretta, Y. Liu, H. D. Waardt, G. D. Khoe, and H. J. S. Dorren. *1x2 optical packet switch using all-optical header processing*. *Electronics Letters*, 37(12):774–775, 2001.
- [22] H. J. S. Dorren, M. T. Hill, Y. Liu, N. Calabretta, A. Srivatsa, F. M. Huijskens, H. de Waardt, and G. D. Khoe. *Optical packet switching and buffering by using all-optical signal processing methods*. *Journal of Lightwave Technology*, 21(1):2–12, 2003.
- [23] G. J. Lasher and A. B. Fowler. *Mutually quenched injection lasers as bistable devices*. *IBM Journal of Research and Development*, 8(4):471–474, 1964.
- [24] J. L. Oudar and R. Kuszelewicz. *Demonstration of optical bistability with intensity-coupled high-gain lasers*. *Applied Physics Letters*, 45(8):831–833, 1984.

- [25] M. T. Hill. *All-optical flip-flop based on coupled laser diodes*. Microwave and Optical Technology Letters, 25(3):157–159, 2000.
- [26] M. T. Hill, H. de Waardt, G. D. Khoe, and H. J. S. Dorren. *All-optical flip-flop based on coupled laser diodes*. IEEE Journal of Quantum Electronics, 37(3):405–413, 2001.
- [27] M. T. Hill, H. J. S. Dorren, T. de Vries, X. J. M. Leijtens, J. H. den Besten, B. Smalbrugge, Y. S. Oei, H. Binsma, G. D. Khoe, and M. K. Smit. *A fast low-power optical memory based on coupled micro-ring lasers*. Nature, 432(7014):206–209, 2004.
- [28] W. D’Oosterlinck, J. Buron, F. Ohman, G. Morthier, and R. Baets. *All-optical flip-flop based on an SOA/DFB-laser diode optical feedback scheme*. IEEE Photonics Technology Letters, 19(5-8):489–491, 2007.
- [29] W. D’Oosterlinck, F. Ohman, J. Buron, S. Sales, A. P. Pardo, A. Ortigosa-Blanch, G. Puerto, G. Morthier, and R. Baets. *All-Optical flip-flop operation using a SOA and DFB laser diode optical feedback combination*. Optics Express, 15(10):6190–6199, 2007.
- [30] W. D’Oosterlinck. *Non-Linear Behaviour in a Semiconductor Optical Amplifier and Laser Diode Feedback Scheme*. PhD thesis, Ghent University, 2007.
- [31] M. Takenaka and Y. Nakano. *Multimode interference bistable laser diode*. IEEE Photonics Technology Letters, 15(8):1035–1037, 2003.
- [32] M. Takenaka, M. Raburn, and Y. Nakano. *All-optical flip-flop multimode interference bistable laser diode*. IEEE Photonics Technology Letters, 17(5):968–970, 2005.
- [33] K. Takeda, M. Takenaka, T. Tanemura, and Y. Nakano. *Experimental Study on Wavelength Tunability of All-Optical Flip-Flop Based on Multimode-Interference Bistable Laser Diode*. IEEE Photonics Journal, 1(1):40–47, june 2009.
- [34] M. Raburn, M. Takenaka, K. Takeda, X. Song, J. S. Barton, and Y. Nakano. *Integrable multimode interference distributed Bragg reflector laser all-optical flip-flops*. IEEE Photonics Technology Letters, 18(13-16):1421–1423, 2006.
- [35] K. Takeda, Y. Kanema, M. Takenaka, T. Tanemura, and Y. Nakano. *Polarization-Insensitive All-Optical Flip-Flop Using Tensile-Strained Multiple Quantum Wells*. IEEE Photonics Technology Letters, 20(21-24):1851–1853, 2008.

- [36] K. Takeda, M. Takenaka, T. Tanemura, and Y. Nakano. *All-optical flip-flop based on Mach-Zehnder interferometer bistable laser diode*. In 35th European Conference on Optical Communication (ECOC '09), 2009.
- [37] H. Kawaguchi. *Bistable laser diodes and their applications: State of the art*. IEEE Journal of Selected Topics in Quantum Electronics, 3(5):1254–1270, 1997.
- [38] J. Y. Zhou, M. Cada, and T. Makino. *All-optical bistable switching dynamics in 1.55- $\mu\text{m}$  two-segment strained multiquantum-well distributed-feedback lasers*. Journal of Lightwave Technology, 15(2):342–355, 1997.
- [39] M. Takenaka and Y. Nakano. *Realization of all-optical flip-flop using directionally coupled bistable laser diode*. IEEE Photonics Technology Letters, 16(1):45–47, jan 2004.
- [40] D. N. Maywar, G. P. Agrawal, and Y. Nakano. *All-optical hysteresis control by means of cross-phase modulation in semiconductor optical amplifiers*. Journal of the Optical Society of America B-Optical Physics, 18(7):1003–1013, 2001.
- [41] M. T. Hill, H. de Waardt, and H. J. S. Dorren. *Fast all optical flip-flop using coupled Mach-Zehnder interferometers*. In Conference on Lasers and Electro-Optics (CLEO '01), page 188, 2001.
- [42] M. T. Hill, H. J. S. Dorren, X. J. M. Leijtens, J. H. den Besten, T. de Vries, J. H. C. van Zantvoort, E. Smalbrugge, Y. S. Oei, J. J. M. Binsma, G. D. Khoe, and M. K. Smit. *Coupled Mach-Zehnder interferometer memory element*. Optics Letters, 30(13):1710–1712, 2005.
- [43] R. Clavero, F. Ramos, J. M. Martinez, and J. Marti. *All-optical flip-flop based on a single SOA-MZI*. IEEE Photonics Technology Letters, 17(4):843–845, 2005.
- [44] R. Clavero, F. Ramos, and J. Marti. *Bistability analysis for optical flip-flops based on a SOA-MZI with feedback*. Journal of Lightwave Technology, 25(11):3641–3648, 2007.
- [45] H. Kawaguchi and I. S. Hidayat. *Gigahertz all-optical flip-flop operation of polarization-bistable vertical-cavity surface-emitting lasers*. Electronics Letters, 31(14):1150–1151, 1995.
- [46] H. Kawaguchi, T. Mori, Y. Sato, and Y. Yamayoshi. *Optical buffer memory using polarization-bistable vertical-cavity surface-emitting lasers*. Japanese Journal of Applied Physics Part 2-Letters & Express Letters, 45(33-36):L894–L897, 2006.

- [47] T. Mori, Y. Yamayoshi, and H. Kawaguchi. *Low-switching-energy and high-repetition-frequency all-optical flip-flop operations of a polarization bistable vertical-cavity surface-emitting laser*. Applied Physics Letters, 88(10):3, 2006.
- [48] T. Katayama, Y. Sato, T. Mori, and H. Kawaguchi. *Polarization bistable characteristics of 1.55  $\mu\text{m}$  vertical-cavity surface-emitting lasers*. Japanese Journal of Applied Physics Part 2-Letters & Express Letters, 46(45-49):L1231–L1233, 2007.
- [49] H. J. S. Dorren, D. Lenstra, Y. Liu, M. T. Hill, and G. D. Khoe. *Nonlinear polarization rotation in semiconductor optical amplifiers: Theory and application to all-optical flip-flop memories*. IEEE Journal of Quantum Electronics, 39(1):141–148, 2003.
- [50] Y. Liu, M. T. Hill, N. Calabretta, H. de Waardt, G. D. Khoe, and H. J. S. Dorren. *Three-state all-optical memory based on coupled ring lasers*. IEEE Photonics Technology Letters, 15(10):1461–1463, 2003.
- [51] S. X. Zhang, D. Owens, Y. Liu, M. Hill, D. Lenstra, A. Tzanakaki, G. D. Khoe, and H. J. S. Dorren. *Multistate optical memory based on serially interconnected lasers*. IEEE Photonics Technology Letters, 17(9):1962–1964, 2005.
- [52] S. Zhang, D. Lenstra, Y. Liu, H. Ju, Z. Li, G. D. Khoe, and H. J. S. Dorren. *Multi-state optical flip-flop memory based on ring lasers coupled through the same gain medium*. Optics Communications, 270(1):85–95, 2007.
- [53] S. Zhang, D. Lenstra, Y. Liu, H. Ju, Z. Li, G. D. Khoe, and H. J. S. Dorren. *Multi-state optical flip-flop memory based on ring lasers coupled through the same gain medium*. Optics Communications, 270(1):85–95, 2006.
- [54] Z. J. Huang, A. Gray, I. Khrushchev, and I. Bennion. *10-Gb/s transmission over 100 Mm of standard fiber using 2R regeneration in an optical loop mirror*. IEEE Photonics Technology Letters, 16(11):2526–2528, 2004.

# 2

## DFB laser all-optical flip-flop

Distributed feedback (DFB) laser diodes are the standard transmitters in most advanced optical communication systems. They have a number of advantages over other laser types such as their stable single-mode behaviour and low noise operation. In this chapter, it will be shown that besides their already widespread use as optical transmitters, DFB laser diodes can also be applied for advanced optical signal processing. It will be demonstrated that they present a hysteresis under the injection of external light and that this hysteresis can be used to obtain fast flip-flop operation with low pulse energies. The fact that the concept comprises a single active element fabricated with a mature technology, is an important asset compared with previously reported all-optical flip-flops.

This chapter will start with a concise introduction on semiconductor laser diodes. The properties of DFB laser diodes with respect to their structure, mode selectivity and carrier dynamics are discussed in more detail. The concept of the hysteresis and the flip-flop operation is first illustrated with simulations and the most important parameters are examined. Experimental results confirm this and it will be shown that fast and robust flip-flop operation is possible. In chapters 6 and 7, we describe how this component can be applied in more system-based approaches such as all-optical packet switching and regeneration.

## 2.1 Semiconductor DFB laser diodes

The concept of distributed feedback lasers was proposed in the early seventies [1, 2]. The first experimental demonstrations were performed using optically pumped devices [3, 4] and, later on, also with electrically pumped devices having a single [5] and double heterostructure [6]. These experiments were done at cryogenic temperatures (80 K) and it took till the mid-seventies for the first demonstrations of DFB laser diodes operating at room temperature [7, 8]. Since the 1990s, DFB laser diodes have become the main optical source in fiber-based telecommunication systems and their properties have been examined extensively during the past decades. Before explaining the concept of all-optical flip-flop operation in a DFB laser diode, we will give a concise introduction on the basic principles of laser operation and the feedback mechanism of a Bragg grating.

### 2.1.1 Introduction

Laser operation requires a material that provides optical gain in combination with feedback from a resonator. The feedback will assure that part of the optical field passing through a given point returns to the point repeatedly. If the delay is equal to an integral number of optical periods, the gain of the laser will add up the fields coherently and in phase through the process of stimulated emission. This will result in a phase condition that will only be fulfilled at specific frequencies. When the optical amplification is sufficiently high, the process of stimulated emission will become dominant and a sustained, self-consistent mode will exist at these frequencies. Through the mode selectivity of the resonator structure, light corresponding to the resonance frequencies will experience more amplification and coherent light emission will occur.

Different materials can provide the required optical gain [9], but we will restrict ourselves to semiconductor compounds in this work. Radiation in a semiconductor material occurs when an electron in the conduction band recombines with a hole in the valence band. The energy of the emitted photon corresponds to the energy of the band gap. Until recently, only materials with a direct band gap could be used for this conversion of electrons to photons. These direct band gap materials are typically III-V semiconductor compounds (such as AlGaAs, InGaAs and InGaAsP). These first semiconductor lasers were demonstrated almost simultaneously by four different groups in 1962 [10–13]. Very recently, also lasing operation in germanium (group IV) was demonstrated [14] which creates new possibilities for integrated photonics but will not be discussed further in this work. The possibility of using an electrical pump (opposed to an optical pump) is the main advantage of semiconductor lasers. Because of their efficient operation, it is possible to fabricate semiconductor

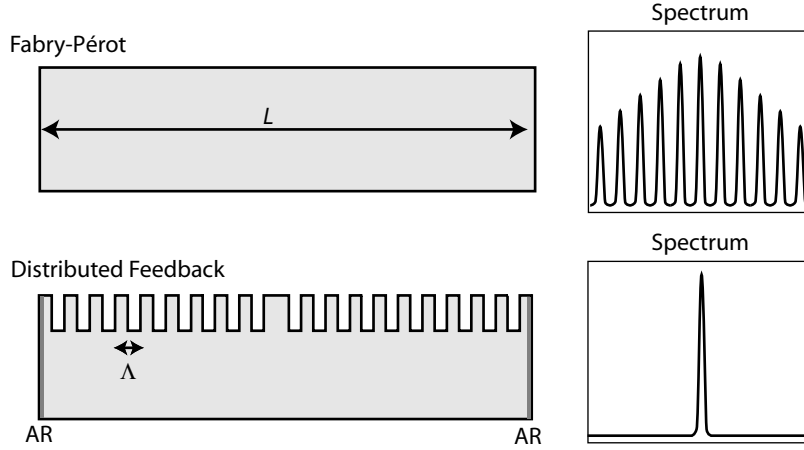


**Figure 2.1:** Schematic representation of a Fabry-Pérot laser cavity and a distributed feedback laser cavity with their respective lasing spectra.

lasers with very small dimensions which allow fast switching and modulation of the optical power. Moreover, the bandgap energy can be continuously varied over a substantial range in ternary and quaternary semiconductor compounds, which facilitates to vary the operating wavelength and thereby to cover most of the visible, near-infrared and mid-infrared spectral areas.

The resonator structure defines the longitudinal modes in which lasing can occur through the phase resonance condition. The most straightforward structure of a laser cavity is given by reflections on the end facets and is referred to as the Fabry-Pérot laser (see Figure 2.1). In this case, the light should fulfill the phase resonance condition requiring that the total phase shift of a complete round trip is a multiple of  $2\pi$ . This condition can be expressed in terms of the wavelength as:

$$\frac{\lambda_m}{n_e} = \frac{2L}{m} \quad (m = 1, 2, \dots) \quad (2.1)$$

with  $L$  the length of the cavity and  $n_e$  the effective refractive index. As can be seen from the above equation, this results in equally spaced cavity modes  $m$  in the frequency domain. The mode spacing is, however, very small ( $\Delta\lambda=0.3$  nm for  $L=400$   $\mu\text{m}$ ). The spectral width of the gain material will therefore extend over multiple longitudinal modes which results in a lasing spectrum with different peaks. The existence of multiple longitudinal modes will limit the use of Fabry-Pérot lasers for telecommunication applications because of chromatic dispersion effects in optical fibers.

Distributed feedback lasers differ from Fabry-Pérot laser diodes in the design of their cavity structure. Instead of using reflections at the end facets,

the feedback is distributed along the cavity by diffraction on a Bragg grating (see Figure 2.1). This is realized by a periodic variation of the thickness of the cladding layers introducing a periodic sequence of layers with a high and low effective index. Subsequent reflections on these layers will generate a coupling between forward and backward propagating waves in a similar way as reflection on the end facets in a Fabry-Pérot structure. The main difference is the strong wavelength selectivity in the coupling which will enable single mode operation. This type of resonance can be described in a similar way as a periodic sequence of multilayer dielectric mirrors and constructive reflection can be expected at

$$\frac{\lambda_m}{n_e} = \frac{2\Lambda}{m} \quad (m = 1, 2, \dots) \quad (2.2)$$

for a given pitch  $\Lambda$ . The above condition ensures that reflections from different unit cells of the periodic perturbation add up in phase and is referred to as the *Bragg condition*. Typically, DFB laser diodes have a length of  $400 \mu\text{m}$  and to operate at the telecommunication wavelength of  $\lambda=1550 \text{ nm}$  their pitch is  $\Lambda=230 \text{ nm}$ . The above Bragg condition is similar to the phase condition of Fabry-Pérot structures (Equation 2.1), but the mode spacing is much wider. Indeed, the difference between two adjacent Bragg windows can be estimated as  $\Delta\lambda=0.75 \mu\text{m}$ . Because the gain material in semiconductors has a spectral range of about  $30 \text{ nm}$ , the grating will force the laser diode to operate unimodal. Therefore, we will omit the higher order Bragg modes in our further description.

The Bragg condition is often represented by the minimization of the Bragg deviation:

$$\Delta\beta = \frac{2\pi n_e}{\lambda} - \frac{\pi}{\Lambda}. \quad (2.3)$$

The strong interaction between forward and backward propagating waves in the vicinity of  $\Delta\beta=0$  will ensure the single mode operation of the laser diode. Changes in the pitch of the periodic variation  $\Lambda$  or the effective index  $n_e$  will directly influence the laser wavelength. This enables a tight wavelength control (e.g. by thermal tuning) but the fabrication of the small pitch also causes technological difficulties.

### 2.1.2 Rate equations

Lasing in a semiconductor material is described in its simplest form by the rate equations. They mathematically represent the interaction between the carrier density  $N$  and the number of photons  $S_m$  in mode  $m$  within the active layer [15]. The first equation describes the evolution of the carrier density  $N$ :

$$\frac{dN}{dt} = \frac{I}{qV_{\text{act}}} - AN - BN^2 - CN^3 - \sum_m \frac{G(N, \lambda_m)S_m}{V_{\text{act}}} \quad (2.4)$$

The first term represents the injection of carriers (with charge  $q$ ) originating from the electrical current  $I$  in the active volume  $V_{\text{act}}$ . The summation corresponds to the stimulated emission in the different cavity modes  $m$ . Spontaneous carrier recombination is represented by the other terms. Recombination via traps (Shockley-Read-Hall) and surfaces involves only one carrier and is therefore represented by  $AN$ . The bimolecular recombination is a process in which an electron and hole are involved and is therefore given by the quadratic term  $BN^2$ . The recombination process where the energy released by electron-hole recombination is transferred to another electron, is referred to as Auger recombination and represented by  $CN^3$ . In some cases, a simpler form of the above equation is used by linearizing the recombination terms in one single term as  $N/\tau_c$  with  $\tau_c$  the carrier lifetime:

$$\frac{dN}{dt} = \frac{I}{qV_{\text{act}}} - \frac{N}{\tau_c} - \sum_m \frac{G(N, \lambda_m)S_m}{V_{\text{act}}} \quad (2.5)$$

The second equation describes the evolution of the number of photons within the active layer of the cavity for the different modes. The relevant processes that are involved are stimulated and spontaneous emission (through which photons are created) and absorption and mirror losses.

$$\frac{dS_m}{dt} = \left( G(N, \lambda_m) - \frac{1}{\tau_p} \right) S_m + R_{\text{sp}} \quad (2.6)$$

The first term (with  $G(N, \lambda_m)$ ) corresponds to the stimulated emission rate which is proportional to the average number of photons. The last term (with  $R_{\text{sp}}$ ) accounts for the spontaneous emission of photons and is sometimes also described as a fraction of the bimolecular recombination  $BN^2$ . The losses inside the cavity are accounted for by the photon lifetime  $\tau_p$  and can be decomposed in two components:

$$\frac{1}{\tau_p} = \nu_g (\alpha_{\text{int}} + \alpha_{\text{fac}}) \quad (2.7)$$

with  $\nu_g$  the group velocity,  $\alpha_{\text{int}}$  the internal cavity losses and  $\alpha_{\text{fac}}$  representing the photons that leave the cavity at the end facets.

The gain  $G$  appearing in the above equations is proportional to the material gain  $g$ :

$$G(N, \lambda_m) = \Gamma g(N, \lambda_m) \nu_g \quad (2.8)$$

with  $\Gamma$  the mode confinement factor which describes how much of the mode is confined in the active region. Both experimental and theoretical studies indicate that the gain  $g$  in a bulk material can be described linearly as:

$$g = g_0(N - N_0) \quad (2.9)$$

where  $g_0 = dg/dN$  is the differential gain (typically  $\sim 10^{-16} \text{ cm}^2$ ) and  $N_0$  is the carrier density at transparency. For quantum wells, the gain will have a sublinear expression.

It is convenient to express the electric field  $E_m$  of mode  $m$  in terms of the number of photons  $S_m$  and the phase  $\phi_m$  [15]:

$$E_m(t) = \sqrt{S_m} \exp(j\phi_m t) \quad (2.10)$$

### 2.1.3 Coupled mode theory for DFB lasers

The above rate equations give insight in the intricate lasing process but they do not allow to describe the influence of the Bragg grating on the coupling between forward and backward propagating waves. Therefore, we will introduce the coupled mode theory for DFB lasers. It will be shown that a  $\lambda/4$ -shift needs to be introduced in the middle of the grating to fulfill the phase resonance condition in order to obtain single mode operation. The derivation can be found in a more elaborate form in standard literature on DFB lasers [15–17].

The field inside the laser diode can be written as the sum of a forward  $F(z)$  and backward  $B(z)$  propagating wave:

$$E(z) = F(z) \exp(j\beta z) + B(z) \exp(-j\beta z) \quad (2.11)$$

with  $\beta$  the wave propagation constant.

The grating will introduce a coupling between the forward and backward propagating waves. The reflected waves will add up constructively with each other at the Bragg wavelength. Typically, the coupling is described by the coupling coefficient  $\kappa$  which is proportional to the variation of the effective index  $\Delta n$ . The spatial evolution of the forward and backward propagating waves can be described with coupled mode equations as [15–17]:

$$\frac{dF(z)}{dz} = (\gamma - j\Delta\beta)F(z) - j\kappa B(z) \quad (2.12)$$

$$\frac{dB(z)}{dz} = -(\gamma - j\Delta\beta)B(z) - j\kappa F(z) \quad (2.13)$$

with  $\gamma$  the gain for the field in a DFB laser with non-reflecting facets (corresponding to  $(\Gamma g - \alpha_{\text{int}})/2$  and  $\Delta\beta$  the Bragg deviation as defined in Equation 2.3.

These equations constitute a set of two coupled, linear, first-order, ordinary differential equations for the functions  $F(z)$  and  $B(z)$ . They can be solved if we know  $F$  and  $B$  at a given point, for example  $z = z_0$ . The general solution can be written as:

$$F(z) = \left( \cosh(Sz) + \frac{\gamma - j\Delta\beta}{S} \sinh(Sz) \right) F(z_0) - \frac{j\kappa}{S} \sinh(Sz) B(z_0) \quad (2.14)$$

$$B(z) = \frac{j\kappa}{S} \sinh(Sz) F(z_0) + \left( \cosh(Sz) - \frac{\gamma - j\Delta\beta}{S} \sinh(Sz) \right) B(z_0) \quad (2.15)$$

with  $S$  given by:

$$S^2 = |\kappa|^2 + (\gamma - j\Delta\beta)^2. \quad (2.16)$$

Hence, the above equations can be developed as a transfer matrix function  $\mathbf{T}$ :

$$\begin{pmatrix} F(z) \\ B(z) \end{pmatrix} = \begin{pmatrix} T_{11}(z - z_0) & T_{12}(z - z_0) \\ T_{21}(z - z_0) & T_{22}(z - z_0) \end{pmatrix} \begin{pmatrix} F(z_0) \\ B(z_0) \end{pmatrix}. \quad (2.17)$$

In order to find the solution of these equations, we need to apply the right boundary conditions. We will start by using the standard DFB laser structure with both facets carrying AR coatings. When setting  $z = L$  and  $z_0 = 0$ , we can then find the resonance condition by setting  $T_{22}(L) = 0$  as boundary condition:

$$SL \coth(SL) - (\gamma L - j\Delta\beta L) = 0 \quad (2.18)$$

The solutions for this equation in the  $\gamma L$  versus  $\Delta\beta L$  plane are depicted in Figure 2.2 for different values of the normalized coupling constant  $\kappa L$ . We can observe that, for this structure, there is no mode at the Bragg wavelength  $\Delta\beta L = 0$ . There is a stop band between the two first order modes situated symmetrically around the Bragg wavelength with a width that increases with increasing values of  $\kappa L$ . Because the two first order modes have exactly the same gain, the laser will show multimode operation at their threshold. The degeneracy can be explained by looking at the sum of the distributed reflections at  $z_1$  and  $z_2$  in Figure 2.3. The phase shift for propagating along half a period  $\Lambda/2$  is  $\pi/2$  and the subsequent interface reflections alternate between 0 and  $\pi$ . Therefore, the fields of the distributed reflections will add up constructively at  $z_1$  and  $z_2$ . When there is no  $\lambda/4$ -shift in the middle of the grating, the bidirectional propagation across  $[z_1, z_2]$  would add an additional phase shift of  $\pi$  which would make the total round-trip time in the cavity  $(2p + 1)\pi$  with  $p$  integer. Therefore, no mode will occur at the Bragg wavelength because the round-trip phase is not a multiple of  $2\pi$ .

This problem can be solved by introducing a  $\lambda/4$ -shift in the middle of the grating [18, 19] as illustrated in Figure 2.3. This will add an additional phase shift of  $\pi$  to the round-trip phase which will lift the mode degeneracy. This can be described mathematically by adjusting the matrix transfer function into  $\mathbf{T}(L/2)\mathbf{T}(\Lambda/2)\mathbf{T}(L/2)$ . After carrying out the matrix multiplications, the oscillation condition is found by:

$$SL \coth\left(\frac{SL}{2}\right) - (\gamma L - j\Delta\beta L \pm \kappa L) = 0 \quad (2.19)$$

The solutions for these equations in the  $\gamma L$  versus  $\Delta\beta L$  plane are depicted in Figure 2.4 for different values of the normalized coupling constant  $\kappa L$ . The structure with a  $\lambda/4$ -shift has a single lowest order mode at the Bragg wavelength ( $\Delta\beta L = 0$ ). Moreover, this mode has a lower loss than the other modes

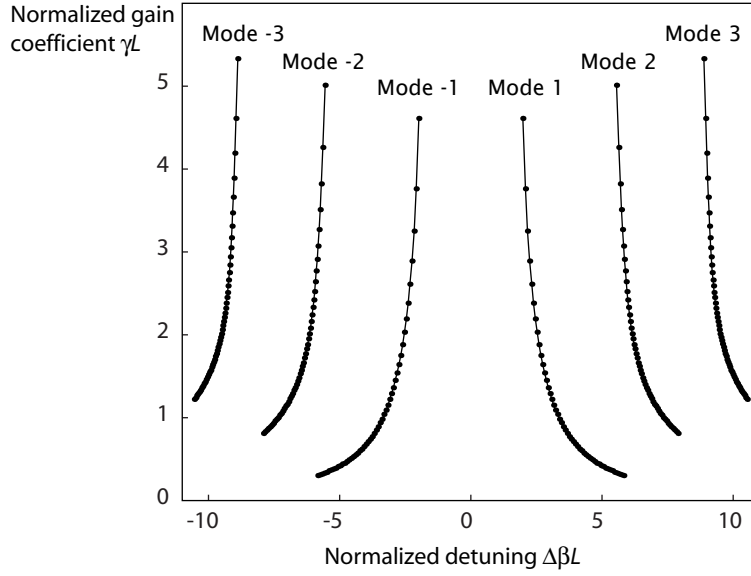


**Figure 2.2:** The solutions of the coupled mode equations for a grating without  $\lambda/4$ -shift have a stop band around  $\Delta\beta = 0$ . The values of the normalized coupling constant  $\kappa L$  range from 0.1 to 5 in steps of 0.1.

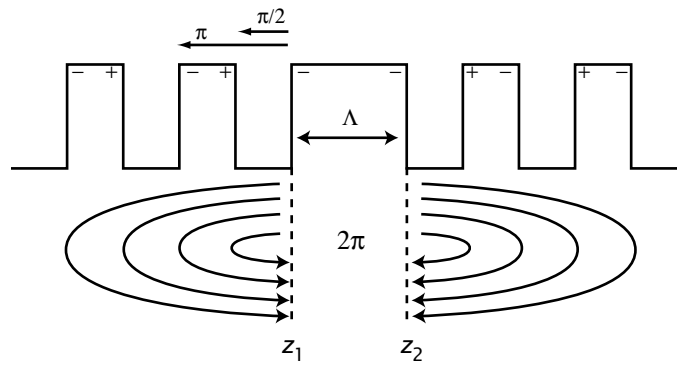


**Figure 2.3:** Physical explanation of the insertion of a  $\lambda/4$ -shift in the middle of the grating [15].

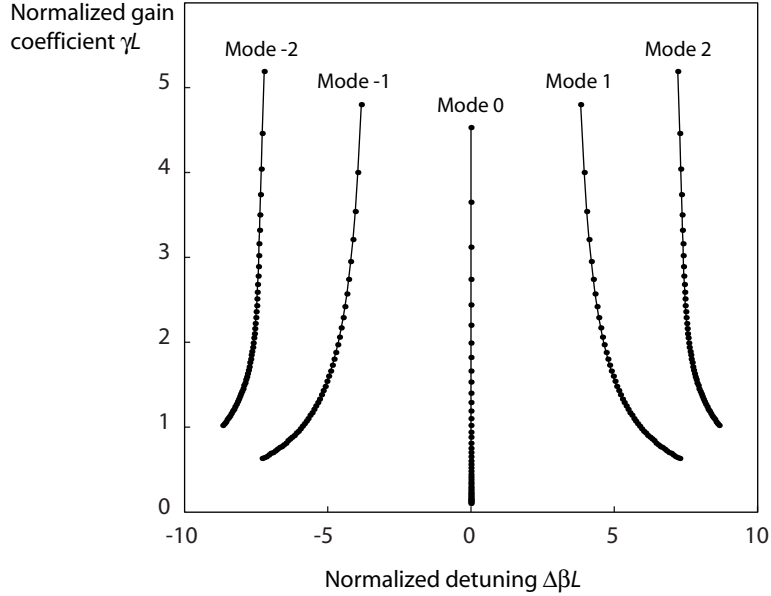


**Figure 2.4:** The insertion of a  $\lambda/4$ -shift results in single mode operation at  $\Delta\beta = 0$ . The values of the normalized coupling constant  $\kappa L$  range from 0.1 to 5 in steps of 0.1.

which means that it will dominate. We can conclude from this analysis that  $\lambda/4$ -shifted DFB lasers with anti-reflection coated facets will exhibit single mode lasing operation at the Bragg wavelength and are therefore the preferred lasers in WDM telecommunication systems.

## 2.2 Concept of the all-optical flip-flop

In this section, we will demonstrate that a longitudinal variation in the carrier density can be established by injecting external light in the laser. It will be shown that these variations affect the index of refraction and therefore the feedback properties of the grating, ultimately resulting in bistable behaviour. Finally, the bistability can be utilized to establish all-optical flip-flop operation by injecting pulses alternately on both sides of the device.

### Longitudinal spatial hole burning

When we introduced the rate equations in section 2.1.2, a uniform distribution of the carriers along the laser cavity was assumed. Here, we will study the effect

of variations in carrier distribution. Such variations on the carrier density are referred to in literature as longitudinal spatial hole burning [20]. A  $\lambda/4$ -shifted DFB laser diode above threshold will have small variations in carrier density, even when it is operating under steady state conditions. These small variations originate from the non-uniform optical power distribution inside the laser cavity. The place along the laser where the spatial hole burning occurs is different depending on the strength of the coupling from the grating [15]. One can distinguish between undercoupled ( $\kappa L < 1$ ) and overcoupled lasers ( $\kappa L > 1$ ). In undercoupled lasers, the holes tend to appear on the edges of the laser while for overcoupled lasers the holes are in the middle of the grating. These variations in the static behaviour of single laser diodes can be considered very small and do not have a large influence on the laser operation. In fact, these small differences will be omitted in our further analysis and we will consider the distribution of the carriers in a single laser diode as (quasi) uniform.

When external light at a wavelength outside the stop-band of the DFB grating is injected in the DFB laser, this light will not experience any feedback while travelling through the laser section. Instead, it will experience an amplification which results in a power increase throughout the cavity. This longitudinal variation in photon density will have a profound effect on the carrier density distribution. Indeed, we can recall the strong interaction between photon and carrier density from the rate equations (Equation 2.4). With an additional term for the externally injected light, we find that under steady state conditions ( $dN/dt=0$ ):

$$\frac{I}{qV_{\text{act}}} - \frac{N(z)}{\tau_c} - \frac{G(N(z), \lambda_{\text{las}})S_{\text{las}}}{V_{\text{act}}} - \frac{G(N(z), \lambda_{\text{inj}})S_{\text{inj}}(z)}{V_{\text{act}}} = 0 \quad (2.20)$$

The gain can be approximated to be linearly dependent on the carrier density for bulk materials. We can then see from the above equation that when the photon density of the injected light  $S_{\text{inj}}(z)$  is sufficiently high, it will cause a strong non-uniformity in the carrier density distribution  $N(z)$ . In Figure 2.5, a simulation result for the longitudinal carrier density with and without injected light is depicted. As described previously, the small bump in the distribution without the injected light originates from the previously mentioned spatial hole burning in the middle of an overcoupled laser. The simulation method and results will be further discussed in section 2.3.

Variations in the carrier density are known to influence the index of refraction of the material [21, 22]. This is caused by the free carrier plasma effect in combination with changes in the spectral shape of the band-gap. Measurements of the change in refractive index due to carrier fluctuations indicate that  $dn/dN = -1.8 \cdot 10^{-20} \text{ cm}^3$ .

The longitudinal variation in the index of refraction will consequently lead to a distortion of the Bragg grating. The  $z$ -dependence of the refractive index

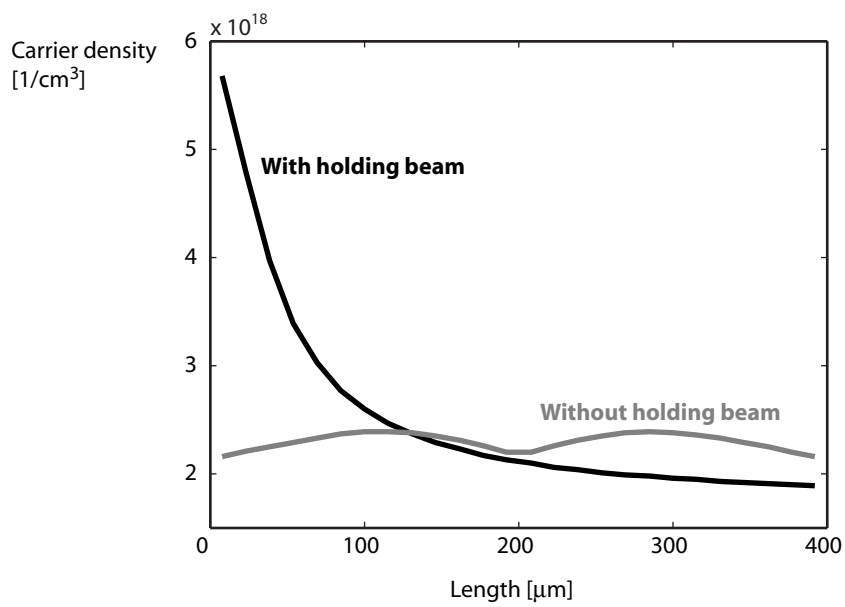


**Figure 2.5:** The distribution of carriers along the laser section with and without external light injection for a DFB laser with  $\kappa L=1.2$  and length  $L=400 \mu\text{m}$ . The holding beam is injected from the left side of the laser.

will result in deviations from the Bragg condition:

$$\Delta\beta(z) = \frac{2\pi n_e(N(z))}{\lambda} - \frac{\pi}{\Lambda}. \quad (2.21)$$

Therefore, when the injected light is sufficiently strong, the feedback from the grating at the Bragg wavelength will not be adequate anymore to support lasing operation. The losses in the laser cavity will increase and lasing will be suppressed.

### **Bistability**

An optical bistability refers to a situation where two different output states are associated with the same input depending on the history of the device [23]. The longitudinal spatial hole burning by injection of external light (as described above) can result in an optical bistability. Indeed, we can distinguish two different states that can both exist under the same level of optical input power:

#### **State 1: laser ON**

In the first state, the laser is lasing which means that the gain is clamped and, therefore, relatively small. Because the wavelength of the injected light is outside the stop-band of the DFB grating, it will pass through the laser without experiencing any feedback. Essentially, the laser will act as an amplifier on the injected light. However, because the gain is clamped, the amplification is very small and its impact on the lasing operation will not be significant. Because the power of the injected light will be quasi uniform throughout the laser cavity, the corresponding Bragg deviations are neglectable.

#### **State 2: laser OFF**

In the second state, the laser is switched off and the injected light experiences a large amplification throughout the laser cavity. As described previously, this power increase through the laser cavity will influence the uniformity of the carrier density and, therefore, introduces changes in the refractive index. The Bragg grating is distorted and the losses at the Bragg wavelength increase significantly. The threshold for lasing will rise and the laser will remain switched off.

Because the two states are self-sustainable, an optical bistability can appear when varying the injected optical power. In Figure 2.6, a simulation result for the bistability in a DFB laser is depicted as a function of the injected optical power. In the simulation, a DFB laser with anti-reflection coated facets and a  $\lambda/4$ -shift in the middle is used having a length of  $L=400 \mu\text{m}$ , normalized coupling constant  $\kappa L=1.2$  and current injection of  $4I_{\text{th}}$ .

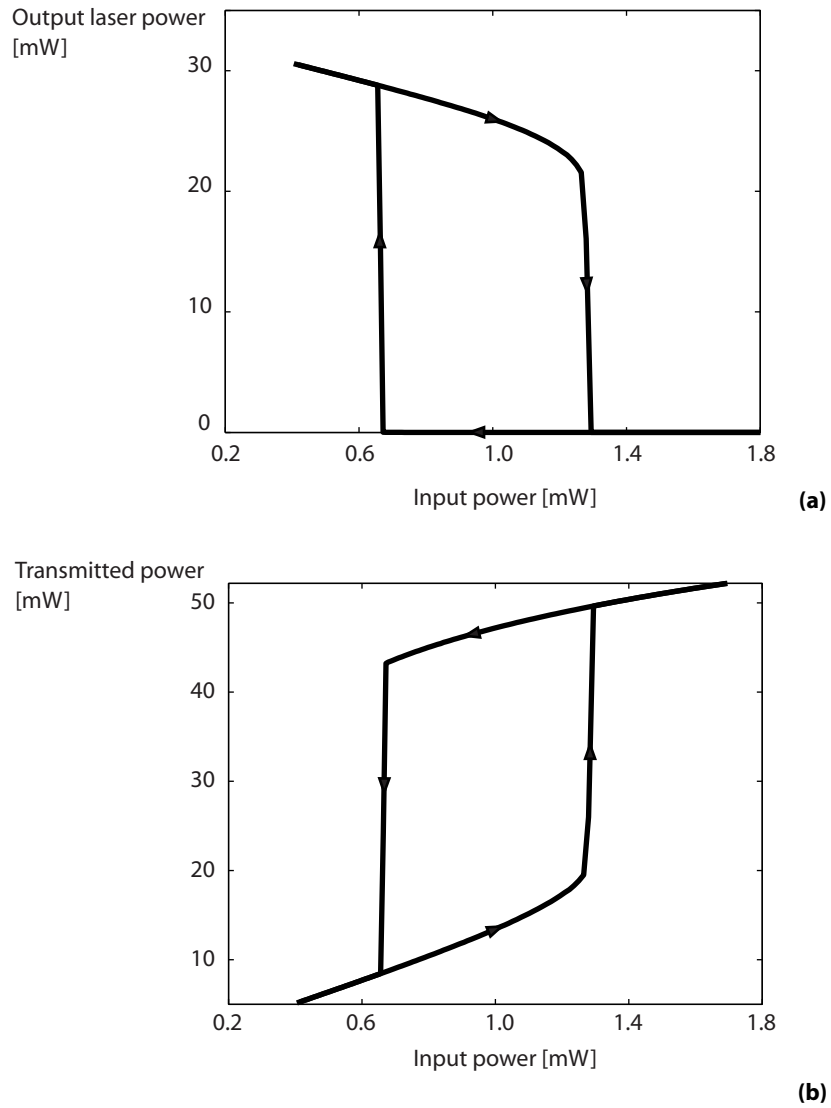


**Figure 2.6:** The bistability in the laser output power (up) and the transmitted power of the holding beam (down) for a DFB laser with length  $L=400 \mu\text{m}$ , normalized coupling constant  $\kappa L=1.2$  and current injection of  $4I_{\text{th}}$ .



**Figure 2.7:** Schematic representation of the flip-flop operation in a single DFB laser.

### Flip-flop operation

The bistability can be used for flip-flop operation by injecting light pulses alternately on both sides of the laser. The principle is depicted in Figure 2.7. We start by injecting a holding beam with a power corresponding (approximately) to the middle of the hysteresis in order to work in the bistable domain. When a pulse is injected at the same side as the holding beam, it will introduce a non-uniform distribution of the carriers which will cause the laser to switch off. When the pulse is gone, the amplification of the holding beam throughout the cavity will ensure the non-uniformity of the carriers leaving the laser switched off. To switch the laser on, a pulse from the other side is injected. This will restore the uniformity of the carrier distribution and restarts laser operation. The switching of the flip-flop can be very fast because it relies on relatively small differences in carriers.

## 2.3 Simulations

### Transmission-line laser model

To simulate the bistability and flip-flop operation in DFB lasers, we make use of the transmission-line laser model (TLLM) [24, 25] implemented in the commercial software package VPI Componentmaker<sup>TM</sup> [26]. This model allows to simulate efficiently the spatial hole burning effects that arise when injecting light in the DFB laser. A complete analysis on the validation of the model compared to other simulation techniques can be found in [27].

A common approach to simulate laser diodes, is to solve a set of rate equations for the photon and carrier density. However, such calculations do not take the longitudinal inhomogeneities of the carrier and photon distribution into account. Transmission-line laser modeling will divide a laser section into different longitudinal segments and solve the rate equations in the time-domain for every segment (see Figure 2.8a-b). In each segment, all the parameters are as-

sumed to be constant, but overall it will enable the study of the longitudinal variation of parameters throughout the laser section. It also allows to work over a continuous range of wavelengths which is a necessity in our calculations because the injected light has a different wavelength than the lasing frequency.

In the transmission-line laser model, each segment contains a scattering node that calculates the gain (stimulated emission), loss (scattering, absorption) and noise (spontaneous emission) experienced by the light during propagation through the segment. These nodes are connected by transmission-lines which represent the waveguide delay during one time step. The scattering will generate reflected forward and backward waves from the incident forward and backward waves. The connections propagate these reflected fields to the adjacent nodes where they become incident waves again on the next time step. The output constitutes therefore of a stream of optical field samples separated by the model time step. Taking a Fourier transform generates the optical spectrum.

To include the feedback originating from the grating in a DFB laser, the TLLM is modified by adding impedance mismatches along the model. Alternate low and high impedance transmission-line sections will resemble the structure of the DFB grating by introducing the required coupling between the forward and backward waves for distributed feedback (see Figure 2.8c). It is also possible to add phase-shifts on one or more sections facilitating the inclusion of the  $\lambda/4$ -shift in the middle of the DFB laser. Studies have shown that a relatively small number of these cross-coupling points can mimic the behaviour of the thousands of periods in a real DFB laser [25].

Using this simulation model, we can study the influence of structural parameters on the static and dynamic behaviour of the DFB all-optical flip-flop. A complete set of parameters is given in [28].

The hysteresis characteristic is simulated by injecting a continuous wave holding beam with a wavelength outside the stop-band of the DFB grating. A sweep of the input power of the holding beam is done by means of a variable attenuator. An optical band-pass filter will separate the laser light from the injected light. The input power values are depicted versus the laser output power (or transmitted power) values and the simulation is done subsequently with increasing and decreasing power levels. For each simulation the stopband frequency was adjusted to operate exactly at a wavelength of  $1.57 \mu\text{m}$  (arbitrarily chosen). The injected light is at a wavelength of  $1.56 \mu\text{m}$  unless stated otherwise. We use  $\lambda/4$ -shifted lasers with AR-coatings to enforce single-mode operation of the laser and increase the spatial hole burning effects.

With dynamic simulations, we can also study the influence of the structural parameters on the switching times of the flip-flop operation. We do this by adding light pulses on both sides of the input of the laser model. This has been done extensively in [28]. In general, the structural differences have very little ef-

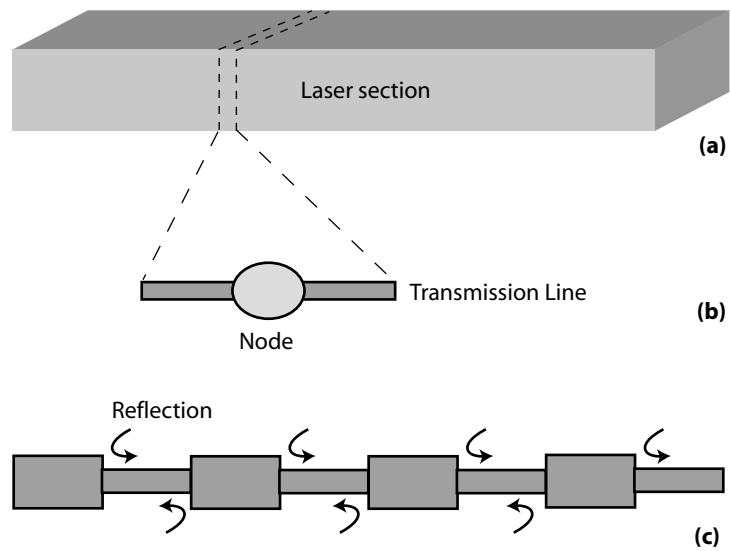


**Figure 2.8:** (a) The transmission-line laser modes divides the laser section into multiple segments. (b) Each segment contains a node where the rate equations are calculated and the fields are transferred to the next node by transmission-lines. (c) To include the feedback from the Bragg grating subsequent high and low impedance lines are placed along the laser section.

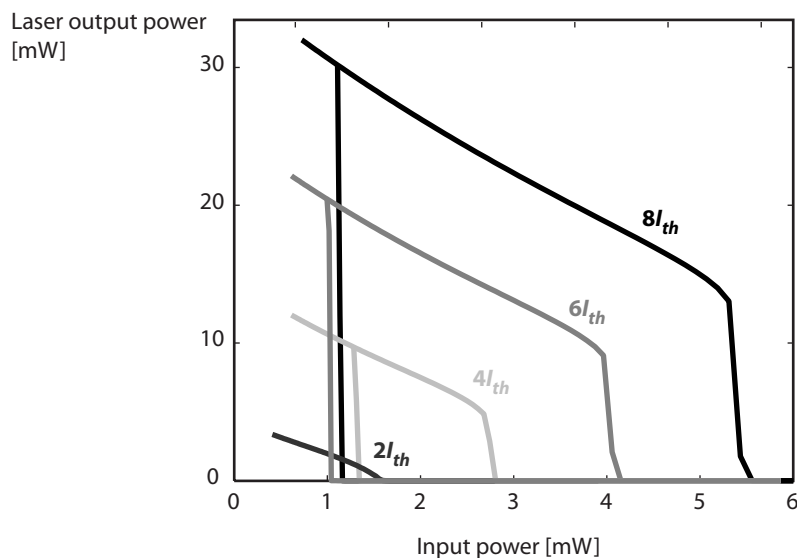


**Figure 2.9:** The influence of the injected current on the bistable characteristic for a DFB laser with length  $L = 600 \mu\text{m}$ ,  $\kappa L = 1.8$  and  $I_{th} = 26.5 \text{ mA}$ .

fect on the dynamic operation and the differences in switching time were mostly within an error margin of 5 ps. The most influential parameter for the switching speed is the normalized coupling coefficient  $\kappa L$  as it has also the largest influence on the static hysteresis properties (see below).

### Influence of current

First, we look at the influence of the bias current on the properties of the hysteresis. An increase in current will not only result in higher output powers, but will also widen the hysteresis (see Figure 2.9). The main reason is that for lower injection currents, the laser will switch off sooner due to the overall carrier depletion by the injected field. As explained later, we observed in experiments also an overall shift towards higher optical input powers.

### Influence of injected wavelength

As mentioned previously, the wavelength of the injected light should be outside the stop-band of the DFB grating. The influence of the wavelength of the injected light on the bistability characteristic is depicted in Figure 2.10. One can see that for wavelengths that differ 2.5 nm from the lasing wavelength, the

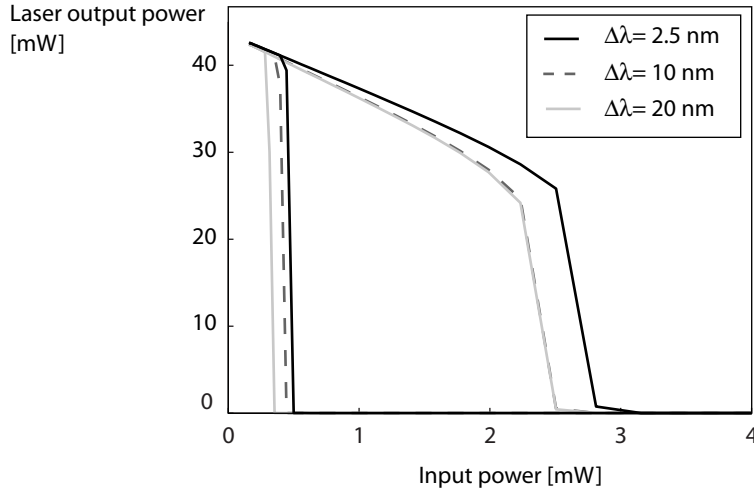


**Figure 2.10:** The influence of the wavelength of the injected light for a DFB laser with length  $L = 400 \mu\text{m}$ ,  $\kappa L = 1.2$  and  $I_{\text{bias}} = 4I_{\text{th}}$ .

same hysteresis characteristic can be obtained throughout the gain spectrum of the laser diode. At closer wavelengths, the injected light will excite higher order modes in the laser by injection-locking. This often results in time-dependent behaviour which does not allow to calculate a static hysteresis curve. The large spectral range over which the hysteresis effect in the DFB laser diode can be demonstrated, allows for broadband operation and is one of the main advantages of this technique.

### Influence of coupling coefficient

As can be seen from Figure 2.11, the hysteresis will narrow and shift to lower input powers for decreasing values of the normalized coupling coefficient  $\kappa L$ . The devices have a current  $I_{\text{bias}} = 4I_{\text{th}}$  and equal lengths ( $L = 400 \mu\text{m}$ ). In general, devices with a lower coupling coefficient will have a higher threshold gain because they generate less feedback. Therefore, the injected light will experience a stronger amplification when the coupling coefficient is low. Hence, the laser will switch off at lower injected powers.

### Validity of $\kappa L$ for classification

Hysteresis curves are plotted for a fixed value of the normalized coupling coefficient ( $\kappa L = 1.2$ ) but with different combinations of length and coupling coeffi-

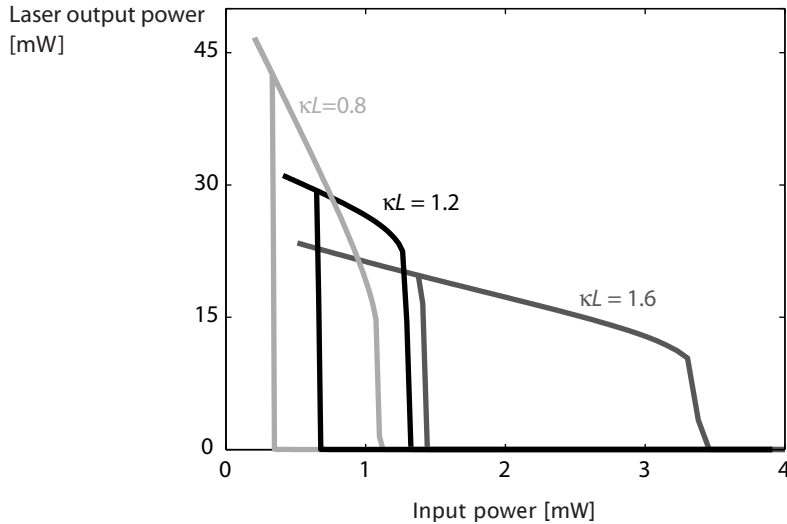


**Figure 2.11:** The influence of the coupling coefficient on the bistable characteristic for a DFB laser with length  $L = 400 \mu\text{m}$  and  $I_{\text{bias}} = 4I_{\text{th}}$ .

cient (see Figure 2.12). The losses are neglected and the bias current is chosen such that the output powers are equal with no light injected. We can see that the variations are small and can conclude that the normalized coupling coefficient is a good measure to characterize the hysteresis effect. However, for laser devices with a longer length, the injected light will experience the amplification over a longer distance which will make the longitudinal spatial hole burning effect more pronounced. Therefore, we can observe a small shift to lower input powers when using longer devices that have lower coupling coefficients. Because the variations are small, we consider the value of the normalized coupling coefficient  $\kappa L$  as an important parameter in the characterization of the hysteresis.

### Influence of carrier lifetime

In Figure 2.13, the influence of the carrier lifetime ( $\tau_c$ ) can be observed. One can clearly observe that the threshold of the bistability shifts towards higher input power levels (resulting in a smaller bistable region) when the carrier lifetime decreases and even disappears completely when the carrier lifetime becomes too small. This is not surprising since a smaller carrier lifetime means that a certain power non-uniformity corresponds to a smaller carrier density

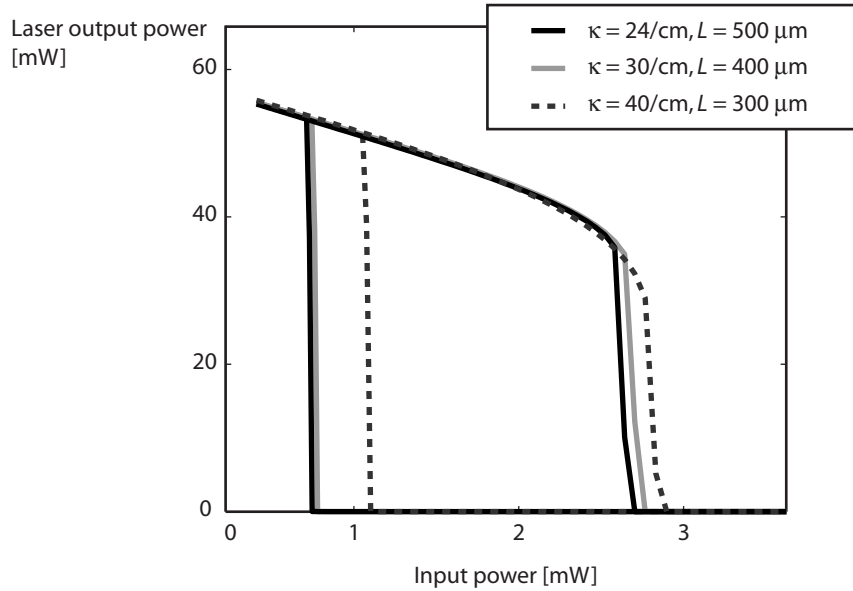


**Figure 2.12:** The bistable characteristics are very similar for fixed values of  $\kappa L$ .

non-uniformity. Therefore, the spatial hole burning will become much weaker. It should be noted, however, that the hysteresis can still be obtained for these smaller carrier lifetimes by increasing the bias current.

Because the influence of the series resistance of the laser diode is similar to that of the carrier lifetime, one can also conclude from this analysis that the series resistance of the laser diode should not be too small. However, this does not account for the thermal effects that can accompany larger values of the series resistance.

### Influence of anti-reflection coated facets

The quality of the anti-reflection coating of the facets has a definite influence on the hysteresis. This is illustrated in Figure 2.14. One can see that the hysteresis disappears for anti-reflection coatings larger than 1%. This can be explained by the backward reflection of the injected light which will destroy the spatial hole burning. Increasing the current can restore the hysteresis again.

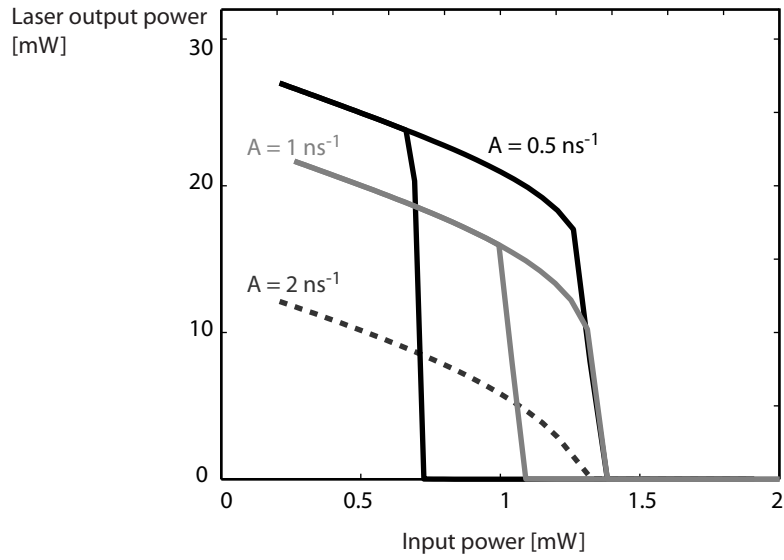


**Figure 2.13:** The influence of the carrier lifetime on the bistable characteristic for a DFB laser with length  $L = 400 \mu\text{m}$ ,  $\kappa L = 1.2$ .

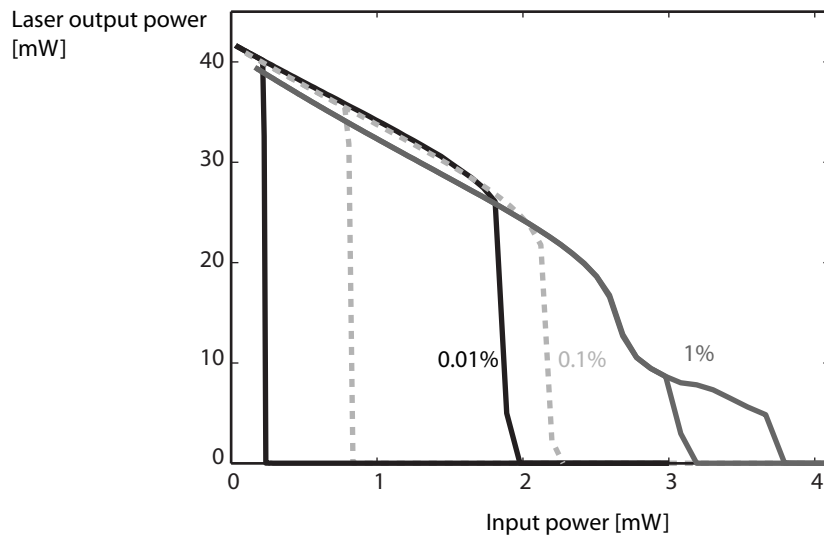


**Figure 2.14:** The influence of the quality of the anti-reflection coating for a DFB laser with length  $L = 400 \mu\text{m}$ ,  $\kappa L = 1.2$ .

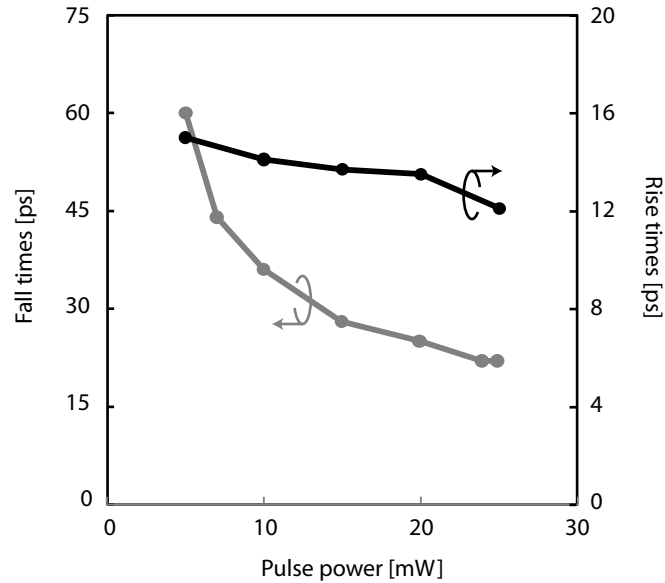


**Figure 2.15:** The simulated switching times for a DFB laser with length  $L = 400 \mu\text{m}$ ,  $\kappa L = 1.2$  and differential gain  $g_0 = 3 \cdot 10^{-16} \text{cm}^2$ . The rectangular pulses have durations of 200 ps for reset and 125 ps for set. (Courtesy of [28])

### Dynamic simulations

Using the same simulation tool, it is possible to study also the switching times of the flip-flop operation [28, 29]. Besides the holding beam, also pulses were injected at both sides of the laser diode. The pulse durations are 200 ps for reset and 125 ps for set. We found minimal switching times of 10-15 ps for the 10%-90% rise time and 20-30 ps for the fall time (see figure 2.15). In general, it was found that most laser parameters have little influence on the simulated switching speed. The normalized coupling coefficient  $\kappa L$  can be considered the most influential parameter [28].

## 2.4 Experimental results

The above concept of flip-flop operation in a DFB laser was demonstrated experimentally. We used a  $\lambda/4$ -shifted DFB laser diode provided by Alcatel-Thales III-V labs. The device has a length of  $400 \mu\text{m}$  and the corrugation has an estimated  $\kappa L$ -value of 1.6. The lasing wavelength is 1553 nm and the threshold current is 30 mA. The laser needs an accurate anti-reflection coating in order

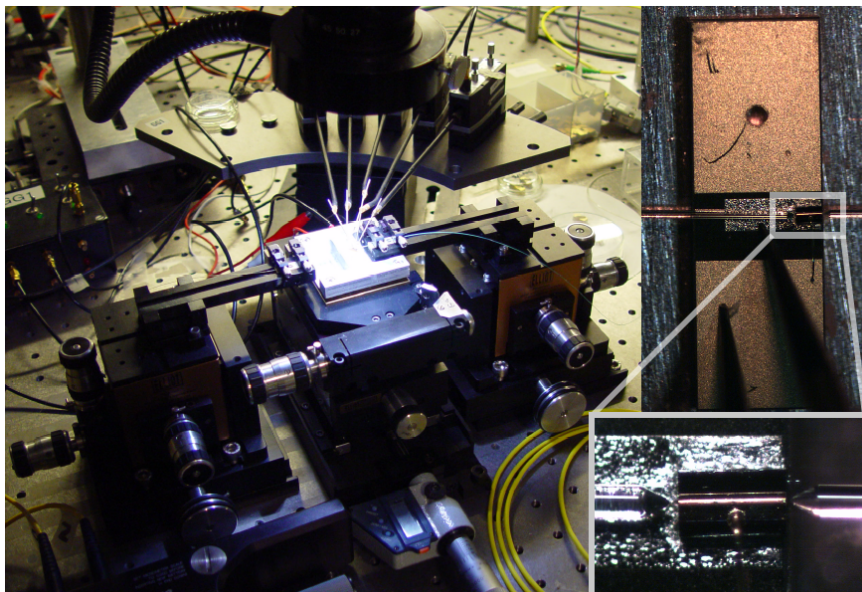


**Figure 2.16:** A photograph of the measurement stage (left) and the device under test (right).

to avoid that backward reflections destroy the spatial hole burning. Therefore, we use laser diodes with an anti-reflection coating of 0.01% at both facets. The device is unpackaged and we use lensed fibers to couple the light at the facets to our test equipment. The coupling with lensed fibers introduces additional losses which can differ in subsequent measurements as the alignment of the fibers is changed. Therefore, the values of the pulse energies and the power of the holding beam that are mentioned below, are the ones measured in-fiber and give an upper-limit of the actual value in the device. The losses of the fiber coupling can typically be estimated to be between 3 and 5 dB. Small distortions due to reflections at opposing fiber facets were also observed which was solved by tilting the device under a small angle.

A picture of the device under measurement conditions is given in Figure 2.16. We connect the electrical contacts of the laser diode by electrical probes through which we sent a current. The device is positioned on a stage which has a built-in Peltier element to control the temperature.

First, we measure the bistability in the DFB laser by injecting continuous wave light in the device. The set-up is depicted in Figure 2.17. The continuous wave light comes from a (tunable) laser diode and is amplified through an erbium-doped fiber amplifier (EDFA). We use a variable attenuator to adjust

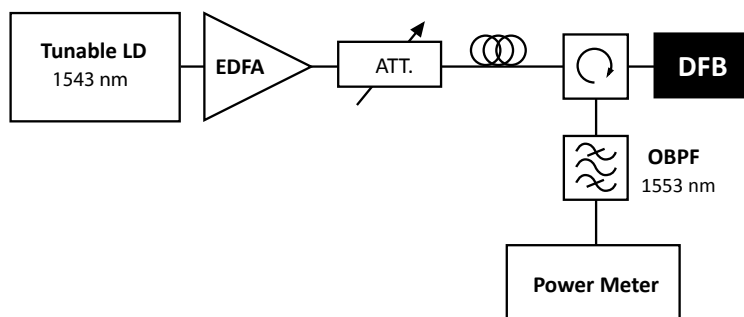


**Figure 2.17:** Schematic of the measurement set-up for the bistability.

the power of this holding beam. A circulator is used to separate the light of the DFB laser from the injected continuous wave. A tunable optical band-pass filter (OBPF) is set at the laser frequency with an optical bandwidth of 0.3 nm. This will filter out the light from the holding beam that is partially reflected on the facets of the lensed fibers. Instead of a filter, it is also possible to measure the power at the lasing frequency on a spectrum analyzer. To avoid unwanted reflections in our measurements, we make use of angled fiber facets (APC) to connect the optical fibers in the set-up. Polarization controlling wheels are used to adjust the polarization of the incoming light because the DFB laser was not designed to be polarization insensitive.

The measured bistabilities for different values of the current injection are depicted in Figure 2.18. The wavelength of the injected holding beam is arbitrarily chosen at 1543 nm. The bistability starts to appear at 120 mA which corresponds to 4 times the threshold current of the device. The widening of the hysteresis at higher injection currents was already discussed in the simulations. However - contrary to the simulations - we observe also a shift towards higher input powers. This shift might be explained by an increase in the internal temperature of the laser which reduces its gain. As can be seen on the graphs, the extinction ratio is over 30 dB.

To measure the flip-flop operation, we conduct dynamic measurements with a set-up as illustrated in Figure 2.19. Light of a tunable laser is sent through a modulator in order to generate pulses. The modulator is driven by a pulse pattern generator (PPG) with the clock at 10 GHz. The pulses have a duration of 100 ps and the repetition rate can be easily adjusted by programming the PPG. The modulator supports only one polarization which can be controlled by polarization controlling wheels. After amplification of the pulses by an EDFA, an optical band-pass filter (OBPF) is used to remove the amplified spontaneous emission (ASE) from the signal. The pulses are split by a 3 dB coupler and sent

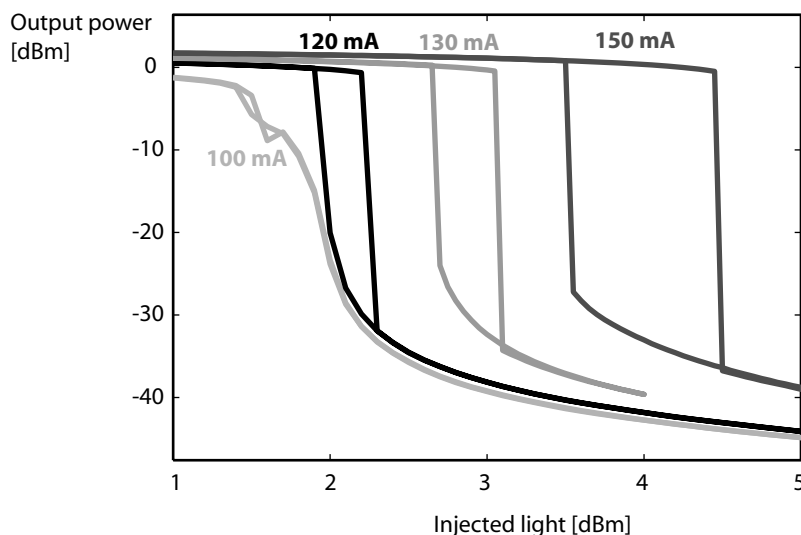


**Figure 2.18:** Experimental result for the bistability in the laser diodes.

to the two laser facets. A short delay line is introduced in one of the two arms to control the time delay between the set and reset pulses. The pulses on the left of the DFB laser are the reset-pulses and are therefore combined with the holding beam (as discussed above). The power of the holding beam corresponds to a value where the DFB laser is bistable. The power and polarization of the set- and reset-pulses can be adjusted by variable attenuators and polarization controlling wheels.

When we perform the experiment, fast flip-flop operation can be observed as illustrated in Figure 2.20. Switching times around 40 ps can be achieved. For these experiments, the minimal pulse energies are in the order of a few hundred femto-Joules (200 fJ set and 500 fJ reset as reported in [30]). However, these values may vary between consecutive experiments because the energies are measured in-fiber without accounting for the variable alignment losses. In Figure 2.21, the evolution of the switching speed as a function of the pulse energies can be observed. The measurement of the fall time was not possible at pulse energies higher than 840 fJ due to limitations of the set-up. The set pulses were injected at a wavelength of 1540 nm and the reset pulses at 1545 nm (arbitrarily chosen). We can observe from this graph that higher pulse energies will result in faster flip-flop operation. However, there seems to be a floor around 40 - 50 ps. In comparing these experimental results with the simulations where switching times between 10-20 ps should be viable, it is important to have in

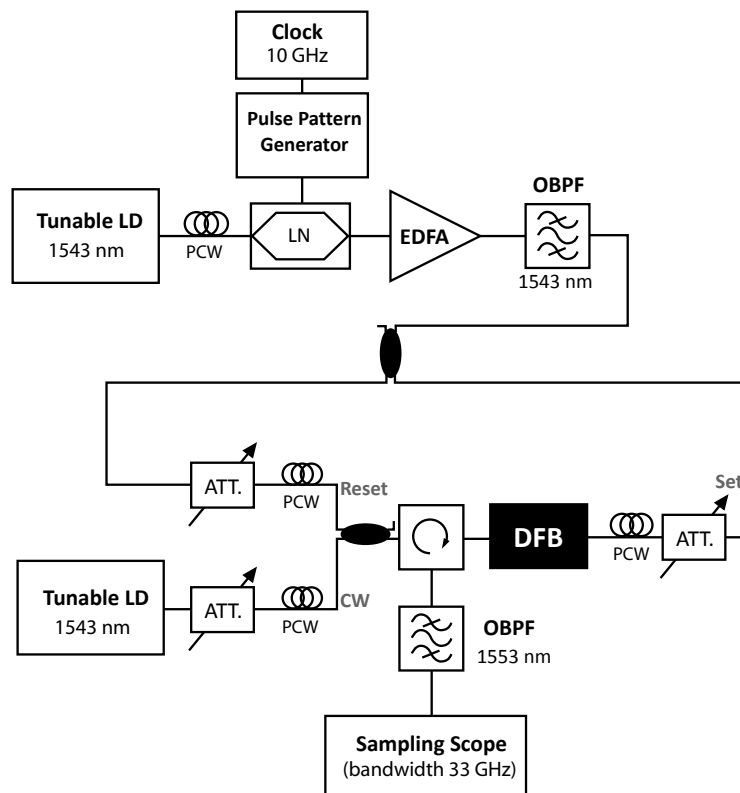


**Figure 2.19:** Schematic of the measurement set-up for the flip-flop operation.

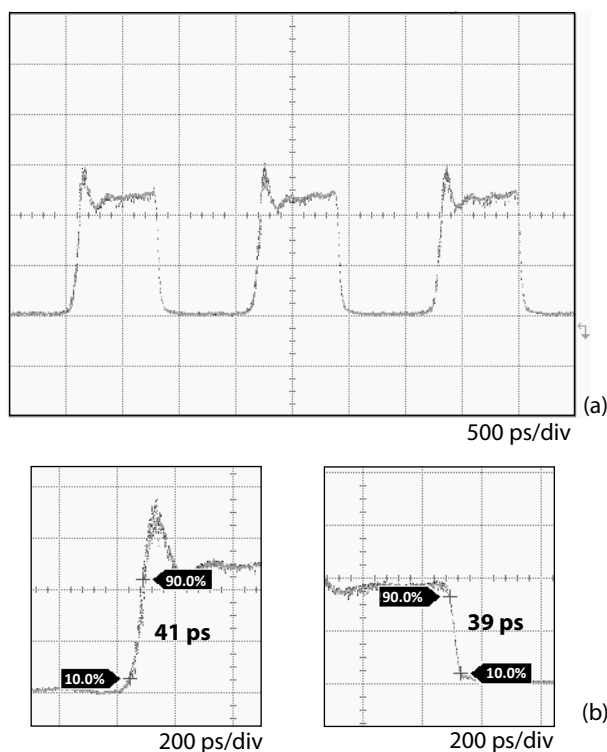


**Figure 2.20:** Experimental demonstration of fast flip-flop operation in a single DFB laser diode under injection of a holding beam. (a) Output of the DFB laser at 1553 nm when subjected to 100 ps long set and reset pulses separated by 1.65 ns. (b) Details of the leading and trailing edges of the laser output enabling the determination of the rise and fall times.

mind that the set and reset pulses in the experiments have rise and fall times of about 30 ps which significantly limits the speed of the switching. The overshoot which is clearly visible from Figure 2.20, will disappear at lower pulse powers.

The same flip-flop experiment was also carried out using very short pulses from an actively mode-locked fiber laser. Because the short pulse source generates pulses at very high repetition rates (5 - 10 GHz), the signal was first sent through an optical modulator to suppress some of the pulses in order to lower the repetition rate (typically between 500 MHz - 3 GHz). Because the modulator has a limited extinction ratio, the pulses are in general not completely suppressed. This resulted in a slightly distorted input signal and complicated the measurements. We used pulses with a duration of 7 ps for the experiment. The

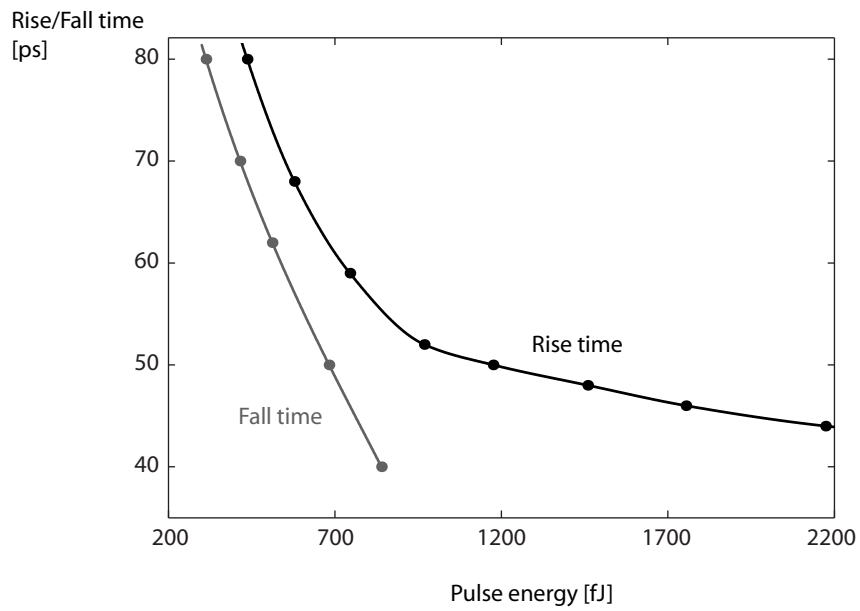


**Figure 2.21:** Experimentally measured rise and fall times for flip-flop operation as a function of pulse energies.

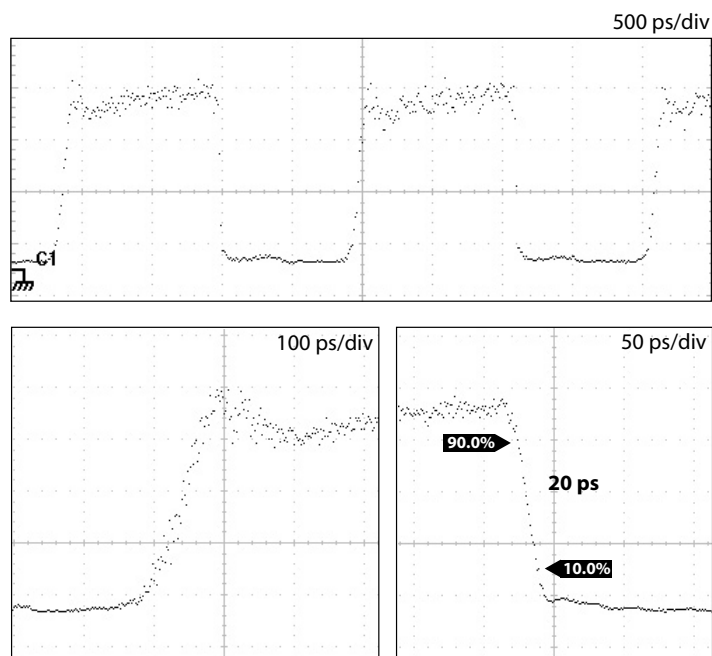


**Figure 2.22:** Experimental demonstration of flip-flop operation in a DFB laser diode with pulse durations of 7 ps.

pulse energies were measured to be 75 fJ (set) and 190 fJ (reset). The flip-flop operation is shown in Figure 2.22. The switch-on time was rather slow (75 ps) but the switch-off was measured to be 20 ps which corresponds to the maximal speed of the sampling scope and could therefore be even faster. The fast switch-off measured with the short pulses suggests that the limited rise and fall time of the pulses in the previous experiments have an influence on the total switching times. Because the distortions on the input signals caused by the limited extinction ratio of the modulator, it was not possible to perform a more complete study of the relationship between the pulse energies and the switching times.

We studied also the influence of the the holding beam power on the switching speeds. One could expect that a holding beam power close to one of the edges of the hysteresis would favor the switching to one specific state. In order to have a broader hysteresis for these experiments, we biased the laser at a higher current (150 mA). In our experiments (Figure 2.23), we see no significant influence of the holding beam power on the switching speed. Because the hysteresis is still rather small, amplitude noise on the input signals may cause the effect (if present) to average out.

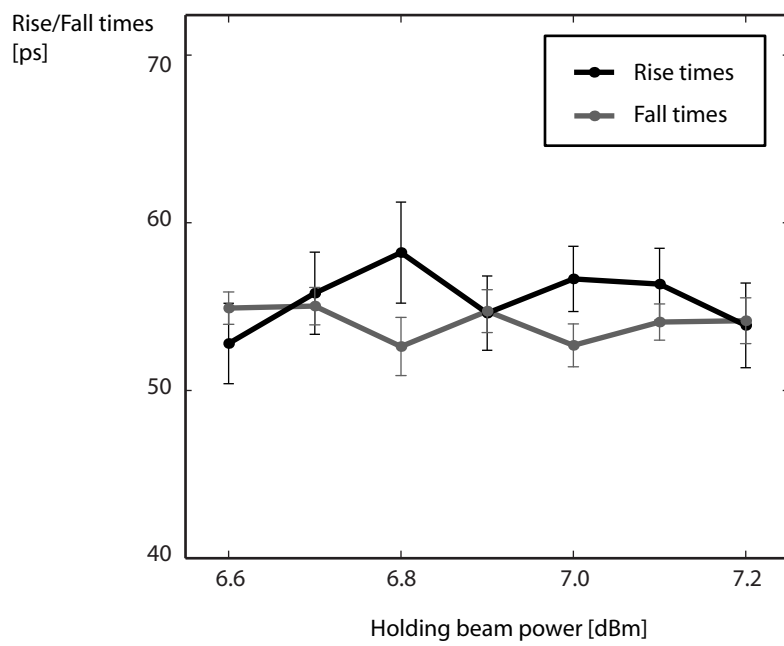


**Figure 2.23:** Changes in the holding beam power have no significant influence on the switching times. The error bars indicate the standard deviation on the averaged switching times.

## 2.5 Discussion and conclusions

It was shown that - under injection of a holding beam - we can obtain a hysteresis in the output of a distributed feedback (DFB) laser diode with anti-reflection coated facets. The effect originates from the longitudinal distribution of the carriers (spatial hole burning). Using simulations with a transmission-line laser model (TLLM), it was investigated which parameters are influential. Experiments show that a hysteresis with an extinction ratio larger than 30 dB is possible. When pulses are injected intermittently from both sides of the laser diode, we can switch between the two states and obtain flip-flop operation. Switching times as low as 40 ps are possible using pulses with a duration of 100 ps. The minimal pulse energies are of the order of a few 100 fJ's.

Compared to most other concepts in literature [31–34], the footprint and power consumption of this device are significantly smaller. The disadvantage of the necessity of a holding beam for the flip-flop operation in a DFB laser can be addressed by distributing one single holding beam over an array of

Moreover, only very complicated set-ups consisting of several active elements [34] are able to outperform the fast switching times but these require a very large power consumption and the use of several optical isolators which are difficult to integrate on-chip. Recent developments of polarization switching in vertical-cavity surface-emitting lasers (VCSELs) [35–37] suggest that they can be a viable alternative. However, VCSELs are less suited for on-chip integration and the best results have been obtained at wavelengths of 980 nm. The coupled ring lasers in [38] have a lower power consumption, footprint and faster switching times but they have only been demonstrated in pulsed operation which complicates their use in practical applications. The recent results we obtained on microdisk lasers [39] (further discussed in chapter 4) are better in terms of power consumption, footprint and pulse energies. However, the small output power, limited extinction ratio and difficult wavelength control of the microdisk lasers makes them rather suitable for on-chip communication instead of long-distance telecommunication networks.

The broadband operation and fast switching makes the DFB flip-flop an ideal candidate to apply in all-optical packet switched networks (chapter 6). The large power consumption will result in high output powers of the flip-flops (due to the efficient lasing in DFB laser diodes) which is advantageous for optical fiber communication. Moreover, DFB lasers have become the standard transmitter in optical networks. Their fabrication has been studied extensively during the past 30 years offering a reliable and already optimized process.

## References

- [1] H. Kogelnik and C. V. Shank. *Stimulated emission in a periodic structure*. Applied Physics Letters, 18(4):152–154, 1971.
- [2] H. Kogelnik and C. V. Shank. *Coupled-wave theory of distributed feedback lasers*. Journal of Applied Physics, 43(5):2327–2335, 1972.
- [3] M. Nakamura, A. Yariv, H. W. Yen, S. Somekh, and H. L. Garvin. *Optically pumped GaAs surface laser with corrugation feedback*. Applied Physics Letters, 22(10):515–516, 1973.
- [4] C. V. Shank, R. V. Schmidt, and B. I. Miller. *Double-heterostructure GaAs distributed-feedback laser*. Applied Physics Letters, 25(4):200–201, 1974.
- [5] D. R. Scifres, R. D. Burnham, and W. Streifer. *Distributed-feedback single heterojunction GaAs diode laser*. Applied Physics Letters, 25(4):203–206, 1974.
- [6] M. Nakamura, K. Aiki, J. Umeda, A. Yariv, H. W. Yen, and T. Morikawa. *GaAs-Ga<sub>1-x</sub>Al<sub>x</sub>As double-heterostructure distributed-feedback diode lasers*. Applied Physics Letters, 25(9):487–488, 1974.
- [7] K. Aiki, M. Nakamura, J. Umeda, A. Yariv, A. Katzir, and H. W. Yen. *GaAs-GaAlAs distributed-feedback diode lasers with separate optical and carrier confinement*. Applied Physics Letters, 27(3):145–146, 1975.
- [8] H. C. Casey, S. Somekh, and M. Ilegems. *Room-temperature operation of low-threshold separate-confinement heterostructure injection laser with distributed feedback*. Applied Physics Letters, 27(3):142–144, 1975.
- [9] O. Svelto. *Principles of lasers*. Plenum Press, fourth edition, 1998.
- [10] R. N. Hall, R. O. Carlson, T. J. Soltys, G. E. Fenner, and J. D. Kingsley. *Coherent light emission from GaAs junctions*. Physical Review Letters, 9(9):366–368, 1962.
- [11] M. I. Nathan, W. P. Dumke, G. Burns, F. H. Dill, and G. Lasher. *Stimulated emission of radiation from GaAs p-n junctions*. Applied Physics Letters, 1(3):62–64, 1962.
- [12] N. Holonyak and S. F. Bevacqua. *Coherent (visible) light emission from Ga(As<sub>1-x</sub>P<sub>x</sub>) junctions*. Applied Physics Letters, 1(4):82–83, 1962.
- [13] T. M. Quist, R. H. Rediker, R. J. Keyes, W. E. Krag, B. Lax, A. L. McWhorter, and H. J. Zeigler. *Semiconductor maser of GaAs*. Applied Physics Letters, 1(4):91–92, 1962.

- [14] J. F. Liu, X. C. Sun, R. Camacho-Aguilera, L. C. Kimerling, and J. Michel. *Ge-on-Si laser operating at room temperature*. Optics Letters, 35(5):679–681, 2010.
- [15] G. Morthier and P. Vankwikelberge. *Handbook of distributed feedback laser diodes*. Artech House Publishers, 1997.
- [16] A. Yariv and P. Yeh. *Photonics - Optical electronics in modern communications*. Oxford University Press, sixth edition, 2007.
- [17] M.-C. Amann, J. Buus, and D.J. Blumenthal. *Tunable laser diodes*. Wiley-Interscience, second edition, 2005.
- [18] H. A. Haus and C. V. Shank. *Anti-symmetric taper of distributed feedback lasers*. IEEE Journal of Quantum Electronics, 12(9):532–539, 1976.
- [19] K. Utaka, S. Akiba, K. Sakai, and Y. Matsushima. *Analysis of quarter-wave-shifted DFB laser*. Electronics Letters, 20(8):326–327, 1984.
- [20] H. Soda, Y. Kotaki, H. Sudo, H. Ishikawa, S. Yamakoshi, and H. Imai. *Stability in single longitudinal mode-operation in GaInAsP-InP phase-adjusted DFB lasers*. IEEE Journal of Quantum Electronics, 23(6):804–814, 1987.
- [21] L. D. Westbrook. *Measurements of  $dg/dN$  and  $dn/dN$  and their dependence on photon energy in  $\lambda=1.5\mu\text{m}$  InGaAsP laser diodes*. IEE Proceedings-J Optoelectronics, 133(2):135–142, 1986.
- [22] B. R. Bennett, R. A. Soref, and J. A. Delalamo. *Carrier-induced change in refractive index of InP, GaAs and InGaAsP*. IEEE Journal of Quantum Electronics, 26(1):113–122, 1990.
- [23] H.M. Gibbs. *Optical bistability: controlling light with light*. Academic Press, second edition, 1985.
- [24] A. J. Lowery. *New dynamic semiconductor laser model based on the transmission-line modeling method*. IEE Proceedings-J Optoelectronics, 134(5):281–289, 1987.
- [25] A. J. Lowery. *Dynamic modeling of distributed-feedback lasers using scattering matrices*. Electronics Letters, 25(19):1307–1308, 1989.
- [26] VPIsystems Inc. *VPIcomponentMaker<sup>TM</sup> Active Photonics*.
- [27] G. Guekos. *Photonic devices for telecommunications*, chapter 7, pages 183–211. Springer-Verlag, 1999.

- [28] A.A. Yimam. *All-optical signal processing using DFB and DBR laser diodes*. Master's thesis, Ghent University, 2009.
- [29] K. Huybrechts, W. D'Oosterlinck, G. Morthier, and R. Baets. *Proposal for an all-optical flip-flop using a single distributed feedback laser diode*. IEEE Photonics Technology Letters, 20(1-4):18–20, 2008.
- [30] K. Huybrechts, G. Morthier, and R. Baets. *Fast all-optical flip-flop based on a single distributed feedback laser diode*. Optics Express, 16(15):11405–11410, 2008.
- [31] M. Takenaka, M. Raburn, and Y. Nakano. *All-optical flip-flop multimode interference bistable laser diode*. Photonics Technology Letters, 17(5):968–970, 2005.
- [32] A. Trita, G. Mezosi, F. Bragheri, Yu Jin, S. Furst, W. Elsasser, I. Cristiani, M. Sorel, and G. Giuliani. *Dynamic operation of all-optical Flip-Flop based on a monolithic semiconductor ring laser*. In 34th European Conference on Optical Communication (ECOC 2008), 2008.
- [33] W. D'Oosterlinck, F. Ohman, J. Buron, S. Sales, A. P. Pardo, A. Ortigosa-Blanch, G. Puerto, G. Morthier, and R. Baets. *All-optical flip-flop operation using a SOA and DFB laser diode optical feedback combination*. Optics Express, 15(10):6190–6199, 2007.
- [34] A. Malacarne, J. Wang, Y. Zhang, A. Das Barman, G. Berrettini, L. Poti, and A. Bogoni. *20 ps transition time all-optical SOA-based flip-flop used for photonic 10 Gb/s switching operation without any bit loss*. IEEE Journal of Selected Topics in Quantum Electronics, 14(3):808–815, 2008.
- [35] H. Kawaguchi, T. Mori, Y. Sato, and Y. Yamayoshi. *Optical buffer memory using polarization-bistable vertical-cavity surface-emitting lasers*. Japanese Journal of Applied Physics Part 2-Letters & Express Letters, 45(33-36):L894–L897, 2006.
- [36] T. Katayama, Y. Sato, T. Mori, and H. Kawaguchi. *Polarization bistable characteristics of 1.55  $\mu\text{m}$  vertical-cavity surface-emitting lasers*. Japanese Journal of Applied Physics Part 2-Letters & Express Letters, 46(45-49), 2007.
- [37] T. Katayama, T. Ooi, and H. Kawaguchi. *Experimental demonstration of multi-bit optical buffer memory using 1.55- $\mu\text{m}$  polarization bistable vertical-cavity surface-emitting lasers*. IEEE Journal of Quantum Electronics, 45(11):1495–1504, 2009.

- 
- [38] M. T. Hill, H. J. S. Dorren, T. de Vries, X. J. M. Leijtens, J. H. den Besten, B. Smalbrugge, Y. S. Oei, H. Binsma, G. D. Khoe, and M. K. Smit. *A fast low-power optical memory based on coupled micro-ring lasers*. *Nature*, 432(7014):206–209, 2004.
- [39] L. Liu, R. Kumar, K. Huybrechts, T. Spuesens, G. Roelkens, E.-J. Geluk, T. de Vries, P. Regreny, D. Van Thourhout, R. Baets, and G. Morthier. *An ultra-small, low-power, all-optical flip-flop memory on a silicon chip*. *Nature Photonics*, 4(3):182–187, 2010.



# 3

## DBR laser all-optical flip-flop

In this chapter, it will be shown that a distributed Bragg reflector laser can be used as an all-optical flip-flop because of a hysteresis effect in its tuning characteristic. The main advantage of this approach compared to using distributed feedback lasers is that there is no need for a holding beam. As before, there is a single lasing wavelength that can be easily tuned to the wavelength division multiplexed (WDM) system. There are however restrictions on the wavelength of the injected pulses as will be discussed further.

First, a short introduction on the mode selectivity in a distributed Bragg reflector laser is given before the underlying physics that create the asymmetric gain suppression responsible for the hysteresis in the tuning characteristic is explained. Afterwards, the concept for all-optical flip-flop operation is discussed and simulated. Experimental results demonstrate that this approach enables fast flip-flop operation with switching times below 100 ps and reasonable pulse energies in the order of several picojoules.

### 3.1 Introduction

Distributed Bragg reflector lasers differ from distributed feedback lasers in the sense that they have a grating *outside* the active section (see Figure 3.1). This grating will act as a wavelength dependent mirror which reflectivity is maximal for those wavelengths that match the Bragg condition ( $\Lambda = m(\lambda_B/2n)$ ).

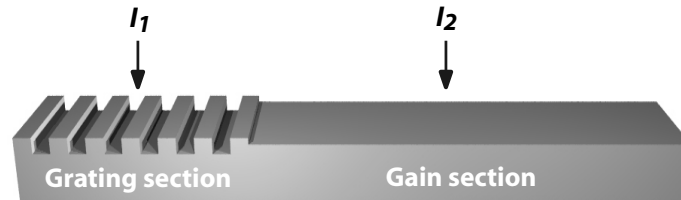


**Figure 3.1:** Illustration of a DBR laser diode with a grating and gain section.

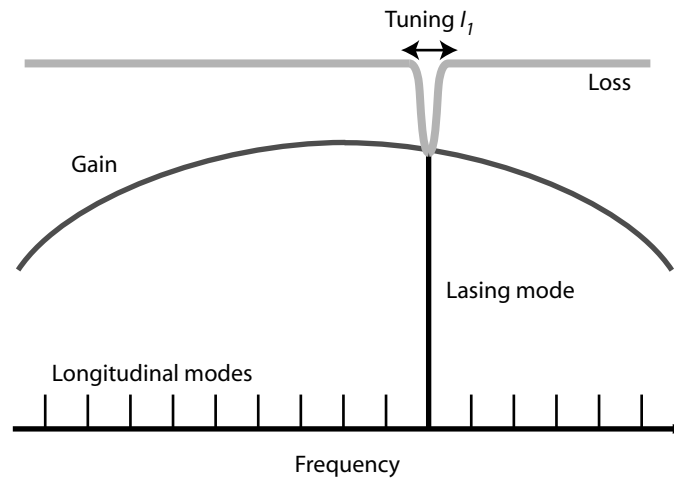


**Figure 3.2:** The wavelength-dependent loss of the DBR grating allows the selection of a specific longitudinal mode.

The feedback for the longitudinal mode that corresponds to this wavelength will therefore be significantly higher and this mode will reach the threshold for lasing first. Once it becomes the dominant mode, it prevents the buildup from spontaneous emission of the other longitudinal modes resulting in a single mode laser.

To tune the wavelength of a distributed bragg reflector laser, we inject a small current on the grating section. The injection of carriers will change the index of refraction [1] and therefore adjust the Bragg wavelength. As shown in Figure 3.2, the lasing wavelength will hop between the different longitudinal modes when the tuning current is changed.

When the current on the active section is raised to higher values (typically above 100 mA), different nonlinear phenomena appear due to the high optical

power in the lasing cavity. As described by Bogatov et al. [2], these nonlinear effects introduce an asymmetric gain suppression in the laser cavity. As will be described further, the asymmetry in the gain around the laser frequency will introduce a hysteresis in the tuning characteristic. The complete theoretical analysis of the underlying physics has been extensively studied in literature [2–7] and falls therefore beyond the scope of this work. However, in the next section a qualitative analysis will be given.

### 3.2 Nonlinear effects

In general, three different effects need to be taken into account to explain the spectral asymmetry in the gain suppression. As will be explained further in this section, four-wave mixing leading to carrier pulsations is strongly present at lower frequencies. At higher frequencies, this effect becomes less pronounced and intraband dynamics such as spectral hole burning and carrier heating become dominant.

In the presence of multiple modes, nonlinear wave mixing causes a pulsation of the carrier density [3]. Consider for example a laser beam at frequency  $\omega_0$  (pump) and a side mode at  $\omega_1$  (probe). The carrier density will then experience a modulation at the beat frequency  $\Omega = \omega_1 - \omega_0$ . Such changes in carrier density affect both the gain and the refractive index [1] of the active region, and generate a dynamic population grating. This will influence the gain in frequencies around the lasing frequency. The effect is limited by the carrier lifetime (typically a few hundred picoseconds), which means that the effect will start decreasing at frequencies higher than 10 GHz.

Very fast intraband effects exist up to 10 THz, however with a much lower amplitude. Intraband dynamics are referred to as processes that affect the shape of the carrier distributions in energy space, but not the corresponding total carrier density. There are basically two different effects associated with intraband dynamics that can distort the gain around the lasing frequency: spectral hole burning and carrier heating [4–7].

Spectral hole burning arises from the high recombination rate of carriers at energy levels that correspond to the lasing frequency. These recombined carriers have to be replaced by newly injected carriers or by carriers from adjacent energy levels in order to keep the gain at a certain level. The replacement of carriers by carriers from adjacent energy levels happens through intraband carrier-carrier scattering on a time scale of 50-100 fs. Because the quasi-equilibrium Fermi distribution is not restored instantaneously, the gain at frequencies around the lasing frequency will be compressed compared to the gain at more distant frequencies. It is obvious that the magnitude of the resulting gain suppression varies with the optical power in the cavity.

Carrier heating describes the fact that the carrier temperatures may be different from the lattice temperature. The carrier temperatures relax towards the lattice temperature by carrier-phonon scattering with a relaxation time of 0.5-1 ps. There are two different processes which will contribute in changing the carrier temperatures in the device. The first is the process of stimulated emission which will remove the 'cool' carriers near the bottom of the band and therefore increases the temperature of the remaining carrier distribution. Second, free carrier absorption will heat up the distribution because almost the entire photon energy is given to the carrier distributions. Both of these heating processes will cause dynamic changes in the energy distribution of the carriers and - as a consequence - they will induce changes in the gain function.

In a standard DBR laser, the cavity lengths range from 500  $\mu\text{m}$  till 1000  $\mu\text{m}$ . The free spectral range of the cavity modes is therefore 0.3-0.6 nm, which means that the beating frequency is below 75 GHz. For such frequencies, all of the above effects contribute to an asymmetry in the gain profile. In figure 3.3, it is shown how an asymmetric gain profile leads to hysteresis in the tuning characteristic [8, 9]. The asymmetry results in a higher gain for lower frequencies. Therefore, the mode hop will occur at a different tuning current depending on the initial lasing state. The relative frequency detuning of the Bragg grating between two lasing modes is indicated by  $\delta\nu_B = (\nu - \nu_0)/\Delta\nu$  with  $\nu_0$  the lasing frequency and  $\Delta\nu$  the mode spacing. When tuning the loss minimum to higher values, the mode hop occurs between  $\delta\nu_B = 0.70$  and  $\delta\nu_B = 0.75$ . The mode hop would have occurred at  $\delta\nu_B = 0.50$  if there was no gain suppression. After the mode hop, the nonlinear gain profile also moves. When tuning the loss minimum in the other direction, the mode hop will occur between  $\delta\nu_B = 0.55$  and  $\delta\nu_B = 0.60$ . This difference in mode hopping frequencies will result in a spectral hysteresis in the tuning characteristic.

### 3.3 Concept

The above-mentioned hysteresis effect can be successfully applied for flip-flop operation. The proposed techniques can be used for either a 2- or 3-section DBR laser diode, or any other variant of the classical DBR laser diodes.

When the tuning current is set within the hysteresis, both frequencies are equally possible. In that case, it is possible to switch between the two frequencies by using injection locking. To injection lock a laser, a light pulse at a certain frequency is injected in the laser cavity so that the injected light will dominate over the existing lasing mode and the laser starts lasing at the frequency of the injected light. By using this technique, it is possible to induce flip-flop operation in the DBR laser. Indeed, by injecting light pulses alternately at the two specified frequencies, it is possible to switch in the frequency domain result-

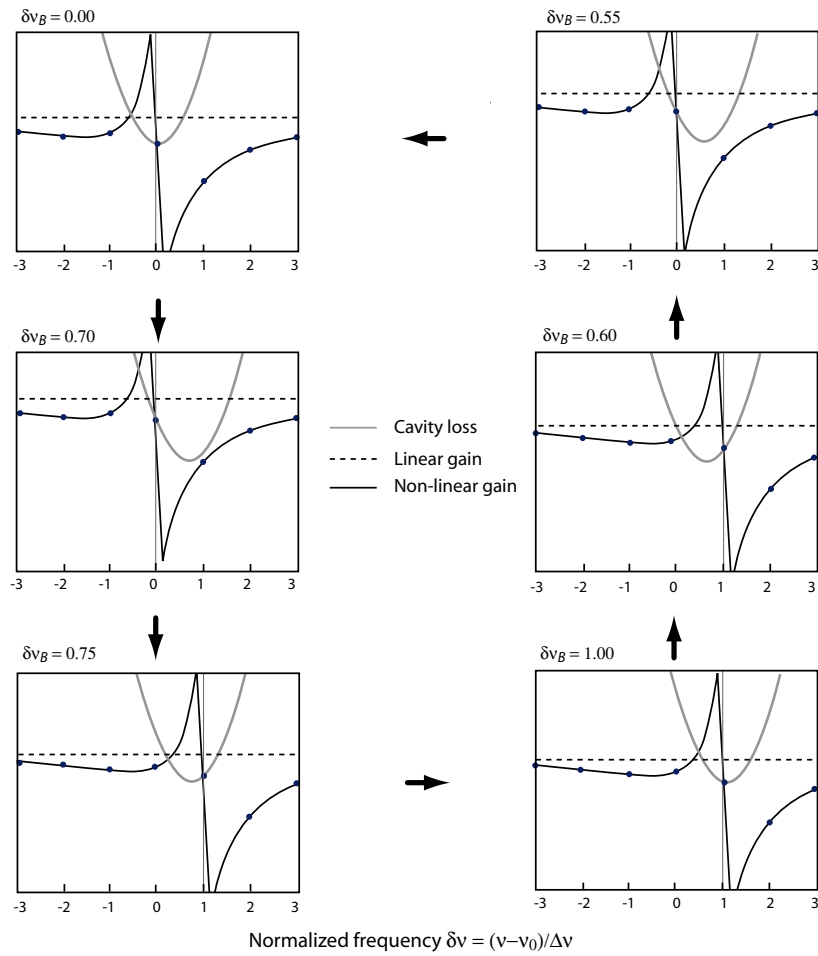


**Figure 3.3:** The asymmetric gain will cause mode hopping at different tuning currents. This results in a hysteresis in the tuning characteristic. (Courtesy of [8]).

ing in wavelength-dependent flip-flop operation. Using a narrow optical band-pass filter (OBPF), it is possible to distinguish between the two lasing modes. This technique has been demonstrated in [10], however with very long pulses (1 ns) and without reporting any specifications on the speed. The advantage of this technique is that the laser can be easily matched with the WDM grid of the network. The frequency alignment with the two different lasing modes is however rather difficult and the flip-flop operation will be distorted by the injected pulses.

It is also possible to switch between two frequencies by using a depletion of carriers. Because the highest frequency corresponds to the lowest carrier density, we can switch from the lowest frequency to the highest by injecting a very short but strong pulse in the laser cavity. Afterwards, the laser will relax back to the state with the lowest carrier density corresponding to the highest frequency. In this case, the injected pulse can have in principle any wavelength. We can therefore realize flip-flop operation by using set and reset pulses with the same wavelength but with a different amplitude and duration. When we inject alternately long pulses (~100 ps) and strong but short pulses (~10 ps) at the lowest frequency of the hysteresis, we also get flip-flop operation in the frequency domain. The long pulse will injection-lock the DBR laser at the lowest frequency. We can make the laser switch back to the highest frequency by depleting the carrier density by injecting the very short pulse. This limits the requirements for wavelength alignment and the signal that is generated at the highest frequency will not get distorted by the injected pulses.

### 3.4 Simulation results

To illustrate the concept, we simulate it with the commercial software packet (VPI) as used in the previous chapter [11]. As explained in the previous chapter, this simulation program makes use of the transmission line laser model (TLLM) which solves the rate equations in different sections of the active material. The effects of carrier heating and spectral hole burning are included in the model and the simulation method does the calculations over a wide bandwidth such that the carrier pulsations are also taken into account.

A standard DBR laser model is used with a gain section of 600  $\mu\text{m}$  and a bias current of 100 mA. The grating section is 300  $\mu\text{m}$  long and has a corrugation with  $\kappa = 60 \text{ cm}^{-1}$ . By varying the tuning current over a wide range, we obtain the bistabilities as depicted in Figure 3.4. The bistability located at the current of 20 mA will be used and the injected pulses are therefore at the wavelength  $\lambda_1$ . We use pulses with a duration of 100 ps and 10 ps and corresponding energies of several pJ (varying from 3 to 6 pJ for set and from 0.5 to 3 pJ for reset). The long pulses will injection-lock the DBR laser at wavelength  $\lambda_1$  while the short

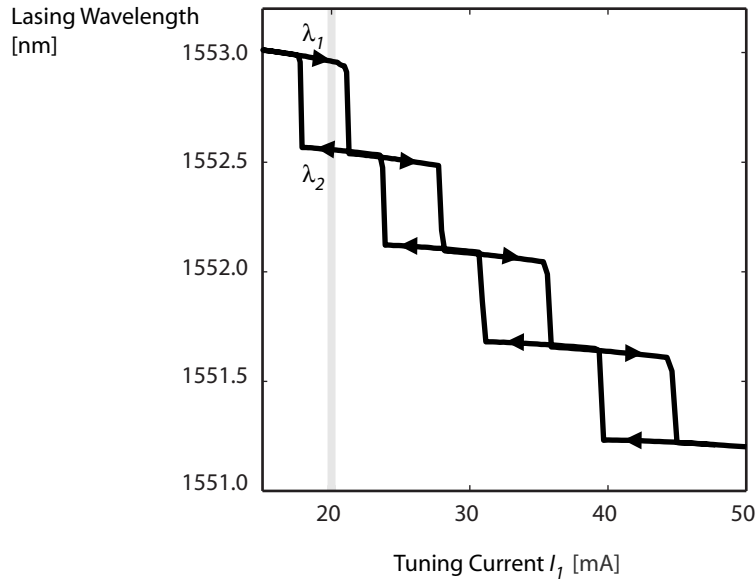


**Figure 3.4:** Simulation of the multiple bistabilities in the tuning characteristic of the lasing wavelength.

pulses will deplete the carrier density such that the state with the lower carrier density at a wavelength  $\lambda_2$  is favoured. The time-resolved frequency is shown in Figure 3.5 and flip-flop operation in the frequency domain can be observed. The rather high value of the tuning current used here (and also in the experiment) is chosen in order to obtain hysteresis over a relatively broad current range which makes the flip-flop less sensitive to small fluctuations. This high current is therefore not strictly required.

### 3.5 Experimental results

We demonstrate the flip-flop operation also experimentally with a standard 2-section DBR laser provided by Alcatel-Thales III-V labs. The active gain section is a multi-quantum well (MQW) layer with a length of  $600 \mu\text{m}$  in which a current of 100 mA is injected. The Bragg section has a length of  $250 \mu\text{m}$  and a corrugation with  $\kappa = 40 \text{ cm}^{-1}$ . The typical tuning range of the wavelength in such devices is 16 nm [9]. Usually, DBR lasers with a shorter active section are used to reduce nonlinear effects and to provide regular tuning control. However, for this application it is important to have a DBR specially designed to have a strong hysteresis and therefore a larger active section.

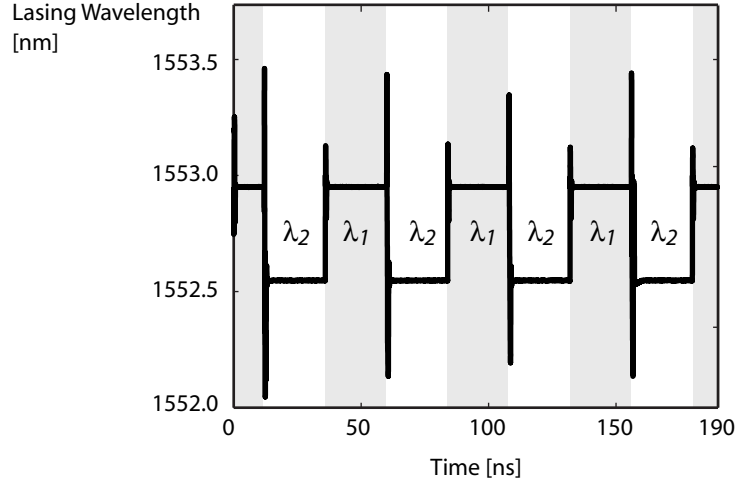


**Figure 3.5:** Simulation of the time-resolved frequency which demonstrates the flip-flop operation.

The bistability as a function of the tuning current is depicted in Figure 3.6. We see that the laser can operate in a bistable region with a width of 0.5 mA at a wavelength of 1561.3 nm and 1560.7 nm. The devices under study were not optimized for polarization-independent operation, but such optimization should be theoretically possible. The extinction ratio between the two lasing modes is 44 dB. This means that the resulting flip-flop operation will have very high extinction ratios.

A schematic of the measurement set-up is given in Figure 3.7. A pico-second pulse source at 1561.3 nm is used to provide pulses of 10 ps with a repetition rate of 10 GHz. By sending these pulses through a standard Lithium Niobate modulator driven by a pulse pattern generator, the repetition frequency can be decreased. Another modulator is used in combination with a tunable laser to generate the 100 ps pulses and a fiber delay line controls the time difference between the set and reset pulses before combining them. Because the modulators attenuate the optical power by 10 dB, the signals are amplified with an erbium-doped fiber-amplifier (EDFA) and the amplified spontaneous emission (ASE) is removed with an optical band-pass filter (OBPF). Using a circulator, we can separate the output signal from the DBR laser. An optical band-pass filter with a very narrow bandwidth (0.3 nm) is used to distinguish between the two different output wavelengths.

Before doing the experiment with pulses of different amplitude and duration, we study the behaviour of the flip-flop operation when the laser is injection locked alternately at the two different wavelengths. We do this by replacing

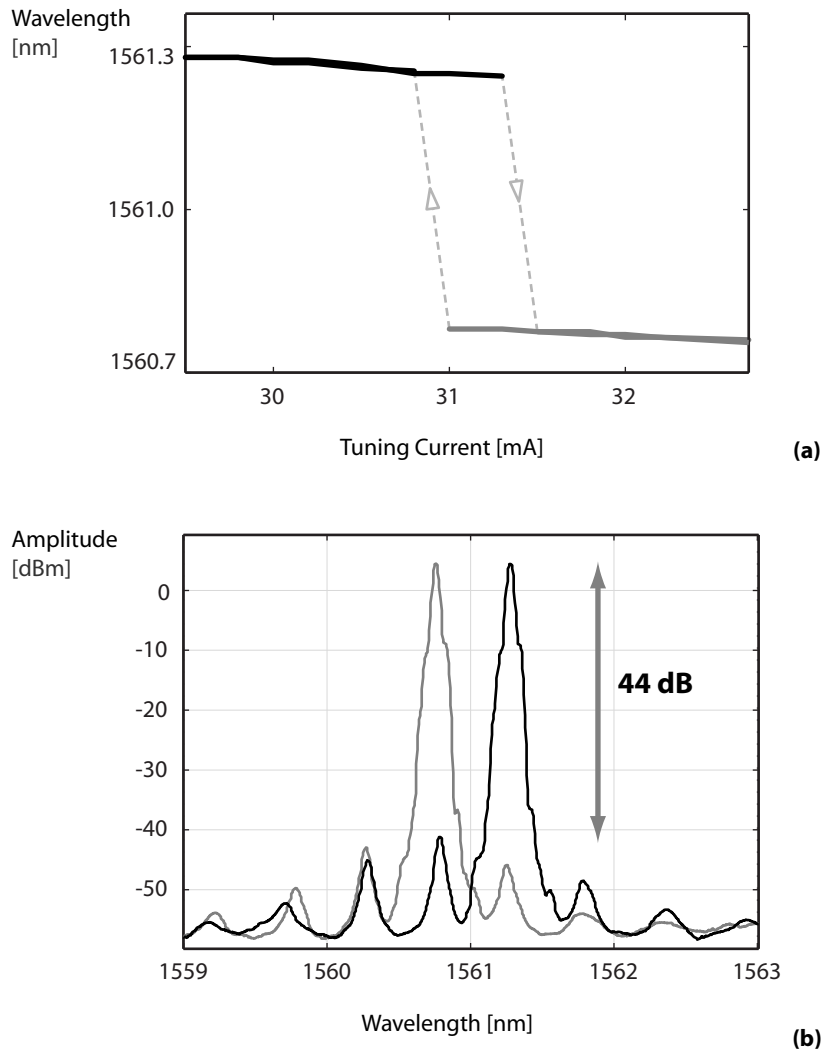


**Figure 3.6:** (a) Bistability in the operating wavelength as a function of the tuning current; (b) Optical spectrum of the two states with side-mode suppression ratio of 44 dB.

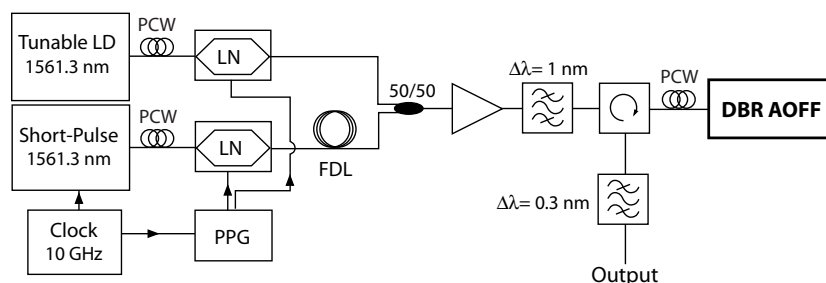


**Figure 3.7:** Schematic of the measurement set-up.

the pico-second pulse source by a standard laser diode tuned at the wavelength corresponding to the lower branch. As mentioned already in the introduction of this chapter, previous studies on this matter were only done by using very long pulses (1 ns) and without giving details on the dynamics [10]. The observed behaviour is shown in Figure 3.8 where flip-flop operation is obtained at both wavelengths. The result was obtained under slightly different conditions as were shown in Figure 3.6 with a tuning current of 11.7 mA, a bias current of 88 mA and the two wavelength branches corresponding to the wavelengths of 1563.4 nm and 1562.4 nm. The rising edge is completely covered by the injected pulses and we can only state that it is shorter than 100 ps. There is some ringing effect due to the injection locking. The switch off behaviour on the other hand can be measured to be about 50 ps. The pulse energies are 1.5 pJ and the small differences between the two graphs are due to slight wavelength detunings and the low extinction ratio of one of the two modulators (about 8-10 dB).

When the experiment is done by a combination of injection locking and carrier depletion [12, 13], we need to use a combination of long (100 ps) and short (10 ps) pulses as explained above. By doing so, the flip-flop operation depicted in Figure 3.9 is obtained. Pulses are injected at the wavelength of 1561.3 nm. The long pulses of 100 ps act as reset-pulses because they injection-lock the laser at the longest wavelength. As before, there is a slight ringing effect in the transients. The short and strong pulses (10 ps) act as set-pulses because they bring the carrier distribution of the laser in depletion and back to the state with the lower carrier densities at 1560.7 nm. We can discriminate between the two different wavelengths using an optical bandpass filter. The signal at the lowest wavelength (1560.7 nm) is free from distortions due to injected pulses and contains the actual flip-flop signal. The noise in the graph of Figure 3.9 is mainly due to the low extinction ratio of one of the modulators. Switching in less than 50 ps was obtained. Part of this switching time is due to the rise and fall times of

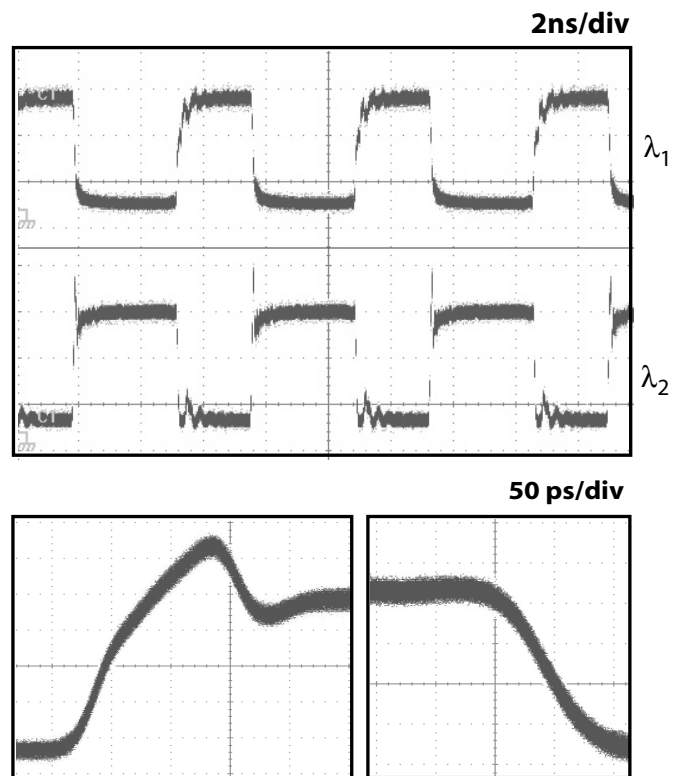


**Figure 3.8:** Flip-flop operation by injection locking at the two separate wavelengths using pulses with a duration of 100 ps. The upper graph presents the output at the two operating wavelengths  $\lambda_1$  and  $\lambda_2$ . Below, details of the leading and trailing edges of the flip-flop output enabling the determination of rise and fall time.

the 10 Gb/s pattern generator and modulator. The pulse energies are 2 pJ (set) and 4 pJ (reset). These values for the pulse energies are measured in-fiber and therefore do not take the coupling loss of the lensed fiber into account.

### **3.6 Conclusion**

We demonstrated experimentally a novel concept for flip-flop operation in a single DBR-laser. Using pulses with different duration and amplitude but with the same wavelength, we obtain switching times of less than 50 ps with pulse energies of a few pJ. The principle can easily be extended to other tunable laser diodes, e.g. widely tunable laser diodes, that exhibit hysteresis in the tuning characteristics.

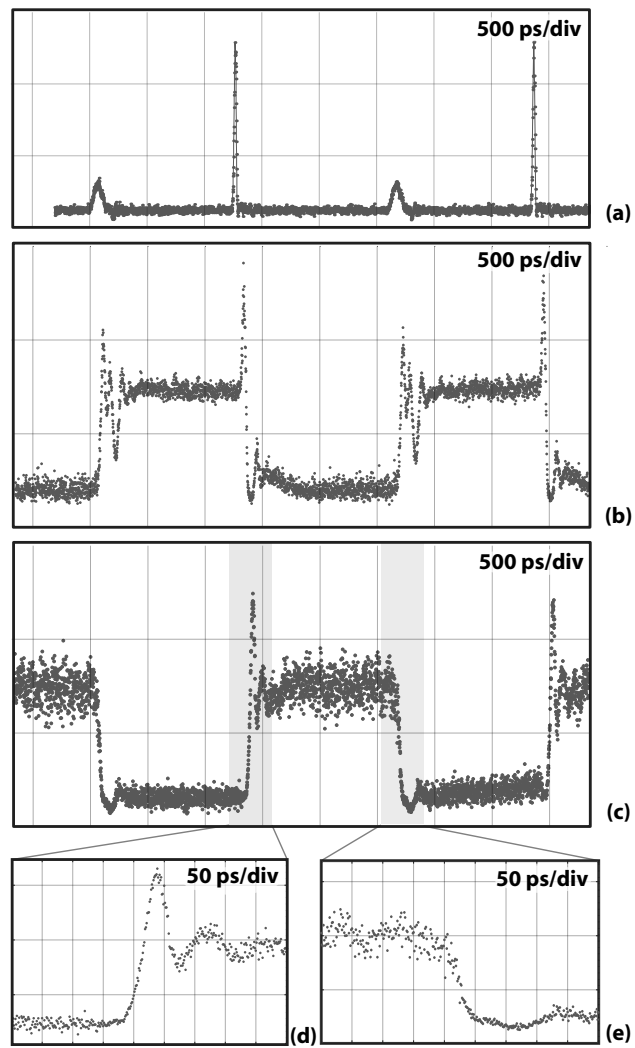


**Figure 3.9:** Flip-flop operation by a combination of injection locking and carrier depletion in a DBR laser. (a) Injected pulses at 1561.3 nm; (b) output at 1561.3 nm; (c) flip-flop operation at 1560.7 nm; (d) switch-on; (e) switch-off.

## References

- [1] B. R. Bennett, R. A. Soref, and J. A. Delalano. *Carrier-induced change in refractive index of InP, GaAs and InGaAsP*. IEEE Journal of Quantum Electronics, 26(1):113–122, 1990.
- [2] A. Bogatov, P. Eliseev, and B. Sverdlov. *Anomalous interaction of spectral modes in a semiconductor laser*. IEEE Journal of Quantum Electronics, 11(7):510–515, 1975.
- [3] G. P. Agrawal. *Population pulsations and nondegenerate 4-wave mixing in semiconductor-lasers and amplifiers*. Journal of the Optical Society of America B-Optical Physics, 5(1):147–159, 1988.
- [4] N. Ogasawara and R. Ito. *Longitudinal mode competition and asymmetric gain saturation in semiconductor injection-lasers - Experiment*. Japanese Journal of Applied Physics, 27(4):607–614, 1988.
- [5] N. Ogasawara and R. Ito. *Longitudinal mode competition and asymmetric gain saturation in semiconductor injection-lasers - Theory*. Japanese Journal of Applied Physics, 27(4):615–626, 1988.
- [6] A. Uskov, J. Mork, and J. Mark. *Wave mixing in semiconductor-laser amplifiers due to carrier heating and spectral-hole burning*. IEEE Journal of Quantum Electronics, 30(8):1769–1781, 1994.
- [7] M. Willatzen, A. Uskov, J. Mork, H. Olesen, B. Tromborg, and A. P. Jauho. *Nonlinear gain suppression in semiconductor-lasers due to carrier heating*. IEEE Photonics Technology Letters, 3(7):606–609, 1991.
- [8] G. Sarlet. *Tunable laser diodes for WDM communication*. PhD thesis, Ghent University, 2001.
- [9] H. Debregeas-Sillard, C. Fortin, A. Accard, O. Drisse, E. Derouin, F. Pommerau, and C. Kazmierski. *Nonlinear effects analysis in DBR lasers: Applications to DBR-SOA and new double bragg DBR*. IEEE Journal of Selected Topics in Quantum Electronics, 13(5):1142–1150, 2007.
- [10] S. Matsuo, T. Kakitsuka, T. Segawa, and H. Suzuki. *Optical Flip-flop Operation Using a DBR Laser*. In Conference on Lasers and Electro-Optics (CLEO '07), 2007.
- [11] *VPI Componentmaker - VPI Photonics*.
- [12] K. Huybrechts, R. Baets, and G. Morthier. *All-Optical Flip-Flop Operation in a Standard Tunable DBR Laser Diode*. Photonics Technology Letters, IEEE, 21(24):1873–1875, December 2009.

- 
- [13] K. Huybrechts, A. Ali, R. Baets, and G. Morthier. *Novel concept for all-optical flip-flop operation in a single DBR laser diode*. In IEEE Photonics Society Annual Meeting Conference Proceedings, pages 648–649, 2009.



# 4

## Microdisk laser all-optical flip-flop

In the past two chapters, the application of edge-emitting laser diodes as all-optical flip-flops was discussed. Because of their large power output (and corresponding footprint and power consumption), their applicability lies more in optical telecommunication networks. For on-chip applications (such as optical logic, shift registers, optical interconnects, ...) a large amount of such components should be integrated on a single chip. In this chapter, we will elucidate how we can obtain flip-flop operation in ultra-small disk lasers (with diameters of  $7.5\ \mu\text{m}$ ) at very low power consumption (3.5 mA bias current). Moreover, these disks are integrated on silicon which is the standard material to manufacture electronic devices. This approach allows a large density of components integrated on a single chip while taking at the same time advantage of the mature technology offered by CMOS.

The results leading to flip-flop operation in a microdisk laser heterogeneously bonded on SOI [1–3] were obtained within the European FP7 Historic project by a large team of researchers from Ghent University - imec, Technical University of Eindhoven and Université de Lyon. These microdisk lasers were initially designed and demonstrated by J. Van Campenhout et al. [4, 5] and, later on, optimized by other team members to allow unidirectional operation [6]. Therefore, the focus in this chapter will *not* be on the fabrication but rather on the high-speed measurement results for which I was responsible.

## 4.1 Introduction

A lot of research has been done on the development of microscale lasers during the past 20 years (such as photonic crystal lasers [7], plasmon lasers [8], ...). Though the optical output power of such ultra-small lasers is very low, they have the important capability of being integrated densely on a chip and are in general expected to have very fast dynamics due to the small cavity roundtrip time. In this chapter, we will look into the flip-flop operation of microdisk lasers. This type of lasers has a circular cavity structure and were proposed for the first time in 1992 [9, 10]. The high-quality resonances in such a microdisk are based on the whispering gallery mode. These are modes confined very close to the edges of the disk, as depicted in Figure 4.1. A situation which is - to some extent - the optical analogue of acoustical waves propagating near the walls of a chapel or theatre. This resemblance also explains their name [11, 12].

The whispering gallery mode in a microdisk consists of a clockwise (CW) and counterclockwise (CCW) propagating mode. When the coupling between the two modes is small, a cross-gain saturation will cause one of the two modes to dominate (see section 4.2). This directional behaviour of the laser can be used for flip-flop operation. Indeed, injecting a pulse into the microdisk will facilitate lasing in the direction of that pulse. When we inject a pulse in the opposite direction, the laser will start to operate in the other directional mode. This bistable behaviour is therefore useful for set-reset flip-flop operation.

The first demonstration of flip-flop operation in ring lasers was done by M. Hill [13] in a structure consisting of two coupled ring lasers. In this structure, the light from one ring laser was used to injection-lock the other. More recently, flip-flop operation was demonstrated in a single ring laser [14]. The ring laser had a racetrack design with a radius of  $150\ \mu\text{m}$  for the circular sections and straight sections of  $200\ \mu\text{m}$ . The reported switching speed was 130 ps (switch-on) and 190 ps (switch-off) at pulse energies of 4 pJ. Using short pulses and high pulse energies, the switching times were reduced further to 20 ps in later experiments [15].

Recently, we reported the first flip-flop on silicon based on a microdisk laser [1–3]. Silicon has an indirect band gap and does therefore not support lasing operation. However, it has many other advantages. Silicon-on-insulator (SOI) offers the ideal platform for photonic integrated circuits as it has a high refractive index contrast. It can benefit from the mature CMOS fabrication technology and it is transparent at 1550 nm [16–18]. The high refractive index of silicon allows a strong light confinement and therefore also a dense integration of photonic and electronic components on a single chip. This results in low-loss waveguides with small bending radii and high quality resonator structures. Only the lack of efficient silicon laser sources has been an obstacle for the

widespread use of silicon photonics.

III-V materials (such as InP) on the other hand, can be used to realize most of the required optical functionalities but the fabrication technology is less mature. This results in a significantly lower fabrication yield compared to silicon which can rely on the decades of research and experience with CMOS technology. Moreover, the integration of passive and active structures often requires the regrowth of layers which is tedious and makes the fabrication procedure expensive. The refractive index contrast is also much lower which limits the integration density.

Heterogeneous integration of both material systems can be considered as a good compromise and combines the best properties of both material systems. This technique involves the bonding of an (active) InP epitaxial layer structure on (passive) silicon-on-insulator [19–22]. This integration can be done by molecular bonding [23] or using an adhesive polymer layer [19]. The advantage is that all the passive structures can be fabricated in silicon-on-insulator, while the active functionalities are provided by the III-V top layer. This technique has led to the fabrication of various lasers and detectors that were integrated on silicon chips [20, 21].

The first demonstration of microdisks molecularly bonded on silicon were optically pumped devices [24, 25]. Later on, the first electrically pumped microdisk laser heterogeneously integrated with a SOI waveguide was demonstrated [4, 5]. Further optimizations of the design and fabrication of the microdisks were reported in [6] and will be shortly summarized in section 4.3.

Besides flip-flop operation, the microdisks can also be used for other optical signal processing applications. Wavelength conversion up to 20 Gb/s has been demonstrated [26, 27], as well as switching of 10 Gb/s NRZ signals [28], modulation at 2.73 Gb/s [29] and multi-wavelength lasing [30].

## 4.2 Theoretical background

An approximate analytical solution of the whispering gallery modes can be found by solving the Helmholtz equation in cylindrical coordinates. This results in Bessel functions of the first kind inside the disk and Hankel functions of the second kind outside the disk. The lowest order mode profile corresponds then to the whispering gallery mode as depicted also in Figure 4.1a. Typically, one can apply a conformal transformation of the refractive index profile to calculate the modes as if in an asymmetric, straight slab waveguide [31] (illustrated in Figure 4.1b). One can see that the lowest order optical mode is confined very close to the edge of the disk. Because disk lasers do not have facets through which the light can be coupled out, an evanescent coupling towards a neighbouring waveguide is assumed in this theoretical approach.

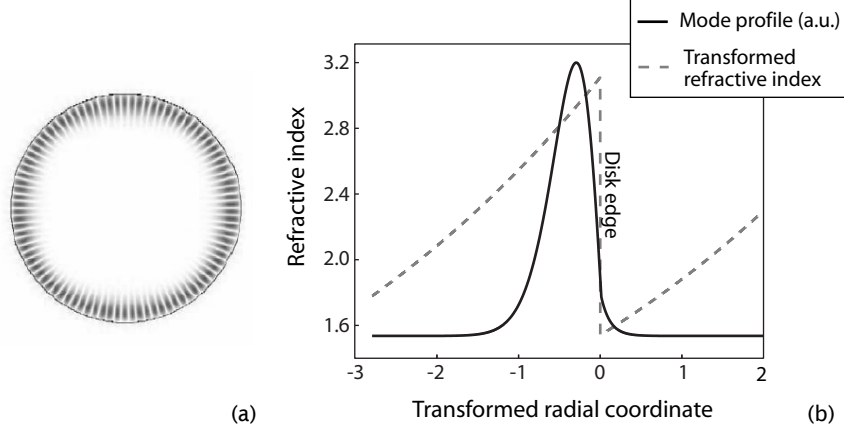


**Figure 4.1:** (a) FDTD simulation of a whispering gallery mode in a disk laser (top view) and (b) the optical mode depicted after a conformal transformation to an asymmetric, straight slab waveguide. It can be seen that the light is located near the edge of the disk. (Courtesy of [5, 32])

To explain the directional behaviour of the microdisk lasers, we formulate the rate equations now in terms of two counterpropagating modes with electric fields  $E^+$  and  $E^-$ . We find [33, 34]:

$$\frac{dE^+}{dt} = \frac{1}{2}(1 + j\alpha) \left[ G^+ - \frac{1}{\tau_p} \right] E^+ - KE^- \quad (4.1)$$

$$\frac{dE^-}{dt} = \frac{1}{2}(1 + j\alpha) \left[ G^- - \frac{1}{\tau_p} \right] E^- - KE^+ \quad (4.2)$$

where  $\alpha$  is the linewidth enhancement factor accounting for phase-amplitude coupling in the semiconductor medium,  $G$  is the modal gain factor which will be described further and  $K = K_d + jK_c$  represents an explicit linear coupling rate between the two modes where  $K_d$  is the dissipative coupling and  $K_c$  the conservative coupling. This coupling describes the effects of reflection at the end facets of the neighbouring waveguide and the reflections due to sidewall roughness.

For the carrier density rate equation, we find:

$$\frac{dN}{dt} = \frac{I}{qV} - \frac{N}{\tau_c} - G^+ |E^+|^2 - G^- |E^-|^2 \quad (4.3)$$

The gain experienced in a semiconductor material is invariably lower the higher the optical intensity. This is due to gain saturation and partly also to gain suppression. The first accounts for the drop of the total carrier population

density  $N$  with an increase in photon density  $P \sim |E|^2$  and is described correctly by the coupled rate equations. The gain suppression takes place even when the total carrier density  $N$  is constant and reflects the reduction of 'resonant carriers' due to spectral hole burning and carrier heating (see chapter 3). To account for this effect, a gain suppression is added in the denominator of the expression for the modal gain:

$$G^+ = \frac{\Gamma g_0 \nu_g (N - N_0)}{1 + \epsilon_s |E^+|^2 + \epsilon_c |E^-|^2} \quad (4.4)$$

$$G^- = \frac{\Gamma g_0 \nu_g (N - N_0)}{1 + \epsilon_s |E^-|^2 + \epsilon_c |E^+|^2} \quad (4.5)$$

where  $\epsilon_s$  reflects the self-gain suppression and  $\epsilon_c$  the cross-gain suppression.

This expression is often linearized to:

$$G^+ = \Gamma g_0 \nu_g (N - N_0) (1 - \epsilon_s |E^+|^2 - \epsilon_c |E^-|^2) \quad (4.6)$$

$$G^- = \Gamma g_0 \nu_g (N - N_0) (1 - \epsilon_s |E^-|^2 - \epsilon_c |E^+|^2) \quad (4.7)$$

It is difficult to give a precise and intuitive understanding of the underlying physical effects, but calculations have shown that  $\epsilon_c = 2\epsilon_s$  [35, 36]. The cross-gain suppression  $\epsilon_c$  will break the symmetry and enforce the unidirectional operation of the laser. The gain suppression is, however, only significant when the photon density is high. This means that at lower powers, a bidirectional regime will be present.

The equations can be transformed into a two-dimensional phase-space analysis [37] which can simplify the study of the ring laser dynamics and allow a more intuitive understanding [38, 39]. However, we will not discuss such analyses in this work.

From the above equations, we can conclude that there are two main effects in the coupling between the two modes:

1. The linear coupling  $K$  due to reflections at the end facets (dissipative) and due to sidewall roughness (conservative). Unidirectional operation is favoured by a lower value of the coupling  $K$ .
2. The nonlinear cross-gain suppression prohibits the counterpropagating cavity mode to build up. This effect is necessary for the unidirectional operation and is present at large values of the photon density.

The above equations have been used to implement a simulation tool to study the influence of the laser parameters. More information on this topic can be found in the Master thesis of Y. De Koninck [32]. In Figure 4.2, a typical light-current (L-I) graph of a ring/disk laser structure is depicted. We can distinguish between three different regimes. The first regime, just after threshold, is the bidirectional regime where the two counterpropagating modes are

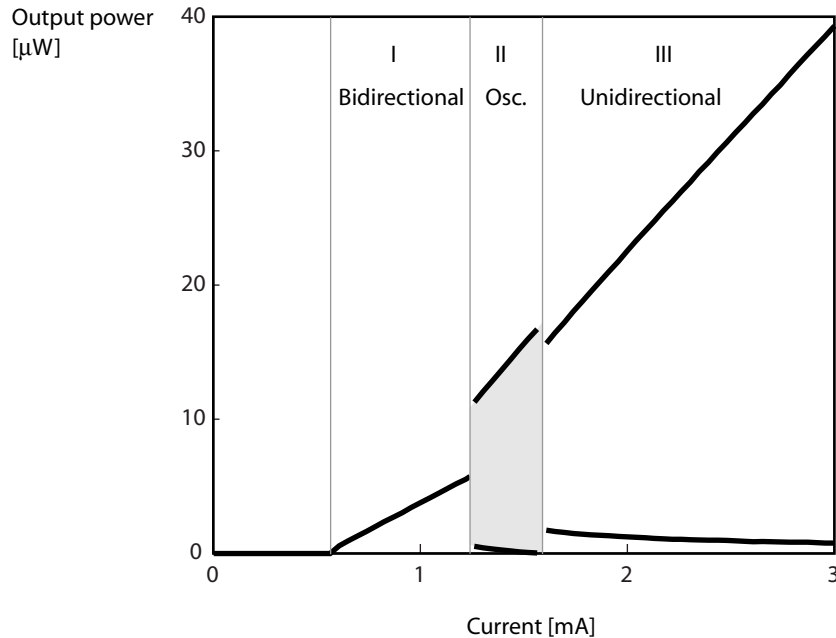


**Figure 4.2:** A simulation of the L-I graph with the different regimes. (Courtesy of [32]).

equally present. There will be a small notch in their spectrum as the coupling between the two modes will introduce a very small frequency splitting. When the injection current is increased, we can have a bidirectional regime with alternating oscillations [33, 40]. In this regime, the intensities of the two counterpropagating modes are modulated with harmonic sinusoidal oscillations. The modulation is out-of-phase (or alternate) which means that the power in one mode is high when it is low in the other mode. The graph depicts the maximal and minimal values of the mode intensities. The last regime corresponds to the unidirectional operation where the initial conditions determine which of the two modes is dominant [41]. By injecting a pulse in one of the modes, one can switch the lasing direction to that mode which results in flip-flop operation.

Using the simulation tool, we can also study the switching dynamics of the flip-flop operation. This has been done extensively in [32, 42]. These simulations indicate that for a microdisk with a diameter of  $10\ \mu\text{m}$  which is biased at 3 mA, a minimal pulse energy of 2.6 fJ is required and switching is possible with a 10%-90% rise time of a few picoseconds. The extinction ratio is predicted to

be 12 dB and can be enhanced by using a structure of two coupled disk lasers. It was also shown by simulations that structures comprised of coupled disks are efficient as chaotic transmitters [43]

### 4.3 Device structure

A schematic of the entire structure with the bonded microdisk is given in Figure 4.3. An unpatterned III-V layer structure was bonded on an SOI circuit by an adhesive die-to-wafer bonding technology [20]. The polymer used for bonding was DVS-BCB (divinylsiloxane-benzocyclobuten). The SOI circuit was fabricated using 193 nm DUV lithography and has a top silicon layer of 220 nm. After removing the InP substrate, contact lithography was used to define the microdisk pattern. This technique allows to carefully align the microdisk patterns with the SOI waveguides. After etching, very small microdisk lasers are obtained with a diameter of only 7.5  $\mu\text{m}$ . After polymer deposition and etching of contact vias, the metal contacts are defined. This results in a structure where electrically driven microdisk lasers are bonded on top of a silicon waveguide. The evanescent field of the microdisk will then couple with the silicon waveguide underneath. The light can be coupled out of the chip into an optical fiber using a grating coupler [44]. Such grating couplers allow an efficiency of about 30%. The presence of a metallic contact on top of the microdisk, will prevent higher order modes to build up as it increases the losses at the center of the disk.

Theory predicts that the unidirectional regime only appears in structures with a low coupling between CW and CCW modes and with a high photon density. Therefore, several improvements were made to the initial microdisk design by team members from the FP7 Historic and Wadimos project, in order to allow stable and unidirectional operation [6]. First of all, the sidewall roughness was reduced by applying an optimized etching process (at TU/e). Second, the thickness of the epitaxial layer structure was altered to 580 nm instead of 950 nm. Moreover, the tunnel junction, consisting of a heavily doped p-layer, was placed on top of the microdisk with an optimized growth process in order to reduce absorption losses. Finally, by adding a heat sink on top of the microdisk, the thermal roll-over improved by a factor of two.

### 4.4 Measurement results

The light-current (L-I) characteristic of the microdisk, measured at the two ends of the SOI waveguide, is depicted in Figure 4.4. This measurement is taken under continuous wave operation and at room temperature. When the thresh-

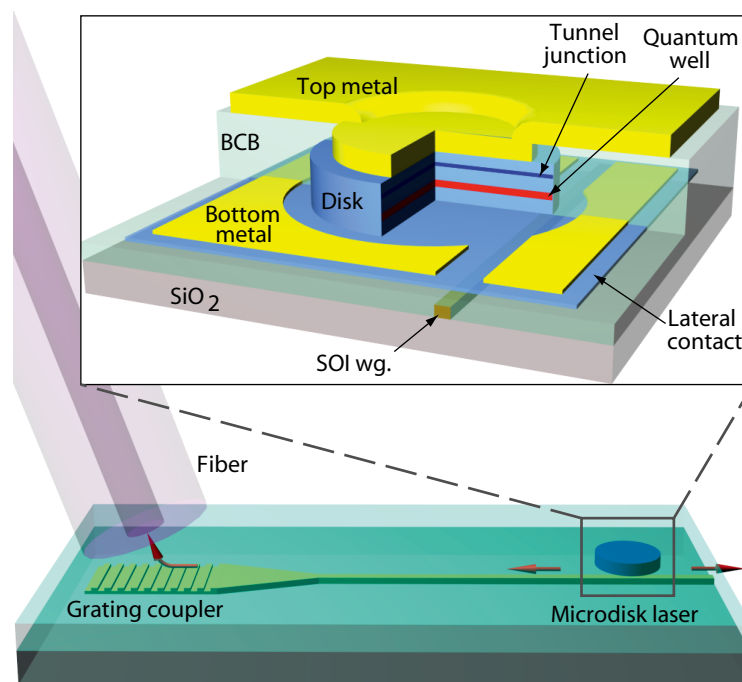


**Figure 4.3:** A schematic of the entire circuit and bonded microdisk. (Courtesy of L. Liu)

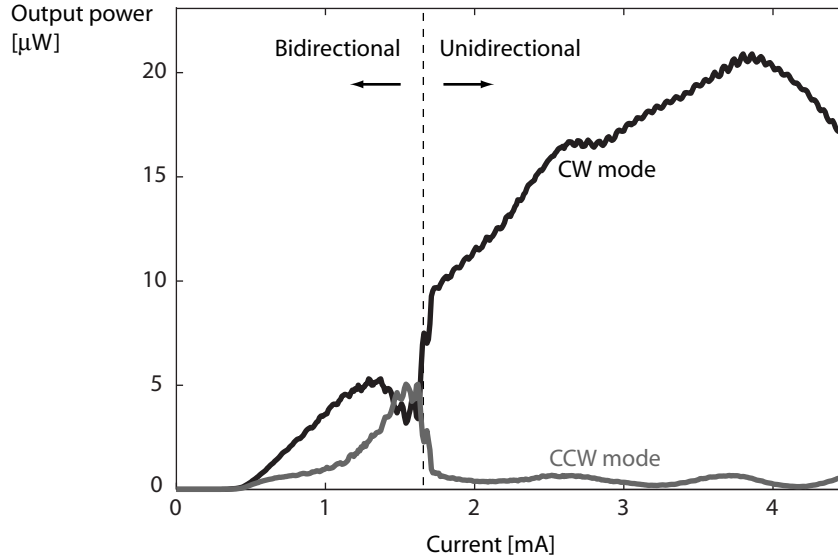


**Figure 4.4:** The measured L-I characteristic of the microdisk indicates that unidirectional operation starts at 1.7 mA.

old current of 0.33 mA is surpassed, a bidirectional regime can be observed. In the bidirectional regime, the clockwise and counterclockwise mode are equally present. The difference in output power between both sides is due to a different attenuation by the waveguides and small alignment mismatches. Between 1.4 mA and 1.7 mA, there is a small periodic oscillating regime due to the reflection feedback from the grating coupler and/or the fibre facet. Because of the low speed of the detector, only the average power of the oscillation is depicted here. The unidirectional, bistable operation starts at 1.7 mA. Due to the improved thermal management, the thermal rollover only starts at 3.8 mA. The maximal optical output power was measured to be  $20 \mu\text{W}$  (normalized with respect to the coupling loss of the grating). In large ring lasers, the lasing direction switches while increasing the current in the unidirectional regime [45]. Theoretical calculations [46] predict that this switching behaviour occurs due to self-heating when the laser mode hops to a different azimuthal order that is several free spectral ranges away. This means that such mode-hopping is unlikely to be present in such a small cavity because the free spectral range is too large.

The lasing spectrum of the clockwise mode is depicted in Figure 4.5. This spectrum is taken at a bias current of 3.8 mA. It clearly indicates that there is single-mode lasing operation and the free spectral range is 30.4 nm. It can be

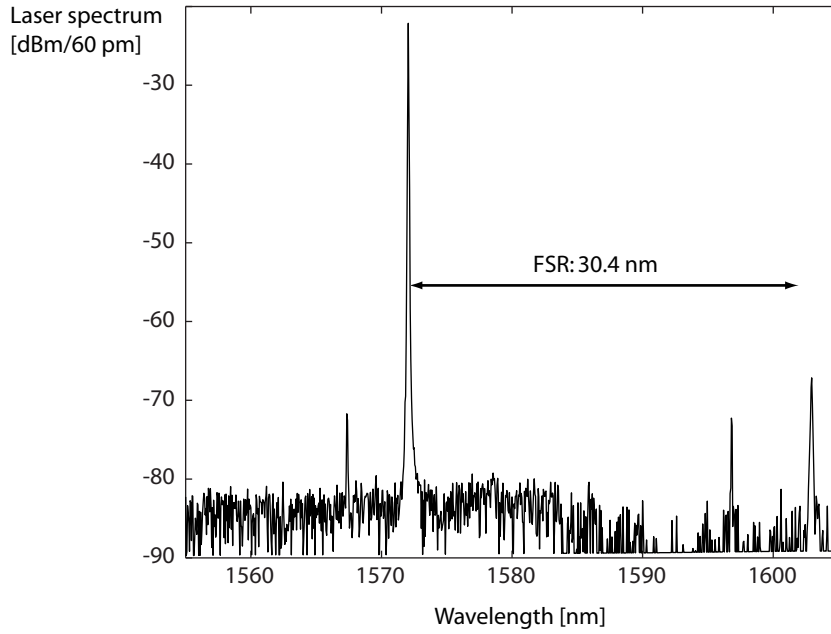


**Figure 4.5:** The spectrum of the clockwise mode of the microdisk at a bias of 3.8 mA indicates unimodal operation with a free spectral range of 30.4 nm.

seen that the side-mode suppression ratio is higher than 40 dB.

The measurement set-up is schematically depicted in Figure 4.6. Light from a tunable laser source is sent through a modulator which is driven by a 10 Gb/s pulse pattern generator. This results in pulses with a width of 100 ps. We use polarization controlling wheels after the laser source because the modulator works only in TE mode. The pulses are split by a 3 dB coupler and a variable optical delay line (ODL) is placed in one of the arms to adjust the relative arrival time between the set and reset pulses. Variable optical attenuators allow to adjust the pulse power. Because the grating couplers are polarization dependent, we use again polarization controlling wheels, before the pulses are sent into the chip. With circulators on both sides, we can monitor the output power of the microdisk on a high-speed optical sampling scope. To overcome the dark current of the detector, the signal power should be larger than 100-200  $\mu\text{W}$ . Therefore, we use an erbium-doped fiber amplifier (EDFA) to increase the signal power ( $\sim 25$  dB amplification) in combination with an optical band-pass filter (OBPF) with  $\Delta\lambda=0.9$  nm to remove amplified spontaneous emission (ASE).

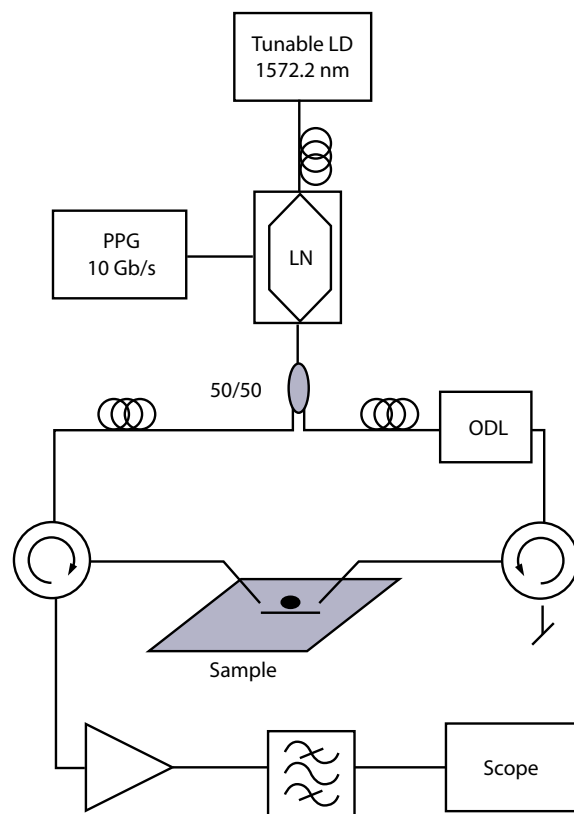


**Figure 4.6:** Schematic of the measurement set-up.

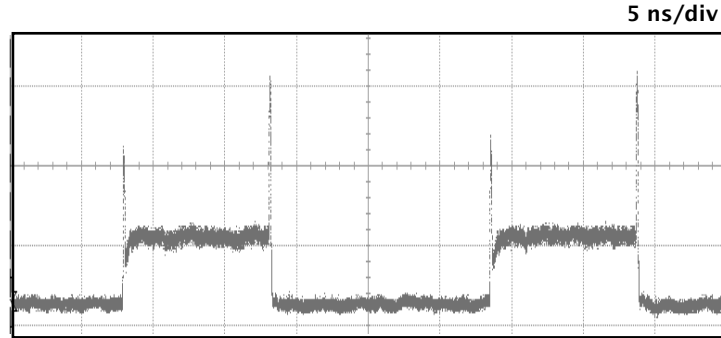


**Figure 4.7:** Measurement result for flip-flop operation in a microdisk laser integrated on silicon.

The high-speed measurement result of the flip-flop operation is depicted in Figure 4.7. The microdisk is biased at 3.5 mA which is about twice the threshold current for unidirectional operation. At too low currents, self-switching due to noise can be observed. When we inject a pulse on the left side of the microdisk, the laser will start to operate in the counter-clockwise dominant state. This state will remain, even after the pulse has passed through. Injection of a (reset) pulse at the other side, will suppress the counter-clockwise mode and induce the clockwise dominant state. The minimal pulse energies needed to switch the microdisk lasers are 1.8 fJ (calculated inside the SOI waveguide by taking into account the efficiency of the grating coupler). The extinction ratio was measured to be 11 dB which was slightly less than observed in a previously done slow-speed measurement (13 dB). This difference is mainly due to the amplified spontaneous emission (ASE) of the EDFA. Further increasing the peak power of injected pulses induced a strong relaxation oscillation at the switch-on transient, due to the deep depletion of the carriers. The injected pulses cover the transient of the microdisk output, making it difficult to determine the exact switching speeds. Even the reset-pulse appears at the output because of reflection at the cleaved facet of the access fibre. This could be suppressed - to some extent- by using an index-matching fluid. A switching time of 60 ps was obtained this way.

## 4.5 Conclusions

In this chapter, we described the flip-flop operation in ultra-small microdisk lasers that were integrated on silicon. The devices have a diameter of only 7.5  $\mu\text{m}$  and require a bias current of only 3.5 mA. The switching energies can

be as low as 1.8 fJ. The small footprint and power consumption of these devices make them interesting for large-scale integration with applications such as optical shift registers or random access memories (RAMs). The principle relies on the unidirectional operation of the disks due to the nonlinear gain suppression from spectral hole burning and carrier heating.

## References

- [1] L. Liu, R. Kumar, K. Huybrechts, T. Spuesens, G. Roelkens, E.-J. Geluk, T. de Vries, P. Regreny, D. Van Thourhout, R. Baets, and G. Morthier. *An ultra-small, low-power, all-optical flip-flop memory on a silicon chip*. *Nature Photonics*, 4(3):182–187, 2010.
- [2] K. Huybrechts, L. Liu, R. Kumar, T. Spuesens, G. Roelkens, E.-J. Geluk, T. de Vries, M.K. Smit, P. Regreny, P. Rojo-Romeo, D. Van Thourhout, R. Baets, and G. Morthier. *Digital photonics using InP microdisk lasers heterogeneously integrated on silicon-on-insulator*. In 15th European Conference on Integrated Optics (ECIO 2010), April 2010.
- [3] R. Kumar, K. Huybrechts, L. Liu, T. Spuesens, G. Roelkens, E.-J. Geluk, T. de Vries, P. Regreny, D. Van Thourhout, R. Baets, and G. Morthier. *An ultra-small, low-power, all-optical flip-flop memory on a silicon chip*. In Optical Fiber Conference and Exposition (OFC), 2010.
- [4] J. Van Campenhout, P. Rojo-Romeo, P. Regreny, C. Seassal, D. Van Thourhout, S. Verstuyft, L. Di Cioccio, J. M. Fedeli, C. Lagahe, and R. Baets. *Electrically pumped InP-based microdisk lasers integrated with a nanophotonic silicon-on-insulator waveguide circuit*. *Optics Express*, 15(11):6744–6749, 2007.
- [5] J. Van Campenhout. *Thin-Film Microlasers for the Integration of Electronic and Photonic Integrated Circuits*. PhD thesis, Ghent University, 2007.
- [6] T. Spuesens, Liu Liu, T. de Vries, P.R. Romeo, P. Regreny, and D. Van Thourhout. *Improved design of an InP-based microdisk laser heterogeneously integrated with SOI*. In 6th IEEE International Conference on Group IV Photonics, 2009, pages 202–204, sep 2009.
- [7] O. Painter, R. K. Lee, A. Scherer, A. Yariv, J. D. O'Brien, P. D. Dapkus, and I. Kim. *Two-dimensional photonic band-gap defect mode laser*. *Science*, 284(5421):1819–1821, 1999.
- [8] R. F. Oulton, V. J. Sorger, D. A. Genov, D. F. P. Pile, and X. Zhang. *A hybrid plasmonic waveguide for subwavelength confinement and long-range propagation*. *Nature Photonics*, 2(8):496–500, 2008.
- [9] S. L. McCall, A. F. J. Levi, R. E. Slusher, S. J. Pearton, and R. A. Logan. *Whispering-gallery mode microdisk lasers*. *Applied Physics Letters*, 60(3):289–291, 1992.

- [10] A.F.J. Levi, R.E. Slusher, S.L. McCall, T. Tanbun-Ek, D.L. Coblentz, and S.J. Pearton. *Room temperature operation of microdisc lasers with submilliamp threshold current*. Electronics Letters, 28(11):1010–1012, may 1992.
- [11] Lord Rayleigh. *The problem of the whispering gallery*. Philosophical Magazine Series 6, 20(120):1001–1004, 1910.
- [12] A. E. Bate. *Note on the whispering gallery of St Paul's Cathedral, London*. Proceedings of the Physical Society, 50(2):293, 1938.
- [13] M. T. Hill, H. J. S. Dorren, T. de Vries, X. J. M. Leijtens, J. H. den Besten, B. Smalbrugge, Y. S. Oei, H. Binsma, G. D. Khoe, and M. K. Smit. *A fast low-power optical memory based on coupled micro-ring lasers*. Nature, 432(7014):206–209, 2004.
- [14] A. Trita, G. Mezosi, F. Bragheri, Yu Jin, S. Furst, W. Elsasser, I. Cristiani, M. Sorel, and G. Giuliani. *Dynamic operation of all-optical flip-flop based on a monolithic semiconductor ring laser*. In 34th European Conference on Optical Communication (ECOC 2008), 2008.
- [15] A. Trita, M.J. Latorre Vidal, M. Zanola, G. Mezosi, J. Javaloyes, M. Sorel, F. Bragheri, I. Cristiani, A. Scire, S. Balle, and G. Giuliani. *All-optical set-reset flip-flop based on semiconductor ring laser: ultrafast response and error-free bit-error-rate operation*. In International Conference on Photonics in Switching (PS '09), sep 2009.
- [16] S.K. Selvaraja, P. Jaenen, W. Bogaerts, D. Van Thourhout, P. Dumon, and R. Baets. *Fabrication of Photonic Wire and Crystal Circuits in Silicon-on-Insulator Using 193-nm Optical Lithography*. Journal of Lightwave Technology, 27(18):4076–4083, sep 2009.
- [17] W. Bogaerts, R. Baets, P. Dumon, V. Wiaux, S. Beckx, D. Taillaert, B. Luyssaert, J. Van Campenhout, P. Bienstman, and D. Van Thourhout. *Nanophotonic waveguides in silicon-on-insulator fabricated with CMOS technology*. Journal of Lightwave Technology, 23(1):401–412, 2005.
- [18] W. Bogaerts. *Nanophotonic Waveguides and Photonic Crystals in Silicon-on-Insulator*. PhD thesis, Ghent University, 2004.
- [19] G. Roelkens, J. Van Campenhout, J. Brouckaert, D. Van Thourhout, R. Baets, P. R. Romeo, P. Regreny, A. Kazmierczak, C. Seassal, X. Letartre, G. Hollinger, J. M. Fedeli, L. Di Cioccio, and C. Lagahe-Blanchard. *III-V/Si photonics by die to wafer bonding*. Materials Today, 10(7-8):36–43, 2007.

- [20] G. Roelkens, D. Van Thourhout, R. Baets, R. Notzel, and M. Smit. *Laser emission and photodetection in an InP/InGaAsP layer integrated on and coupled to a Silicon-on-Insulator waveguide circuit*. Optics Express, 14(18):8154–8159, 2006.
- [21] J. Brouckaert, G. Roelkens, D. Van Thourhout, and R. Baets. *Thin-film III-V photodetectors integrated on silicon-on-insulator photonic ICs*. Journal of Lightwave Technology, 25(4):1053–1060, 2007.
- [22] G. Roelkens. *Heterogeneous III-V/Silicon Photonics: Bonding Technology and Integrated Devices*. PhD thesis, Ghent University, 2007.
- [23] U. Gosele and Q. Y. Tong. *Semiconductor wafer bonding*. Annual Review of Materials Science, 28:215–241, 1998.
- [24] C. Seassal, P. Rojo-Romeo, X. Letartre, P. Viktorovitch, G. Hollinger, E. Jalaguier, S. Pocas, and B. Aspar. *InP microdisk lasers on silicon wafer: CW room temperature operation at 1.6  $\mu\text{m}$* . Electronics Letters, 37(4):222–223, feb 2001.
- [25] H. T. Hattori, C. Seassal, E. Touraille, P. Rojo-Rmeo, X. Letartre, G. Hollinger, P. Viktorovitch, L. Di Cioccio, M. Zussy, L. El Melhaoui, and J. M. Fedeli. *Heterogeneous integration of microdisk lasers on silicon strip waveguides for optical interconnects*. IEEE Photonics Technology Letters, 18(1-4):223–225, 2006.
- [26] L. Liu, J. Van Campenhout, G. Roelkens, D. Van Thourhout, P. Rojo-Romeo, P. Regreny, C. Seassal, J. M. Fedeli, and R. Baets. *Ultralow-power all-optical wavelength conversion in a silicon-on-insulator waveguide based on a heterogeneously integrated III-V microdisk laser*. Applied Physics Letters, 93(6):3, 2008.
- [27] O. Raz, R. Kumar, G. Morthier, D. Van Thourhout, P. Regreny, P. Rojo-Romeo, T. de Vries, and H.J.S. Dorren. *Compact, low power and low threshold electrically pumped micro disc lasers for 20Gb/s non return to zero all optical wavelength conversion*. In The Optical Fiber Communication Conference and Exposition (OFC 2010), 2010.
- [28] Liu Liu, G. Roelkens, T. Spuesens, R. Soref, P. Regreny, D. Van Thourhout, and R. Baets. *Low-power electro-optical switch based on a III-V microdisk cavity on a silicon-on-insulator circuit*. In 2009 Asia Communications and Photonics Conference and Exhibition (ACP 2009), Shanghai, China, 2009.

- [29] L. Liu, J. Van Campenhout, G. Roelkens, R. A. Soref, D. Van Thourhout, P. Rojo-Romeo, P. Regreny, C. Seassal, J. M. Fedeli, and R. Baets. *Carrier-injection-based electro-optic modulator on silicon-on-insulator with a heterogeneously integrated III-V microdisk cavity*. Optics Letters, 33(21):2518–2520, 2008.
- [30] J. Van Campenhout, L. Liu, P. Rojo-Romeo, D. Van Thourhout, C. Seassal, P. Regreny, L. Di Cioccio, J. M. Fedeli, and R. Baets. *A compact SOI-integrated multiwavelength laser source based on cascaded InP microdisks*. IEEE Photonics Technology Letters, 20(13-16):1345–1347, 2008.
- [31] N. C. Frateschi and A. F. J. Levi. *Resonant modes and laser spectrum of microdisk lasers*. Applied Physics Letters, 66(22):2932–2934, 1995.
- [32] Y. De Koninck. *Niet-lineaire dynamica van enkelvoudige en gekoppelde microschijflasers*. Master's thesis, Ghent University, 2009.
- [33] M. Sorel, G. Giuliani, A. Scire, R. Miglierina, S. Donati, and P. J. R. Laybourn. *Operating regimes of GaAs-AlGaAs semiconductor ring lasers: Experiment and model*. IEEE Journal of Quantum Electronics, 39(10):1187–1195, 2003.
- [34] T. Numai. *Analysis of signal voltage in a semiconductor ring laser gyro*. IEEE Journal of Quantum Electronics, 36(10):1161–1167, 2000.
- [35] E. J. D'angelo, E. Izaguirre, G. B. Mindlin, G. Huyet, L. Gil, and J. R. Tredicce. *Spatiotemporal dynamics of lasers in the presence of an imperfect  $O(2)$  symmetry*. Physical Review Letters, 68(25):3702–3705, 1992.
- [36] M. Sargent. *Theory of a multimode quasi-equilibrium semiconductor-laser*. Physical Review A, 48(1):717–726, 1993.
- [37] G. Van der Sande, L. Gelens, P. Tassin, A. Scire, and J. Danckaert. *Two-dimensional phase-space analysis and bifurcation study of the dynamical behaviour of a semiconductor ring laser*. Journal of Physics B-Atomic Molecular and Optical Physics, 41(9):095402, 2008.
- [38] L. Gelens, S. Beri, G. Van der Sande, J. Danckaert, N. Calabretta, H. J. S. Doreen, R. Notzel, Eajm Bente, and M. K. Smit. *Optical injection in semiconductor ring lasers: backfire dynamics*. Optics Express, 16(15):10968–10974, 2008.
- [39] L. Gelens, G. Van der Sande, S. Beri, and J. Danckaert. *Phase-space approach to directional switching in semiconductor ring lasers*. Physical Review E, 79(1):016213, 2009.

- 
- [40] M. Sorel, P. J. R. Laybourn, A. Scire, S. Balle, G. Giuliani, R. Miglierina, and S. Donati. *Alternate oscillations in semiconductor ring lasers*. *Optics Letters*, 27(22):1992–1994, 2002.
- [41] M. Sorel, P. J. R. Laybourn, G. Giuliani, and S. Donati. *Unidirectional bistability in semiconductor waveguide ring lasers*. *Applied Physics Letters*, 80(17):3051–3053, 2002.
- [42] T. Pérez, A. Scirè, G. Van der Sande, P. Colet, and C. R. Mirasso. *Bistability and all-optical switching in semiconductor ring lasers*. *Optics Express*, 15(20):12941–12948, 2007.
- [43] Y. De Koninck, K. Huybrechts, G. Van der Sande, J. Danckaert, R. Baets, and G. Morthier. *Nonlinear dynamics of asymmetrically coupled microdisk lasers*. In 22nd Annual Meeting of the IEEE Photonics Society, Turkey, 2009.
- [44] D. Taillaert, W. Bogaerts, P. Bienstman, T. F. Krauss, P. Van Daele, I. Moerman, S. Verstuyft, K. De Mesel, and R. Baets. *An out-of-plane grating coupler for efficient butt-coupling between compact planar waveguides and single-mode fibers*. *IEEE Journal of Quantum Electronics*, 38(7):949–955, 2002.
- [45] G. Mezosi, M. J. Strain, S. Furst, Z. Wang, S. Yu, and M. Sorel. *Unidirectional Bistability in AlGaInAs Microring and Microdisk Semiconductor Lasers*. *IEEE Photonics Technology Letters*, 21(1-4):88–90, 2009.
- [46] S. Furst, A. Perez-Serrano, A. Scire, M. Sorel, and S. Balle. *Modal structure, directional and wavelength jumps of integrated semiconductor ring lasers: Experiment and theory*. *Applied Physics Letters*, 93(25):3, 2008.

# 5

## Network motifs of coupled nonlinear cavities

In the previous chapter, it was shown that nonlinear effects in the gain material are able to break the directional symmetry of a microdisk laser, resulting in a regime with unidirectional operation. In this chapter, we will use a different form of symmetry breaking which is based on the Kerr nonlinearity in structures composed of multiple (passive) resonators. The Kerr nonlinearity will introduce a slight shift in the index of refraction at high optical powers and therefore also shift the resonance frequency of the cavities. We will show that these frequency shifts result in symmetry breaking for small ring-like network motifs consisting of three and four identical cavities. This means that, when an equal amount of light is injected in the different (coupled) cavities, the optical output powers will differ, even when the structure itself (and its excitation) is completely symmetrical.

Using coupled-mode theory, we will derive analytical conditions for which symmetry breaking can occur. Time-domain calculations show that it is possible to switch between the different asymmetric states by injecting optical pulses. Cyclical switching action is presented leading to multi-stable, all-optical flip-flop operation. This chapter differs from others in the sense that combinations of passive structures are used instead of single laser diodes. Moreover, the results are only of a theoretical nature and have not yet been demonstrated

experimentally.

## 5.1 Introduction

The rich and intricate dynamical behaviour exhibited by structures with coupled nonlinear photonic cavities opens up a whole new range of applications such as photonic reservoir computing [1], slow light engineering [2] and all-optical flip-flop operation [3]. Therefore it is important to develop clear insights into the possible states and instabilities of progressively more complex designs. By now, networks of hundreds of coupled cavities have been studied experimentally in the linear regime [4] and the logical next step is to study the effects of the nonlinearities in smaller networks. Network motifs consisting of three or four nodes [5] already have a significant degree of complexity, and here our aim is to examine the nonlinear properties of such photonic cavity designs.

Symmetry breaking is a counterintuitive physical effect that describes the appearance of asymmetric states while the structure under study, and its excitation, is completely symmetric. In previous work [3, 6], it was shown that two coupled nonlinear cavities can exhibit symmetry breaking: when equal power is injected on both sides of the coupled cavities, the reflected output power is different on both sides due to the nonlinear effects. The symmetry breaking would not be possible in a linear structure, but is based on the nonlinear Kerr effect. This Kerr effect (or quadratic electro-optic effect) can be mathematically represented by a refractive index  $n$  which depends linearly on the intensity of the light ( $\sim|E|^2$ ):

$$n = n_0 + n_2|E|^2 \quad (5.1)$$

with  $n_0$  the linear refractive index of the material and  $n_2$  the Kerr coefficient. This means that the refractive index of the cavities will undergo a small change which affects their resonance wavelength.

Here, we will couple three and four passive cavities with a Kerr-based nonlinearity in a symmetric structure. In addition, the system is excited equally from all sides with a holding beam. We show that these symmetric setups result in different nonlinear regimes with various kinds of asymmetric states. Using coupled-mode theory, we derive analytical conditions for the symmetry breaking detuning requirements. Furthermore, using time-domain studies, we demonstrate multi-state flip-flop operation [7, 8]. In these cases a cyclical switching action is obtained.

Our description is quite general and therefore independent of the exact implementation. The system could be implemented with compact nonlinear photonic crystal cavities [9–11] or ring resonators [12]. Recently demonstrated hybrid material systems are also a promising solution [13].

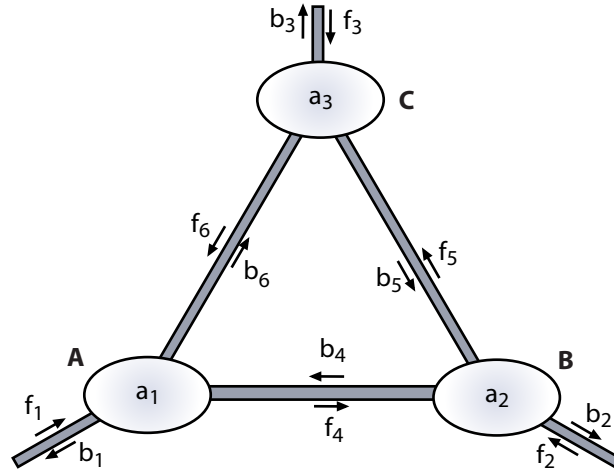


**Figure 5.1:** A schematic representation of a symmetric structure of three coupled cavities.

We will start by discussing the behaviour of three cavities in a triangular configuration. Using coupled-mode theory we derive an analytical condition for symmetry breaking in this structure. Afterwards we look at the different asymmetric states under steady state conditions and we conclude by studying the dynamical behaviour with the multi-state flip-flop operation. We do the same for a configuration of four cavities: after deriving an analytical condition for symmetry breaking and discussing the steady state behaviour, we give insight in the switching between the asymmetric states.

## 5.2 Three coupled cavities

### 5.2.1 Symmetry breaking condition

We apply coupled-mode theory on a symmetric structure consisting of three coupled nonlinear cavities as depicted in Figure 1. The time dependence of the

amplitude  $a_i$  of the resonance modes of the cavities is given by [14, 15]:

$$\frac{da_1}{dt} = \left[ j(\omega_0 + \delta\omega_1) - \frac{1}{\tau} \right] a_1 + df_1 + db_4 + df_6 \quad (5.2)$$

$$\frac{da_2}{dt} = \left[ j(\omega_0 + \delta\omega_2) - \frac{1}{\tau} \right] a_2 + df_2 + db_5 + df_4 \quad (5.3)$$

$$\frac{da_3}{dt} = \left[ j(\omega_0 + \delta\omega_3) - \frac{1}{\tau} \right] a_3 + df_3 + db_6 + df_5 \quad (5.4)$$

Here  $f_i$  and  $b_i$  are the forward and backward propagating mode amplitudes in the waveguides. We assume the three cavities have the same resonant mode with center frequency  $\omega_0$  and with at least a three-fold symmetry (e.g. monopole) in order to have the same coupling  $d$  to the three waveguides. The nonlinear frequency shift due to the Kerr nonlinearity is given by

$$\delta\omega_i = \frac{-|a_i|^2}{P_0\tau^2} \quad (5.5)$$

with  $P_0$  the characteristic nonlinear power of the cavity [14] and  $\tau$  the lifetime of the cavity which can be related to the  $Q$ -factor as  $Q = \omega_0\tau/2$ . A formula for the coupling  $d$  between the waveguide modes and the cavity can be derived by applying energy conservation laws on the coupled-mode equations [15] and we find

$$d = j\sqrt{\frac{2}{3\tau}} \exp\left(j\frac{\phi}{2}\right) \quad (5.6)$$

Here,  $\phi$  represents the phase depending on the waveguide length and the reflection properties. For high- $Q$  cavities and small detunings,  $\phi$  will be quasi independent of the frequency.

The amplitudes of the forward and backward propagating waves are coupled by [16]:

$$f_4 = \exp(j\phi)b_4 + da_1 \quad (5.7)$$

$$b_4 = \exp(j\phi)f_4 + da_2 \quad (5.8)$$

Similar equations hold for the other waveguides.

The analysis will be done in the frequency domain so  $d/dt$  will be replaced by  $j\omega$  (with  $\omega$  the operating frequency). The forward and backward internal waveguide amplitudes can be eliminated in equations (5.2-5.4) and we obtain:

$$\left[ j(\omega_0 - \omega + \delta\omega_1) - \frac{1}{\tau} \right] a_1 + \kappa(2\gamma a_1 + a_2 + a_3) = -df_1 \quad (5.9)$$

$$\left[ j(\omega_0 - \omega + \delta\omega_2) - \frac{1}{\tau} \right] a_2 + \kappa(2\gamma a_2 + a_1 + a_3) = -df_2 \quad (5.10)$$

$$\left[ j(\omega_0 - \omega + \delta\omega_3) - \frac{1}{\tau} \right] a_3 + \kappa(2\gamma a_3 + a_1 + a_2) = -df_3 \quad (5.11)$$

with  $\gamma = \exp(j\phi)$  and  $\kappa = d^2/(1 - \gamma^2)$ . In our further analysis, we will use dimensionless cavity energies  $A = -|a_1|^2/P_0\tau$ ,  $B = -|a_2|^2/P_0\tau$  and  $C = -|a_3|^2/P_0\tau$ , and a dimensionless detuning  $\Delta = \tau(\omega_0 - \omega)$ . This detuning  $\Delta$  can be expressed also in terms of the linewidth  $\delta\Omega$  of the cavity mode as  $\Delta = 2(\omega_0 - \omega)/\delta\Omega$ . To examine the effect of symmetry breaking we assume equal input powers and phases from all sides (i.e.  $f_1 = f_2 = f_3$ ). Elimination of  $f_1$  in the above equations gives:

$$\left[-\frac{1}{3} + j(\Delta' + A)\right] a_1 = \left[-\frac{1}{3} + j(\Delta' + B)\right] a_2 \quad (5.12)$$

$$= \left[-\frac{1}{3} + j(\Delta' + C)\right] a_3 \quad (5.13)$$

with

$$\Delta' = \Delta - \frac{2\cos(\phi) - 1}{3\sin(\phi)}. \quad (5.14)$$

We take the modulus squared of equation (5.12) and after factoring we get:

$$(A - B) \left( B^2 + (A + 2\Delta')B + A^2 + 2\Delta'A + \Delta'^2 + \frac{1}{9} \right) = 0. \quad (5.15)$$

A similar equation holds for the relation between  $A$  and  $C$ . Apart from the symmetric solutions derived from the first factor ( $A = B = C$ ), there is also the possibility of an asymmetric solution (second factor) if the detuning  $\Delta'$  is chosen correctly and if the solution is stable. The factor of the asymmetric solution can be seen as a quadratic equation in  $B$  for which the discriminant has to be positive for the existence of real solutions:

$$-3A^2 - 4\Delta'A - \frac{4}{9} > 0 \quad (5.16)$$

This condition is fulfilled if  $A$  lies between the values

$$-\frac{2\Delta'}{3} \pm \frac{2\sqrt{9\Delta'^2 - 3}}{9} \quad (5.17)$$

Thus the asymmetric solution exists if  $|\Delta'| > 1/\sqrt{3}$ . In case of a self-focusing Kerr effect (positive nonlinearity),  $A$  is negative and therefore the condition for symmetry breaking is:

$$\Delta' > \frac{1}{\sqrt{3}} \quad (5.18)$$

### 5.2.2 Static solutions

By solving the coupled-mode equations under steady state conditions, we can find the static solutions as a function of the input power. In addition, a stability analysis needs to be performed to determine which of the possible states are stable, and thus excitable in experiments.

The linear stability analysis is created by evaluating the eigenvalues of the Jacobian matrix for the obtained states. Therefore we rewrite equations (5.2-5.4) into 6 ordinary differential equations (ODE's) where the phase and amplitude are considered separately. The elements of the Jacobian matrix are obtained by taking the derivatives of these equations to each of the variables (amplitude and phase of  $a_i$ ). After evaluating this  $6 \times 6$  Jacobian matrix in the possible solutions, we can determine the corresponding eigenvalues. If the real part of all these eigenvalues is negative, the system will move into the direction of the equilibrium point.

The stable output powers are depicted as a function of the input power in two different configurations where the condition for symmetry breaking (Equation 5.18) is fulfilled (Figure 5.2). One can clearly observe that besides the symmetric solution (all output powers the same and equal to  $P_{in}$ ), asymmetric solutions show up for a certain range of input powers (regions I, II and III). With increasing input power, we uncover a distinctive progression through three possible symmetry breaking regimes. In region I of Figure 5.2a, we distinguish solutions where two out of three output powers are equal and have a higher value than the third output which is low. By increasing the input power, the two equal outputs split up (region II) and the symmetry breaking in the system is complete: all three output powers are different. This state then transforms to region III where two low output powers are equal and the third output is high. When we change the phase  $\phi$ , we find the bifurcation depicted in Figure 5.2b where the same states appear but in a different order. The parameters of the two examples are chosen in order to show the three possible regimes in a single example, but were not optimized for possible other conditions. Higher values for the detuning  $\Delta$  seem to increase the extinction ratio but also moves the asymmetric regime to higher input powers. However, we did not perform extensive analysis on this matter.

To have more insight in the symmetric solution of Figure 5.2a, we depict the energy of the resonant modes in the cavities as a function of the input power (Figure 5.3). It appears that the symmetric solution itself exhibits also a bifurcation structure. Despite this bifurcation in the cavity energies of the symmetric solutions, this asymmetry does not show up in the output powers of Figure 2 because the two branches have equal output powers (cfr. conservation of energy), but a different phase. In the lower branch, the symmetric solution becomes unstable for certain input powers and in that range the asymmetric solutions are possible. This means that we can avoid the symmetric solutions of the upper branch if we stay below the input power threshold of  $P_{in} \approx 4.5P_0$ . For the second case (with  $\phi = 2.0$ ), this bistability in the symmetric solution does not show up and we find that only stable asymmetric solutions appear in the region of symmetry breaking.

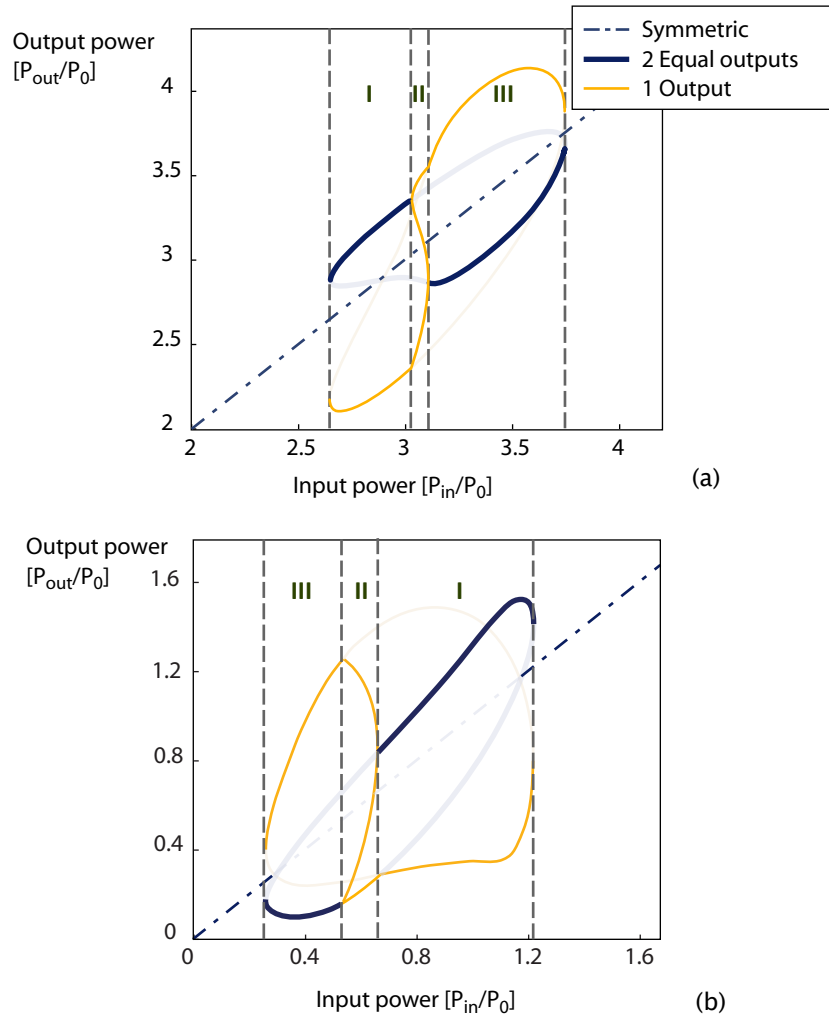


**Figure 5.2:** The states of the output power as a function of the input power for a structure with (a)  $\Delta = 0.1$  and  $\phi = -0.5$  and (b)  $\Delta = 0.1$  and  $\phi = 2.0$ . The unstable states are shaded.

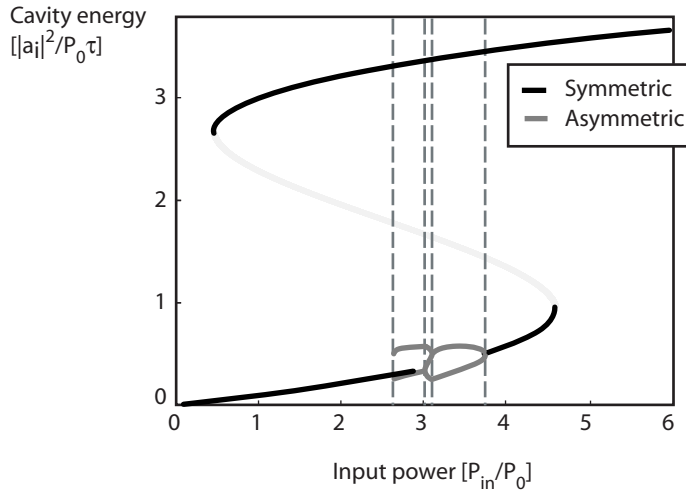


**Figure 5.3:** The stable states of the cavity energies as a function of the input power for a structure with  $\tau(\omega - \omega_0) = 0.1$  and  $\phi = -0.5$ . The unstable states of the symmetric solutions are shaded.

To see the influence of the parameters  $\Delta$  and  $\phi$ , we depict the appearance of the different states in Figure 5.4 for a constant input power of  $3.0 P_0$ . We can clearly observe the same three regions as described before.

### 5.2.3 Dynamic behaviour

We can study the dynamical behaviour by solving the equations 5.2-5.4 in the time domain. In the third regime of Figure 5.2a, it is possible to switch between asymmetric states where one of the outputs is high and the other two outputs are low. This results in multi-stable flip-flop operation [7, 8]. When a short pulse is applied to two of the three ports, the system will evolve to a state where the third output port has the high output power. In Figure 5.5, the switching is done between the three possible output states. The time is expressed in units of the characteristic lifetime  $\tau$  of the cavity. A constant input power of  $3.3 P_0$  is injected in the three cavities. To achieve switching, this input power is increased in two of the three input ports to  $3.5 P_0$  during a time  $30\tau$ .

We do the same for the bifurcation diagram of Figure 5.2b. We work in the same regime as before and find that by injecting a single pulse in one of the output ports, the system switches to a state where that output is high and the other outputs low. This is demonstrated for an input power of  $0.5 P_0$  which is increased to  $1.2 P_0$  in case of a pulse (Figure 5.5b). We observed robust switching

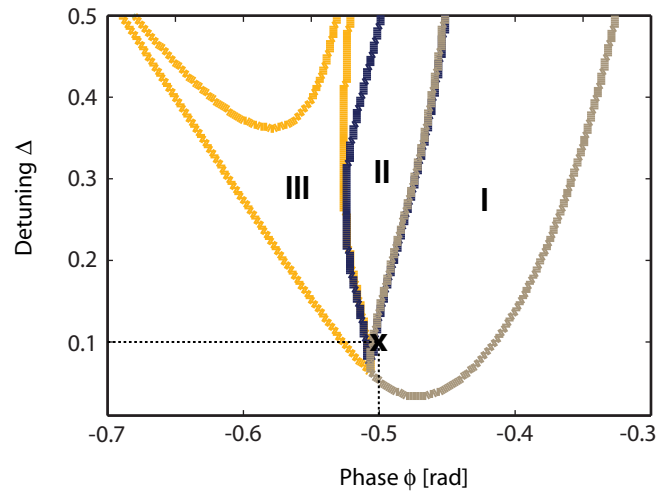


**Figure 5.4:** The different working regimes for different parameters of  $\Delta$  and  $\phi$  with a constant input power of  $P_{in}/P_0 = 3.0$ . I: two equal solutions in the upper branch and one in the lower branch (bounded by orange line); II: three different outputs (bounded by blue line); III: two equal solutions in the lower branch and one in the higher branch (bounded by brown line). The cross indicates the working point of Figure 2a.

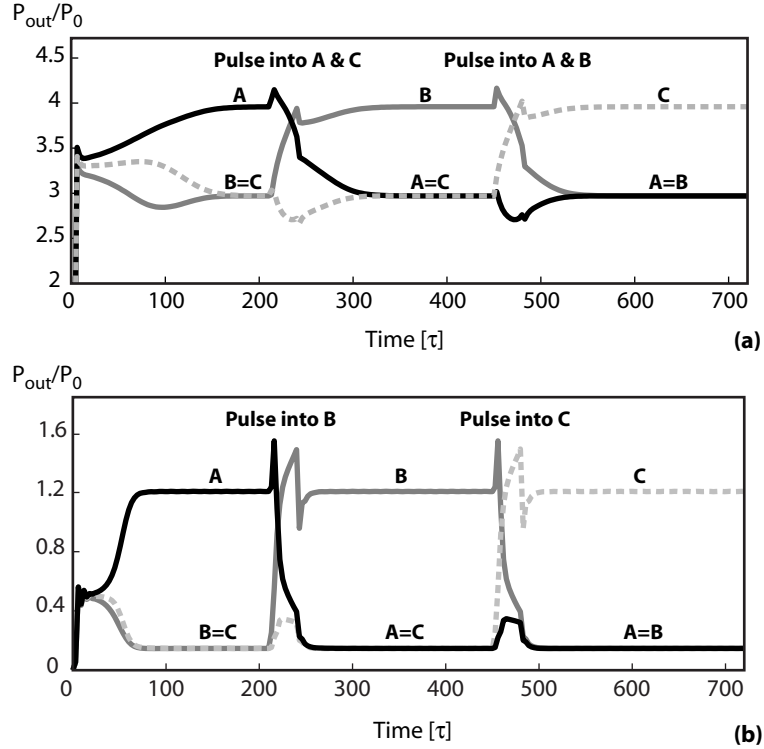


**Figure 5.5:** Switching between the three different states of region III.

behaviour: small variations on the input power do not cause switching and a variation of 30% on the values of  $\Delta$  of the different cavities is possible when using higher pulse powers.

The switching times scale with the  $Q$ -factor of the cavity. If we assume the cavity has a  $Q$ -factor of 4000, the switching time can be predicted to be 520 ps. This rather slow switching speed is due the fact that the system has to travel over a large distance in phase space. It can be reduced by also adjusting the phase of the injected pulses, as demonstrated for a single cavity in [17]. The energy needed to enter the bistable regime is proportional to the Kerr-nonlinearity and becomes lower if the mode has a small volume. In literature, we find typically a value of 2.6 mW for photonic crystal cavities [14]. In silicon ring resonators with a  $Q$ -factor of 14 000 an operational value of about 6 mW is necessary [12]. Two possible suggestions for a practical implementation of the proposed scheme are depicted in Figure 5.6 as an illustration: the first using a photonic crystal cavity with a hexagonal symmetry in the cavity mode and the other consisting of ring resonators coupled to waveguides.

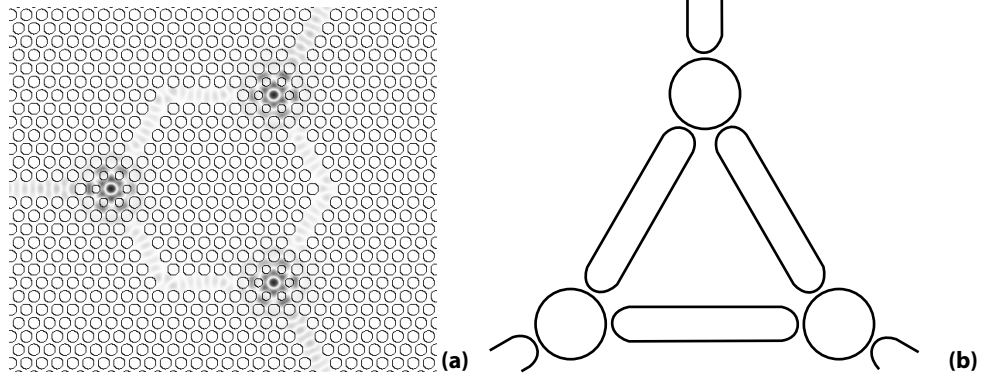


**Figure 5.6:** Two possible implementations of the proposed scheme using (a) photonic crystal cavities and (b) ring resonators.

## 5.3 Four coupled cavities

### 5.3.1 Symmetry breaking conditions

The analysis for the symmetric structure of four coupled cavities (Figure 5.7) is similar to the previous one. The time dependance of the resonant modes of the cavities is now:

$$\frac{da_1}{dt} = \left[ j(\omega_0 + \delta\omega_1) - \frac{1}{\tau} \right] a_1 + df_1 + db_5 + df_8 \quad (5.19)$$

$$\frac{da_2}{dt} = \left[ j(\omega_0 + \delta\omega_2) - \frac{1}{\tau} \right] a_2 + df_2 + db_6 + df_5 \quad (5.20)$$

$$\frac{da_3}{dt} = \left[ j(\omega_0 + \delta\omega_3) - \frac{1}{\tau} \right] a_3 + df_3 + db_7 + df_6 \quad (5.21)$$

$$\frac{da_4}{dt} = \left[ j(\omega_0 + \delta\omega_4) - \frac{1}{\tau} \right] a_4 + df_4 + db_8 + df_7 \quad (5.22)$$

By using the same definitions as before and equations (5.7-5.8), we rewrite these in the following form:

$$\left[ j(\omega_0 - \omega + \delta\omega_1) - \frac{1}{\tau} \right] a_1 + \kappa(2\gamma a_1 + a_2 + a_4) = -df_1 \quad (5.23)$$

$$\left[ j(\omega_0 - \omega + \delta\omega_2) - \frac{1}{\tau} \right] a_2 + \kappa(2\gamma a_2 + a_1 + a_3) = -df_2 \quad (5.24)$$

$$\left[ j(\omega_0 - \omega + \delta\omega_3) - \frac{1}{\tau} \right] a_3 + \kappa(2\gamma a_3 + a_4 + a_2) = -df_3 \quad (5.25)$$

$$\left[ j(\omega_0 - \omega + \delta\omega_4) - \frac{1}{\tau} \right] a_4 + \kappa(2\gamma a_4 + a_3 + a_1) = -df_4 \quad (5.26)$$

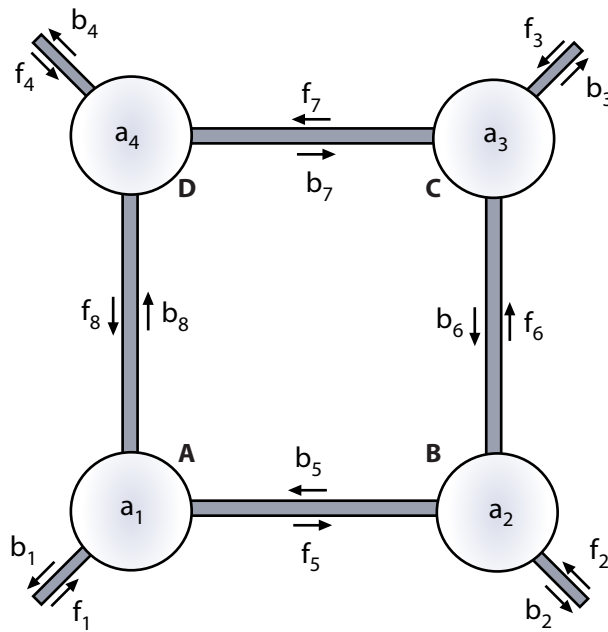


**Figure 5.7:** Schematic representation of a symmetric structure of 4 cavities coupled by waveguides.

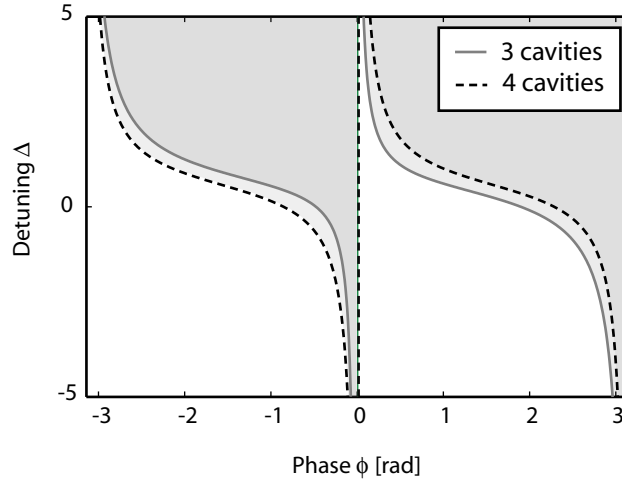


**Figure 5.8:** Schematic representation of the symmetry breaking condition for three and four coupled cavities. In the dark regions, the symmetry breaking condition holds.

To find a condition for symmetry breaking, it is assumed that all inputs are equal ( $f_1 = f_2 = f_3 = f_4$ ). By combining the first and the third equation, we obtain an equation similar to equation 5.13:

$$\left[ -\frac{1}{3} + j(\Delta'' + A) \right] a_1 = \left[ -\frac{1}{3} + j(\Delta'' + C) \right] a_3 \quad (5.27)$$

with

$$\Delta'' = \Delta - \frac{2}{3} \cot \phi \quad (5.28)$$

The same relation can be derived for  $B$  and  $D$  when combining the second and the fourth equation.

When we apply the same reasoning as in the previous case of three coupled cavities, we find the following condition for symmetry breaking with a self-focusing Kerr effect (positive nonlinearity):

$$\Delta'' > \frac{1}{\sqrt{3}} \quad (5.29)$$

In Figure 5.8 the conditions for three and four coupled cavities are depicted graphically as a function of  $\Delta$  and  $\phi$ .

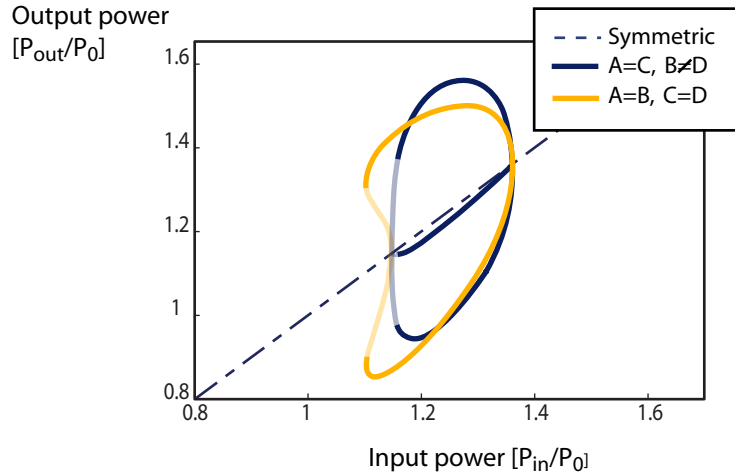


**Figure 5.9:** Stable states of the output power as a function of the input power for a structure consisting of four cavities with  $\Delta = -0.35$  and  $\phi = 0.6$ . The unstable states are plotted with a thin line.

### 5.3.2 Static solutions

We can solve the coupled-mode equations again under steady state conditions and perform a stability analysis which takes now a Jacobian matrix of 64 elements to be evaluated at each point. We can depict the stable output powers as a function of the input power for a configuration where the symmetry breaking condition is fulfilled, see Figure 5.9. In this configuration, there are two different asymmetric solutions. The first one to show up has a left-right symmetry with two pairs of equal output power (e.g.  $A = B$  and  $C = D$ ). In the next solution, two opposing cavities have the same output power and the other two outputs are respectively higher and lower (e.g.  $A = C$  and  $B < A < D$ ). By increasing the detuning a whole range of other states can be found, resulting in very complex state diagrams.

When analyzing the energy in the cavities, we observe a similar behaviour as in Figure 5.3 where we have a bifurcation in the symmetric solution which becomes unstable in the lower branch.

### 5.3.3 Dynamic behaviour

As demonstrated in Figure 5.10, we can again switch between the different states by injecting pulses. We describe in more detail the solution with two pairs of

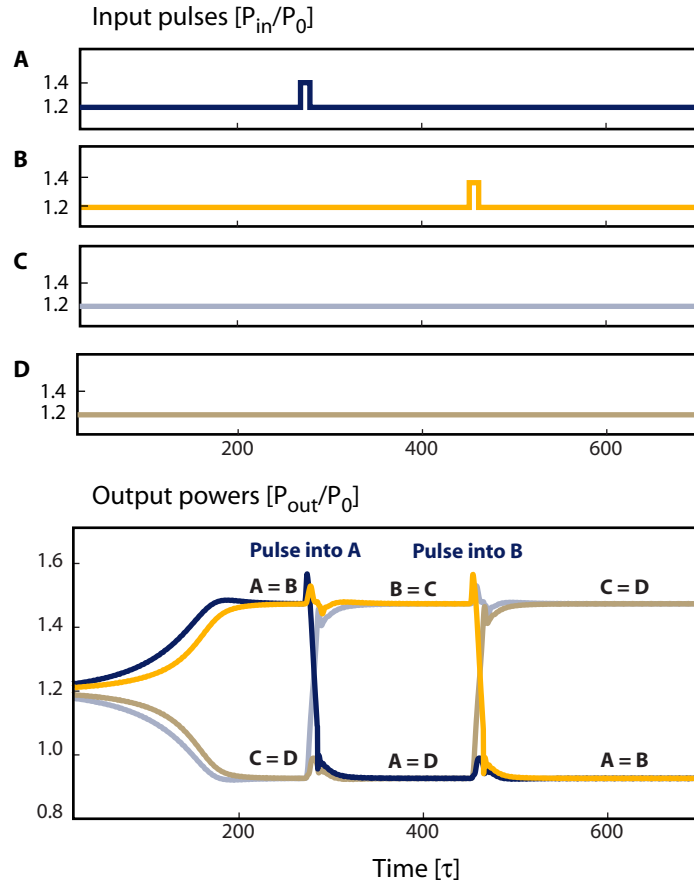


**Figure 5.10:** Switching between different states in a configuration of 4 cavities.

equal output. By injecting a short pulse in a port with a high output, that output becomes low and the port at the opposite side will become high. We inject the pulses by increasing the input power from  $1.2 P_0$  till  $1.4 P_0$  during a period of  $5\tau$ . A cyclical switching action ensues: the state rotates as a result of the switching pulse.

## 5.4 Conclusion

We demonstrated analytically and numerically symmetry breaking in structures composed of 3 and 4 cavities. Intricate bifurcation behavior with different

regimes is uncovered and dynamical studies demonstrate multi-stable and cyclical flip-flop operation. With currently hundreds of coupled cavities being studied experimentally in the linear regime [4], nonlinear dynamics in smaller networks are the logical next step.

## References

- [1] K. Vandoorne, W. Dierckx, B. Schrauwen, D. Verstraeten, R. Baets, P. Bienstman, and J. Van Campenhout. *Toward optical signal processing using Photonic Reservoir Computing*. Optics Express, 16(15):11182–11192, 2008.
- [2] M. Soljacic, S.G. Johnson, S.H. Fan, M. Ibanescu, E. Ippen, and J.D. Joannopoulos. *Photonic-crystal slow-light enhancement of nonlinear phase sensitivity*. Journal of the Optical Society of America B, 19(9):2052–2059, 2002.
- [3] B. Maes, M. Soljacic, J. D. Joannopoulos, P. Bienstman, R. Baets, S. P. Gorza, and M. Haelterman. *Switching through symmetry breaking in coupled nonlinear micro-cavities*. Optics Express, 14(22):10678–10683, 2006.
- [4] M. Notomi, E. Kuramochi, and T. Tanabe. *Large-scale arrays of ultrahigh-Q coupled nanocavities*. Nature Photonics, 2(12):741–747, 2008.
- [5] O. D’Huys, R. Vicente, T. Erneux, J. Danckaert, and I. Fischer. *Synchronization properties of network motifs: Influence of coupling delay and symmetry*. Chaos, 18(3):037116, 2008.
- [6] B. Maes, P. Bienstman, and R. Baets. *Symmetry breaking with coupled Fano resonances*. Optics Express, 16(5):3069–3076, 2008.
- [7] S. X. Zhang, D. Owens, Y. Liu, M. Hill, D. Lenstra, A. Tzanakaki, G. D. Khoe, and H. J. S. Dorren. *Multistate optical memory based on serially interconnected lasers*. Photonics Technology Letters, 17(9):1962–1964, 2005.
- [8] S. Zhang, D. Lenstra, Y. Liu, H. Ju, Z. Li, G. D. Khoe, and H. J. S. Dorren. *Multi-state optical flip-flop memory based on ring lasers coupled through the same gain medium*. Optics Communications, 270(1):85–95, 2007.
- [9] P. E. Barclay, K. Srinivasan, and O. Painter. *Nonlinear response of silicon photonic crystal microresonators excited via an integrated waveguide and fiber taper*. Optics Express, 13(3):801–820, 2005.
- [10] M. Notomi, A. Shinya, S. Mitsugi, G. Kira, E. Kuramochi, and T. Tanabe. *Optical bistable switching action of Si high-Q photonic-crystal nanocavities*. Optics Express, 13(7):2678–2687, 2005.
- [11] T. Uesugi, B. S. Song, T. Asano, and S. Noda. *Investigation of optical nonlinearities in an ultra-high-Q Si nanocavity in a two-dimensional photonic crystal slab*. Optics Express, 14(1):377–386, 2006.
- [12] Q. F. Xu and M. Lipson. *Carrier-induced optical bistability in silicon ring resonators*. Optics Letters, 31(3):341–343, 2006.

- 
- [13] G. Roelkens, L. Liu, D. Van Thourhout, R. Baets, R. Notzel, F. Raineri, I. Sagnes, G. Beaudoin, and R. Raj. *Light emission and enhanced nonlinearity in nanophotonic waveguide circuits by III-V/silicon-on-insulator heterogeneous integration*. *Journal of Applied Physics*, 104(3):033117, 2008.
- [14] M. Soljacic, M. Ibanescu, S.G. Johnson, Y. Fink, and J.D. Joannopoulos. *Optimal bistable switching in nonlinear photonic crystals*. *Physical Review E*, 66(5), 2002.
- [15] S. H. Fan, W. Suh, and J. D. Joannopoulos. *Temporal coupled-mode theory for the Fano resonance in optical resonators*. *Journal of the Optical Society of America a-Optics Image Science and Vision*, 20(3):569–572, 2003.
- [16] B. Maes, P. Bienstman, and R. Baets. *Switching in coupled nonlinear photonic-crystal resonators*. *Journal of the Optical Society of America B-Optical Physics*, 22(8):1778–1784, 2005.
- [17] H. Kawashima, Y. Tanaka, N. Ikeda, Y. Sugimoto, T. Hasama, and H. Ishikawa. *Numerical study of impulsive switching of bistable states in nonlinear etalons*. *IEEE Photonics Technology Letters*, 19(9-12):913–915, 2007.

# 6

## All-optical packet switching

The increasing demand for network traffic creates a technological bottleneck on future optical routing systems. New internet-based services are gaining more public attention and will increase the need for higher bitrates. However, the router forwarding capacity does not match the fibre bandwidth at these high bitrates. The opto-electronic and electro-optic conversions (O/E/O) that are needed to process data in the network nodes are power consuming and require expensive electronic circuits. Moreover, most electro-optic switches have rather slow switching times (more than 1 ns). Transparent networks based on all-optical packet switching offer a potential solution because all the processing is done completely in the optical layer [1–6].

All-optical flip-flops are important building blocks in the implementation of all-optical packet switches because they act as optical memory elements which can store the header information while the output of the flip-flop is directly used to route the payload to the correct output port without any O/E/O-conversions [4]. In the previous chapters, we discussed several novel concepts for all-optical flip-flop memories based on single laser diodes. Here, we will demonstrate the use of the distributed feedback (DFB) laser flip-flop in an all-optical packet switching scheme for data rates up to 40 Gb/s. Because DFB lasers are already the standard transmitters in most optical network systems, the added functionality as a fast optical memory element makes them very suitable for this application.

## 6.1 Introduction

An all-optical router system is composed of several components and processes in order to switch packets in a network [1, 2]. First of all, it will extract the header information or ‘label’ which contains the routing information (eg. destination node address). This label is normally placed at the beginning of the packet. However, it can be encoded also in different ways, for example, at a different wavelength than the payload or in-band at a much lower bitrate. Afterwards, the header information is being processed, typically by comparing it with a pre-defined bitsequence using an optical correlator [7–12]. When the destination address of an arriving packet matches the signature of an optical correlator, autocorrelation pulses are generated that are above a given threshold. If there is no match, cross-correlation pulses below threshold are generated. Therefore, simple threshold detection at the output of the optical correlator allows to recognize the destination address of the packet.

These autocorrelation pulses are typically used to switch the state of an all-optical flip-flop. This allows to store the processed label information while the payload is routed to the correct output port. Several concepts to perform this switching have been proposed in the past. The most well-known technique in literature is based on wavelength routing [4] and has been described already in the introductory chapter (see Figure 1.4). The all-optical flip-flop is assumed to be able to switch between two different wavelengths and its output is used as probe signal for a wavelength conversion of the payload. An arrayed waveguide grating (AWG) can be used afterwards to separate the two wavelengths spatially to different output ports. A slightly different technique [6] is depicted in Figure 6.1. The label signal is first converted by a serial-to-parallel converter in order to store it by an array of flip-flop elements. The output of the flip-flops drives a network of optical switches which sends the payload to the output port corresponding to the bit information in the label. Recently, optical packet switching without the use of flip-flops was demonstrated. This was done by incorporating the continuous wave signal that drives the optical switches and/or wavelength converters, as an in-band address label [5] (see Figure 6.2). In this case, the label comprises a number of wavelength bands, each representing a bit of the header information. Using optical filters to distinguish between the different wavelengths, the light is sent to a series of switches. This technique can be used to implement packet switches without the use of optical memory elements.

The implementation of all-optical packet switching where both the packet header and payload are processed entirely in the optical domain is challenging due to the lack of optical random access memory (RAM) and the difficulty to execute complex computations and logical operations within the optical domain.

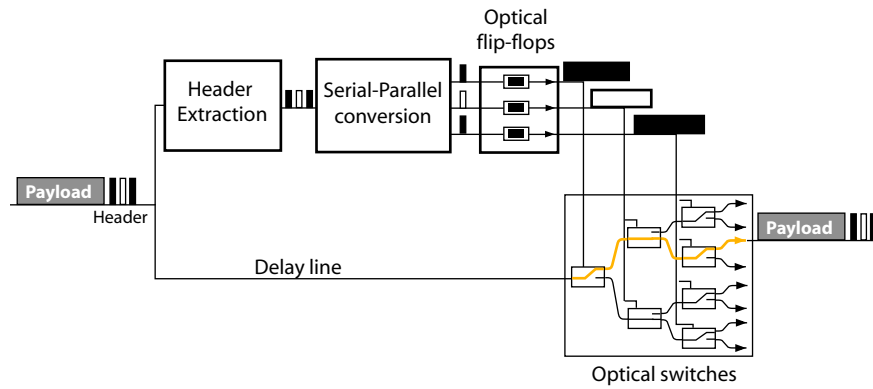


**Figure 6.1:** Packet switch based on a network of optical switches driven by optical flip-flops.

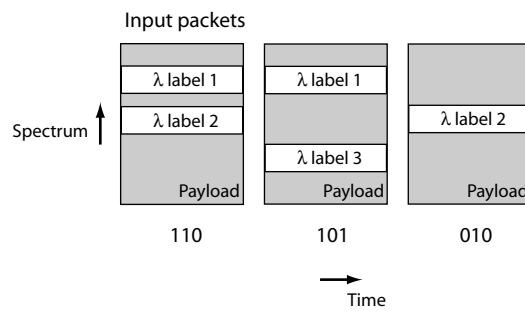


**Figure 6.2:** Alternative approach using in-band address labels [5].

Therefore, most implementations rely on optical label switching (OLS) where the packet header (label) is processed electronically while the payload remains in the optical domain [1]. Typically, one will encode the label at a lower bit-rate in order to avoid fast electronic processing. A state-of-the-art demonstration of this technique is given in [13–15]. Such optical label switching approaches can be expected to be realized in the short term. The disadvantage of these techniques is, however, that they require rather long guard times (typically multiple nanoseconds) and can be less efficient as the opto-electro-optic conversions come into play.

In optical packet switched networks, a contention may occur as two or more packets try to leave through the same output port on the same wavelength at the same time. Therefore, there is a clear need for buffering techniques and controlling systems. Different optical buffering techniques have been proposed based on recirculating loops [16, 17], slow light [18, 19] or arrays of optical memory elements (eg. microdisks). These optical buffering techniques often suffer from the disadvantage of the small buffering time that can be achieved without significant attenuation/distortion of the signal. The footprint and power consumption are also a concern in delay-line-based buffers. The buffering of signals and the contention resolution management will, however, not be further discussed in this work.

In this chapter, we will discuss the application of DFB laser flip-flops (see chapter 2) in an all-optical packet switch. In most optical networks, the optical signals are wavelength-division multiplexed (WDM) on different optical carriers in order to exploit the huge bandwidth potential of optical fibers. These carriers are often created by an array of DFB laser diodes, each emitting light at one channel of the WDM grid. In electronic switching configurations, the packets are demultiplexed and converted to electrical signals by an array of photodiodes. After processing in the electrical layer, the signals are converted back to one of the optical carriers of the WDM grid by an array of DFB lasers. The functionality as optical memory elements will allow the same array of DFB lasers to switch the packets all-optically while they are directly matched with the WDM grid.

The principle is illustrated in Figure 6.3 and shows the packet switch based on a DFB laser array. First, the header is processed and with an optical set pulse the DFB laser, with the wavelength that matches the header information, is switched on. The other optical flip-flops remain switched off. The payload of the signal has been delayed during the optical header processing and sent to a wavelength converter. This will convert the payload to the wavelength provided by the continuous light output of the DFB laser. An arrayed waveguide grating (AWG) can subsequently separate the packets spatially to different output ports according to their new wavelength. When using packets with a fixed length, the

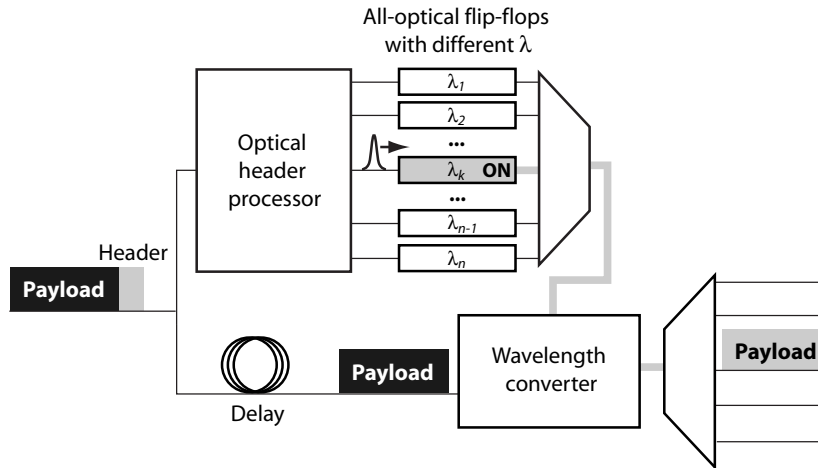


**Figure 6.3:** Concept for all-optical packet switching based on an array of DFB lasers with different wavelengths. The two arrayed waveguide gratings (AWG's) can be identical.

set-pulse generated by the optical header processor can be delayed over a fiber delay line corresponding to the length of the packets. Afterwards, it is sent into the DFB laser on the other side as a reset pulse. To work with packets with a variable length, we insert a pulse at the end of the packet to switch off the laser again.

The technique illustrated here allows very fast switching compared to electronic switches. As indicated in chapter 2, switching times as low as 45 ps can be obtained. Even more important is the advantage that DFB lasers are already a mature technology and that they can be easily matched with the WDM grid. The device can work under broadband operation: the only restriction on the wavelength of the pulses and holding beam is that they should be outside the stopband of the DFB grating. The disadvantage of the necessity of a holding beam for the flip-flop operation in a DFB laser can be addressed by distributing one single holding beam over all the lasers of the array. The devices under study are dependent on the polarization of the pulses. In theory, optimized designs for the laser section could be used that are insensitive to the polarization.

## 6.2 Experiment

To demonstrate the concept, we use one single DFB laser as all-optical flip-flop to switch 40 Gb/s packets. We do this for packets with a fixed and a variable

duration. The labels are color-coded, i.e. pulses at a different wavelength than the payload, in order to simplify the header extraction process.

### Fixed duration

The experimental set-up for all-optical switching of packets with a fixed duration is depicted in Figure 6.4. First, 40 Gb/s non-return-to-zero (NRZ) packets are created by the 40 Gb/s packet transmitter. The payload is generated by a standard lithium-niobate (LN) modulator driven by a 40 Gb/s pulse pattern generator (PPG) using standard pseudo-random bit-sequence (PRBS) data. The wavelength of the payload is 1540 nm. The payload is combined with label-encoded pulses with a 150 ps duration and at a wavelength of 1543 nm. The packets have a duration of 180 ns and are created alternately with and without a matching optical label. The payload together with the labels is depicted in Figure 6.5a. This signal is being amplified by an erbium-doped fiber amplifier (EDFA). In a practical implementation, there could be a long-haul fiber link after the EDFA.

When the signal arrives at an optical node, it will be split by a 50:50 coupler. Part of the signal will be used for label processing and storage in the upper arm. In our set-up, we omit advanced header recognition and an optical band-pass filter (OBPF) is used to extract the label pulse which will be used as a set-pulse in our set-up. As mentioned before, there is no strict limitation on the wavelength of the pulses because the DFB flip-flop works broadband when operated outside the stop-band of the grating. A holding beam of approximately 3 dBm at a wavelength of 1546 nm is used to bias the DFB laser in its bistable regime. The reset-pulses are the same pulses as the set-pulses but delayed by a fiber delay line (FDL) which is matched with the duration of the packets (180 ns). After the set-pulse from the label is sent into the DFB all-optical flip-flop, the laser will start lasing at a wavelength of 1553 nm. The pulse energies can be as low as 200 fJ, but switching times improve when larger energies are used. The DFB laser output is extracted by a circulator and an optical band-pass filter and sent directly to the wavelength converter afterwards. The corresponding output of the flip-flop can be observed in Figure 6.5b.

While the laser is switched on, the wavelength of the payload is converted to the operating wavelength of the DFB laser by a MZI-SOA (Mach-Zehnder interferometer with SOAs in the arms) [20]. The principle is illustrated in Figure 6.6. This wavelength conversion is based on a combination of cross-gain modulation and cross-phase modulation. The payload is only injected in the upper arm of the MZI and the probe signal originating from the flip-flop travels through both arms. In the upper arm, cross-gain modulation of the probe signal will occur in the SOA (biased at 600 mA). This means that the amplifi-

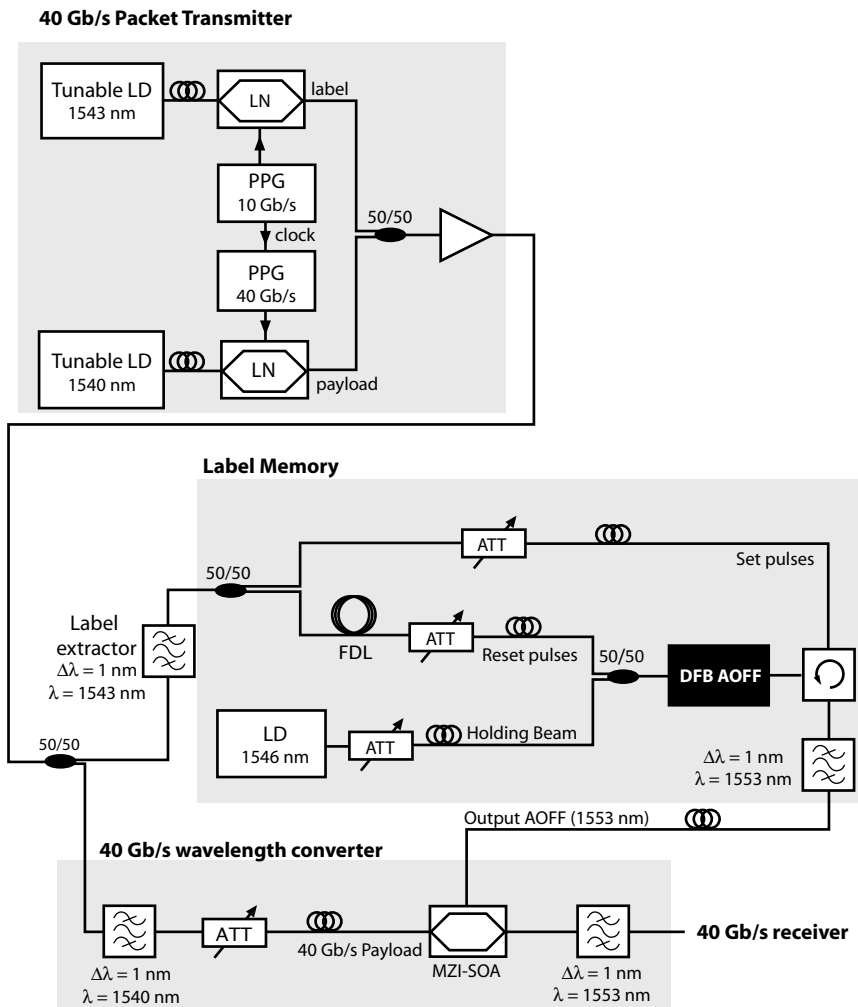


**Figure 6.4:** Schematic of the measurement set-up for all-optical switching of packets with a fixed duration using a DFB AOFF. (LD: Laser Diode, ATT: attenuator, FDL: fiber delay line, PPG: pulse pattern generator, LN: lithium niobate modulator)

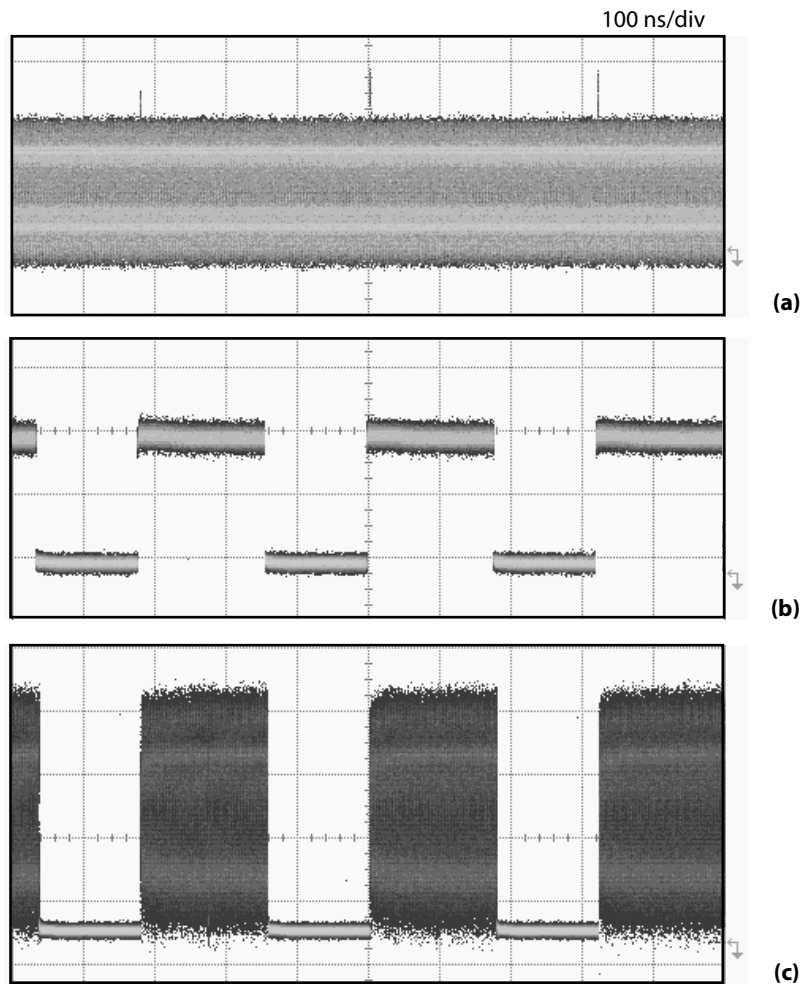


**Figure 6.5:** Results for all-optical switching of packets with a fixed duration.  
(a) Payload with labels; (b) output of DFB all-optical flip-flop; (c) optically switched packets

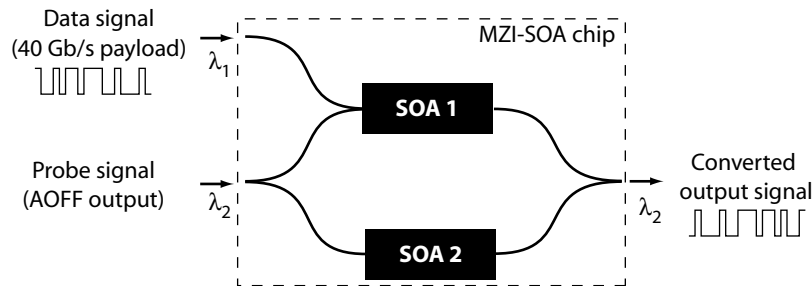


**Figure 6.6:** Schematic of the wavelength conversion in the optical packet switch.

cation of the payload signal will modulate the gain because it consumes carriers and will inversely modulate the carrier density. These dynamic changes in gain will affect the amplification of the probe signal as such. However, not only the gain is modulated by the original payload signal, but also the refractive index of the upper SOA. This will induce changes in the phase, leading to cross-phase modulation. The interferometric configuration allows to exploit these changes in the phase and, therefore, the current of the second SOA is adjusted to obtain a proper level of interference by amplification of the probe signal (typically 340 mA). The MZI-SOA consists of an optimized active-layer structure to reduce the carrier lifetime, enabling 40 Gb/s non-return-to-zero (NRZ) wavelength conversion without push-pull operation.

The switched packets (now at 1553 nm) are shown in Figure 6.5c with their corresponding transient behaviour depicted in Figure 6.7. One can see that a guard time of only 150 ps should be taken into account. This is much lower than typical optical label switches (in the order of multiple nanoseconds) or previously reported all-optical packet switching (305 ps in [6]). The longer switching time (compared to chapter 2) is due to the lower pulse energies (500 fJ) and the more complicated set-up. Error free operation can be obtained as illustrated in the bit-error rate (BER) curve of Figure 6.8. The power penalty of 2.4 dB is mostly due to the wavelength conversion.

### Variable duration

We do the same experiment also for packets with a variable duration (see Figure 6.9). Therefore, we do not only add a pulse at the start (set-pulses at 1543 nm), but also at the end of the packet (reset-pulses at 1548 nm). After amplification of this signal through an erbium-doped fiber amplifier, the set-pulses and reset-pulses are extracted separately by an optical filter. The extracted set- and reset-

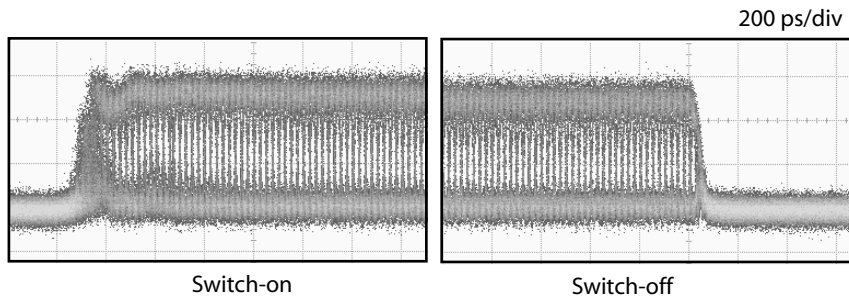


**Figure 6.7:** Transient behaviour at the start and end of the switched packets.

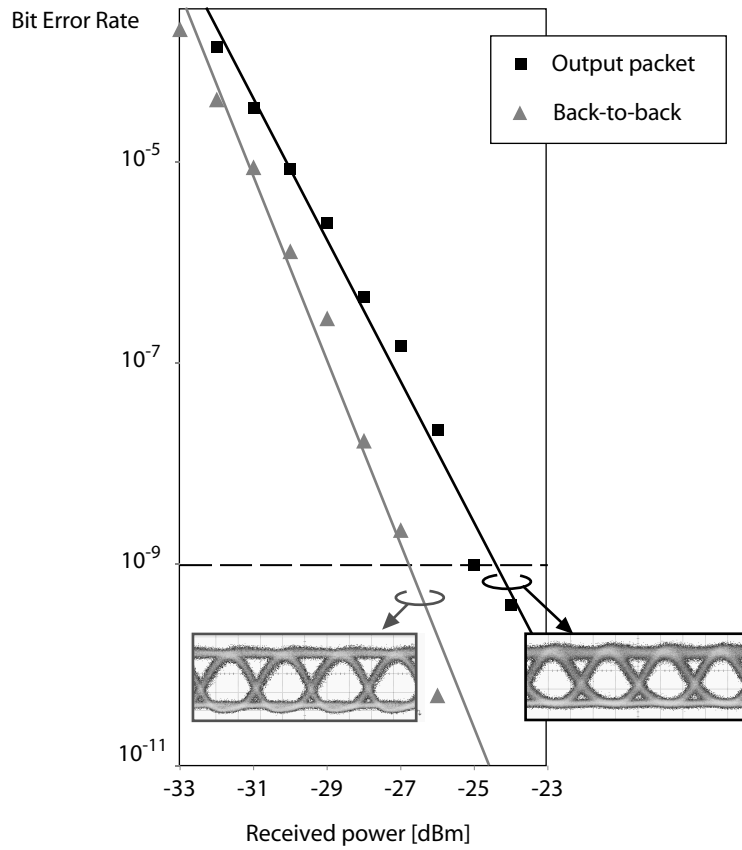


**Figure 6.8:** Bit-error rate measurements for the back-to-back and output.

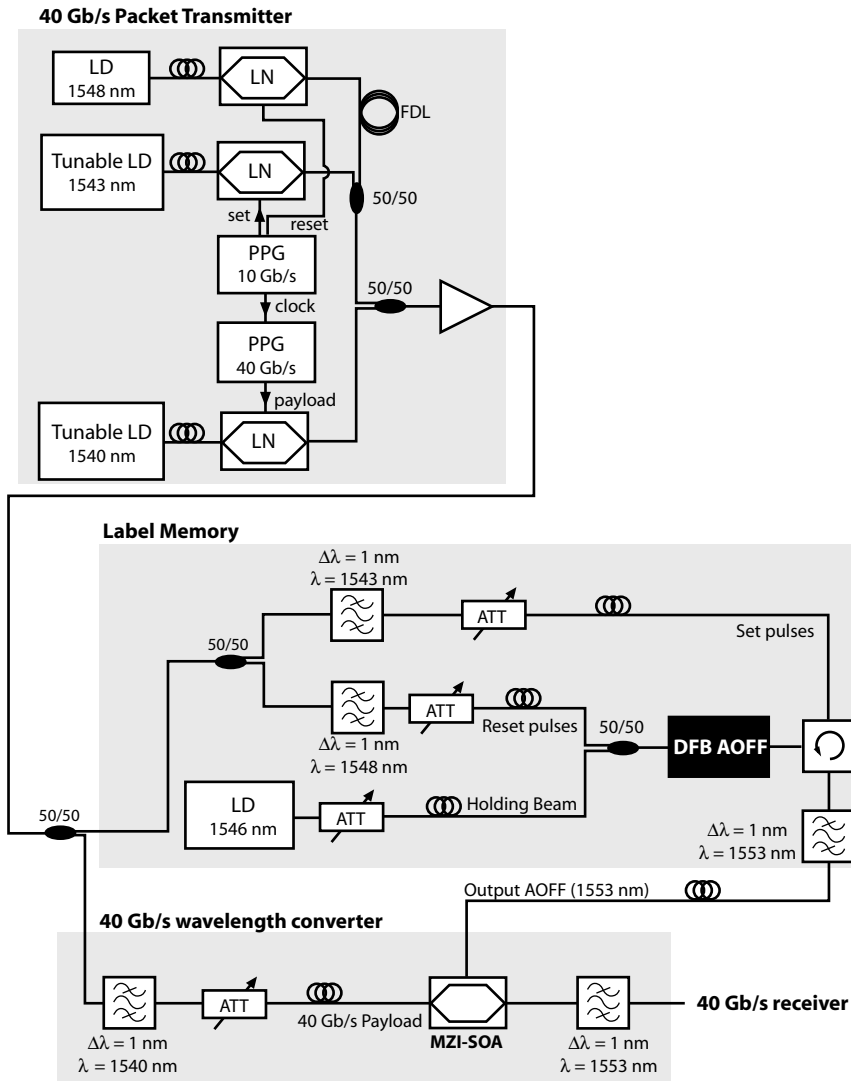


**Figure 6.9:** Schematic of the measurement set-up for optical packet switching with a DFB AOFF (LD: Laser Diode, ATT: attenuator, FDL: fiber delay line, PPG: pulse pattern generator, LN: lithium niobate modulator)

pulses are depicted in Figure 6.10 together with the corresponding output of the all-optical flip-flop and the switched 40 Gb/s packets. The packets have an alternating length of 140 ns and 40 ns.

### 6.3 Conclusion

A fast and practical method is demonstrated to switch 40 Gb/s optical packets using an off-the-shelf distributed feedback laser as all-optical flip-flop. Packets with a variable duration can be switched by adding an extra label at the end of the packet. A guard time of 150 ps has been achieved which is (to the author's knowledge) much shorter than previously reported optical packet switching schemes in literature. In the future, the DFB laser array should be integrated on a single chip together with the all-optical header processor, wavelength converter, and AWG's. Such a chip would have a great potential for a compact integrated all-optical packet switching circuit.

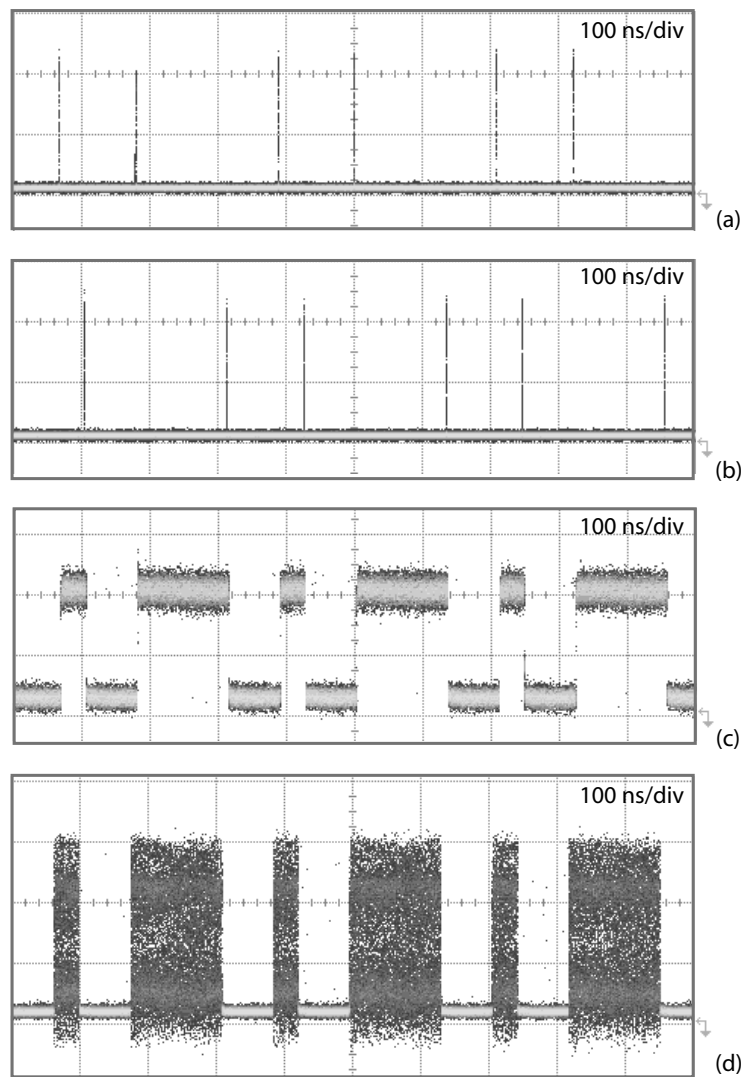


**Figure 6.10:** Results for all-optical packet-switching with a DFB AOFF. (a) set-pulses; (b) reset-pulses; (c) output of DFB all-optical flip-flop; (d) optically switched packets

## References

- [1] S. J. B. Yoo. *Optical Packet and Burst Switching Technologies for the Future Photonic Internet*. Journal of Lightwave Technology, 24(12):4468–4492, dec 2006.
- [2] M. Maier. *Optical switching networks*. Cambridge University Press, 2008.
- [3] J. Herrera, O. Raz, E. Tangdiongga, Y. Liu, H. C. H. Mulvad, F. Ramos, J. Marti, G. Maxwell, A. Poustie, M. T. Hill, H. de Waardt, G. D. Khoe, A. M. J. Koonen, and H. J. S. Dorren. *160-Gb/s all-optical packet switching over a 110-km field installed optical fiber link*. Journal of Lightwave Technology, 26(1):176–182, 2007.
- [4] H. J. S. Dorren, M. T. Hill, Y. Liu, N. Calabretta, A. Srivatsa, F. M. Huijskens, H. de Waardt, and G. D. Khoe. *Optical packet switching and buffering by using all-optical signal processing methods*. Journal of Lightwave Technology, 21(1):2–12, 2003.
- [5] N. Calabretta, H.D. Jung, J. Herrera, E. Tangdiongga, A.M.J. Koonen, and H.J.S. Dorren. *1x4 all-optical packet switch at 160 Gb/s employing optical processing of scalable in-band address labels*. Optical Fiber Communication Conference (OFC/NFOEC), 2008. Post deadline paper 33.
- [6] M. Takenaka, K. Takeda, Y. Kanema, and Y. Nakano. *All-optical switching of 40 Gb/s packets by MMI-BLD optical label memory*. Optics Express, 14(22):10785–10789, 2006.
- [7] A.E. Willner, D. Gurkan, A.B. Sahin, J.E. McGeehan, and M.C. Hauer. *All-optical address recognition for optically-assisted routing in next-generation optical networks*. IEEE Communications Magazine, 41(5):38 – 44, may 2003.
- [8] J. M. Martinez, E. Ramos, and J. Marti. *All-optical packet header processor based on cascaded SOA-MZIs*. Electronics Letters, 40(14):894–895, 2004.
- [9] N. Calabretta, Y. Liu, F. M. Huijskens, M. T. Hill, H. de Waardt, G. D. Khoe, and H. J. S. Dorren. *Optical signal processing based on self-induced polarization rotation in a semiconductor optical amplifier*. Journal of Lightwave Technology, 22(2):372–381, 2004.
- [10] N. Calabretta, H. de Waardt, G. D. Khoe, and H. J. S. Dorren. *Ultrafast asynchronous multioutput all-optical header processor*. IEEE Photonics Technology Letters, 16(4):1182–1184, 2004.

- [11] M. S. Rasras, I. Kang, M. Dinu, J. Jaques, N. Dutta, A. Piccirilli, M. A. Cappuzzo, E. Y. Chen, L. T. Gomez, A. Wong-Foy, S. Cabot, G. S. Johnson, L. Buhl, and S. S. Patel. *A programmable 8-bit optical correlator filter for optical bit pattern recognition*. IEEE Photonics Technology Letters, 20(9-12):694–696, 2008.
- [12] I. Kang, M. Rasras, M. Dinu, L. Buhl, S. Cabot, M. Cappuzzo, L.T. Gomez, Y.F. Chen, S.S. Patel, C.R. Giles, N. Dutta, A. Piccirilli, and J. Jaques. *Latency-free all-optical recognition of 32-bit optical bit patterns at 40 Gb/s using a passive optical correlator*. European Conference on Optical Communication (ECOC), 2008. Th.3.E.6.
- [13] I. M. Soganci, T. Tanemura, K. A. Williams, N. Calabretta, T. de Vries, E. Smalbrugge, M. K. Smit, H. J. S. Dorren, and Y. Nakano. *Monolithically Integrated InP 1x16 Optical Switch With Wavelength-Insensitive Operation*. IEEE Photonics Technology Letters, 22(3):143–145, 2010.
- [14] N. Calabretta, I. M. Soganci, T. Tanemura, W. Wang, O. Raz, K. Higuchi, K. A. Williams, T.J. de Vries, Y. Nakano, and H. J. S. Dorren. *1x16 optical packet switch sub-system with a monolithically integrated InP optical switch*. In Optical Fiber Communication Conference (OFC/NFOEC), 2010.
- [15] M.Y. Jeon, Z. Pan, J. Cao, Y. Bansal, J. Taylor, Z. Wang, V. Akella, K. Okamoto, S. Kamei, J. Pan, and S.J.B. Yoo. *Demonstration of all-optical packet switching routers with optical label swapping and 2R regeneration for scalable optical label switching network applications*. Journal of Lightwave Technology, 21(11):2723 – 2733, Nov 2003.
- [16] K.L. Hall and K.A. Rauschenbach. *All-optical buffering of 40-Gb/s data packets*. IEEE Photonics Technology Letters, 10(3):442 –444, mar 1998.
- [17] H. Park, J.P. Mack, D.J. Bluementhal, and J.E. Bowers. *An integrated recirculating optical buffer*. Opt. Express, 16(15):11124–11131, 2008.
- [18] Y. A. Vlasov, M. O’Boyle, H. F. Hamann, and S. J. McNab. *Active control of slow light on a chip with photonic crystal waveguides*. Nature, 438(7064):65–69, 2005.
- [19] F. N. Xia, L. Sekaric, and Y. Vlasov. *Ultra-compact optical buffers on a silicon chip*. Nature Photonics, 1(1):65–71, 2007.
- [20] T. Hatta, T. Miyahara, Y. Miyazaki, K. Takagi, K. Matsumoto, T. Aoyagi, K. Motoshima, K. Mishina, A. Maruta, and K. Kitayama. *Polarization-insensitive monolithic 40-Gbps SOA-MZI wavelength converter with narrow active waveguides*. IEEE Journal of Selected Topics in Quantum Electronics, 13(1):32–39, 2007.



# 7

## All-optical 2R regeneration

In previous chapters, it was argued that the logical next step in network evolution is the implementation of all-optical network nodes. Therefore, novel techniques were described to implement optical memory elements and perform packet switching within the optical domain. The drawback of such all-optical approaches is the limited cascability of all-optical network nodes due to the accumulation of noise from optical amplifiers and cross-talk from switches. Indeed, the opto-electro-optic (O/E/O) conversions also act as repeaters in the network and they significantly reduce the noise on the signals. Therefore, there is a clear need for all-optical regenerators that operate at low power consumption, at high bitrates and independent of the incoming wavelength.

In this chapter, it will be demonstrated that the bistability in the amplification characteristic of a DFB laser can be employed for this purpose. It is also shown that the very fast switching dynamics of the hysteresis do not only reduce the noise on an optical signal but also allow to improve the bit error rate (BER). A theoretical approach is given to clarify the concept of hysteresis in a decision characteristic. Using a standard DFB laser diode, 2R regeneration and BER improvement is demonstrated experimentally at bitrates up to 25 Gb/s. Moreover, it is shown that this regeneration is robust and holds even after transmission through a dispersion compensated fiber link with a length of 160 km.

## 7.1 Introduction

There are different noise mechanisms that can degrade optical signals in wavelength-division-multiplexed (WDM) networks. The main cause of degradation is the attenuation by propagation in the optical fiber. This attenuation can be overcome by using erbium-doped fiber amplifiers (EDFAs) which will re-amplify the signal. EDFAs are therefore also referred to as '1R regenerators' in some cases. The amplification by EDFAs will, however, also add noise to the signal. Other sources of signal degradation are mere distortions than noise and can be ascribed to the nonlinearities in the fiber (such as self-phase modulation, cross-phase modulation, four wave mixing, ...) and dispersion effects (chromatic as well as polarization dispersion). The combination of all these different degradation effects can influence the shape of the pulses and add intensity noise to the signal. This distortion can be reduced by using '2R regenerators' in the network (comprising re-amplifying and reshaping functionality). When there are also distortions in the time domain (timing jitter), a '3R regenerator' is needed which performs a retiming in addition to the 2R functionality. The different types of regeneration are depicted in Figure 7.1.

In this work, we will limit ourselves to 2R regeneration techniques on intensity modulated non-return-to-zero (NRZ) signals. Most of the concepts for regeneration at high speeds solely offer the ability to handle return-to-zero (RZ) signals while most commercial systems are currently still deployed as NRZ. The retiming used by 3R regeneration has been demonstrated to be a reliable technique for transmission over practically unlimited distances (1 000 000 km with 2500 hops [1]). However, this requires clock extraction/recovery techniques which become complicated in all-optical packet switched networks since the packets arrive at burst rates. 2R regeneration is far simpler and more cost-effective. Experiments have shown that even without correcting the time degradations, it is still possible to achieve all-optical packet switching at 10 Gb/s by cascading up to 16 optical nodes and using multistage 2R regeneration [2–4]. It has also been demonstrated that transmission over large distances (100 000 km) is possible without performing a retiming [5, 6].

All-optical 2R regenerators are typically based on elements with a very steep nonlinear transmission characteristic, ideally resembling a step-like function (see Figure 7.2). This steep transition will act as the decision level between the logical zeros and logical ones. When a bit pattern with noise is inserted, there will be a much lower amplification for the logical zeros than for the logical ones. This will reduce the noise on the signal and thus increase the optical signal-to-noise ratio (OSNR).

All-optical regenerators have been studied extensively in the past. Most of them are based on a combination of semiconductor optical amplifiers (SOA) in

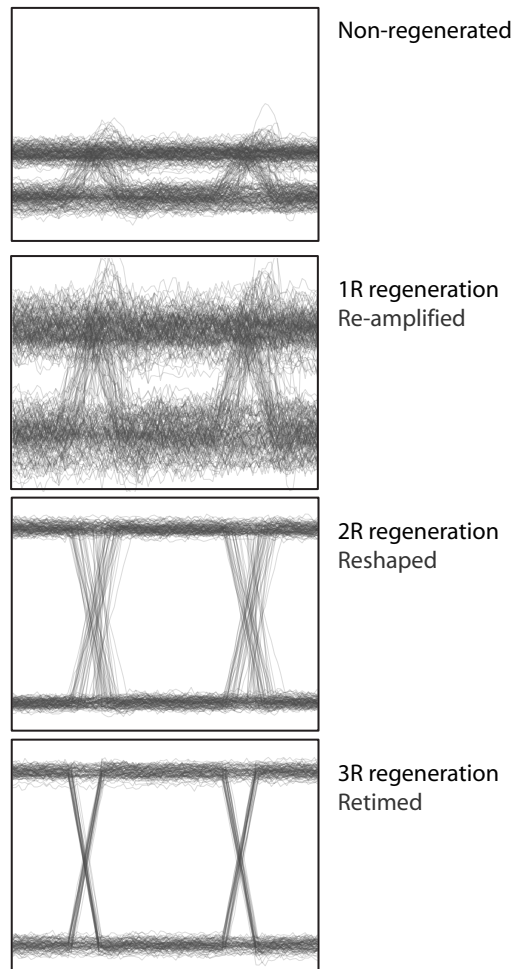


**Figure 7.1:** Schematic representation of the different types of regeneration.

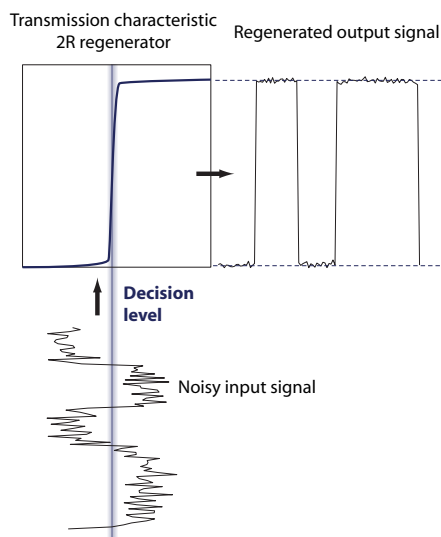


**Figure 7.2:** Principle of 2R regeneration using a static decision level.

interferometric structures such as active Mach-Zehnders [7–14] or multi-mode interferometers (MMI) [15–17]. These differential schemes have been shown useful for regeneration at high bitrates (40 Gb/s in [12]), but are in general not independent of the bitrate because of the interference effects. The simultaneous wavelength conversions are also unwanted in most practical realizations and the combination of multiple active elements increases not only the power consumption and footprint but also complicates the fabrication process.

Structures that are based on single active elements have been proposed such as laser diodes (using injection locking [18, 19] or Q-switching [20]) and electroabsorption modulators (EAM). Electroabsorption modulators are based on the Franz-Keldysh effect [21–23] according to which the effective semiconductor bandgap decreases with increasing electric field. For wavelengths close to the bandgap, the absorption will therefore increase when a voltage is applied over the semiconductor because the bandgap will shrink [24]. The absorbed light will create carriers which induce an electric field in the opposite direction. A probe signal that is sent through the EAM simultaneously with the data signal, will therefore experience a cross-absorption modulation (XAM) effect [25–28]. The disadvantage here is the need for high optical power inputs (18 dBm in [26]) and the simultaneous wavelength conversion.

More recently, the directional bistability in a semiconductor ring laser (as discussed in chapter 4), has been demonstrated to be useful for optical regen-

eration [29, 30], however at extremely slow bitrates (155 Mb/s) and with almost no improvement in power penalty (a mere 0.5 dB).

Besides the use of active devices, also fiber-based (passive) methods have been studied for 2R regeneration. The most well-known is the so-called ‘Mamyshhev regenerator’ based on the self-phase modulation (SPM) in nonlinear fibers [31–33]. This technique is based on the spectral broadening of the pulses due to Kerr nonlinearities in optical fibers. A consecutive filter with a slight detuning from the central wavelength can then suppress the noise. A similar effect can be used in Sagnac interferometers by using cross-phase modulation [34, 35]. These passive methods allow regeneration at high bitrates but their main disadvantage is the requirement of very high optical input powers (typically several 100 mW’s). Moreover, they are only applicable to return-to-zero (RZ) signals.

The above overview of the state of the art suggests that there is a clear need for low power 2R regenerators that have a simple design and operate in a colourless mode independent of the bitrate. However, the decision circuit of electronic repeaters offer in general a qualitatively better result because they are often implemented using hysteresis effects (Schmitt trigger) to increase their tolerance to noise. No successful demonstration of all-optical regeneration using hysteresis has been proposed before. The bistability used in semiconductor ring laser regenerators [29, 30] did not yet result in qualitatively good results (small power penalty improvement at very low bitrates).

As shown before, the hysteresis in the DFB laser power under the injection of a holding beam can successfully be applied to obtain flip-flop operation (chapter 2) and packet switching (chapter 6). There is, however, also a simultaneous hysteresis in the amplification characteristic of the externally injected light (see Figure 7.4a). It will be shown in this chapter that this steep nonlinearity combined with a hysteresis is very effective for all-optical 2R regeneration. The advantage of using a hysteresis in the decision characteristic is illustrated in Figure 7.4. The decision level will move dynamically with the signal which increases its ability to reduce noise. Indeed, when we are at the lower side of the hysteresis (corresponding to the logical zeros), the decision level will move up which facilitates the suppression of noise fluctuations on the zero level. The same reasoning holds for the upper side of the hysteresis corresponding to the logical ones. Moreover, because the amplification characteristic is used, the regenerator will work independent of the wavelength (only the wavelengths within the stopband of the DFB grating can not be used) and preserves the original wavelength. The proposed regenerator consists of a single element which eliminates the fabrication difficulties (stemming from passive/active integration) and the bitrate dependencies of the active interferometer implementations [7–14]. The total (electrical) power consumption is therefore also limited

to 0.6 W (including the cooling of the DFB laser).

A distinct decision level for the logical ones and zeros (as offered by the hysteresis) brings up the notion of BER improvement. According to a theoretical study by Rochette et al. [33, 36], it is not possible to improve the bit error rate of a signal using 2R regenerators with a single static function as in Figure 7.2. The regenerator can only reduce the noise on the signal, but cannot, in principle, improve bits that would be detected erroneous at the detector. Only regenerators with a distinct transfer function for the logical ones and zeros can improve the bit error rate of a signal. These regenerators are called class II regenerators [33, 36] to distinguish them from standard regeneration techniques using a single static decision level. Regenerators with a static decision level (class I) will redistribute the noise so the signal can be detected at lower input powers on the receiver. Indeed, because the noise of the receiver adds to the noise of the signal, noise reduction means a shift to the left in a BER vs. received optical power diagram (as indicated in Figure 7.3). The optical noise of the signal will, however, also lead to a noise floor in the BER diagram. Even at higher optical powers where the noise of the receiver does not come into account anymore, the signal noise will prevent correct detection of a number of bits. Only a regenerator with a distinctive and different transfer function for the ones and zeros is able to overcome this noise floor and can shift the curve downwards [33, 36]. As far as known in literature, the only all-optical 2R regenerator that can improve the bit error rate is the Mamyshev regenerator [31]. We will show with experimental results that the DFB laser regenerator can improve the BER of a signal with multiple orders of magnitude. In the next section, a theoretical approach will be given to illustrate the ability to perform BER improvement using hysteresis-based decision characteristics.

## 7.2 Theoretical approach

The experimental results that will be presented in this chapter suggest that the hysteresis in the transmission characteristic plays an important role. In this section, we will give the basis for a theoretical approach on 2R regeneration using a hysteresis in the decision characteristic. For this theoretical study, we will consider the BER as a stochastic quantity corresponding to the probability of detecting a wrong bit. The textbook definition [37, 38] for the BER is therefore given in terms of the probability  $P(0|1)$  of deciding zero when a one is expected and the probability  $P(1|0)$  of deciding one when a zero is expected. Since one and zero bits are equally likely to occur, the BER can be defined as:

$$\text{BER} = \frac{1}{2} (P(0|1) + P(1|0)) \quad (7.1)$$

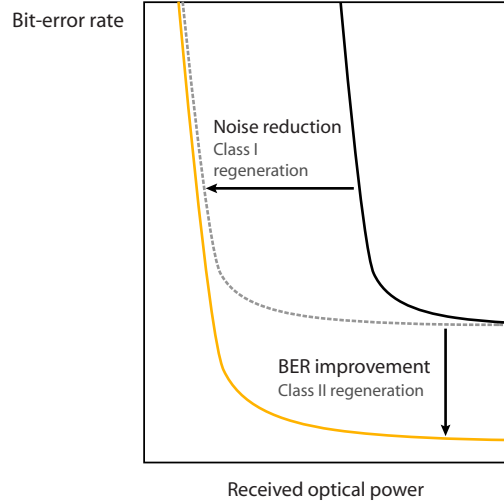
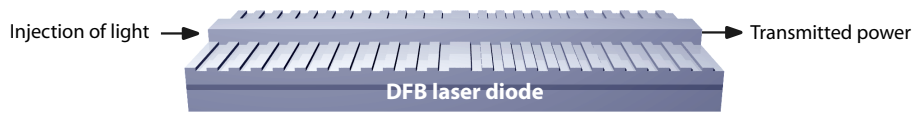


**Figure 7.3:** Schematic of the difference between noise reduction (class I regenerators) and BER improvement (class II regenerators).

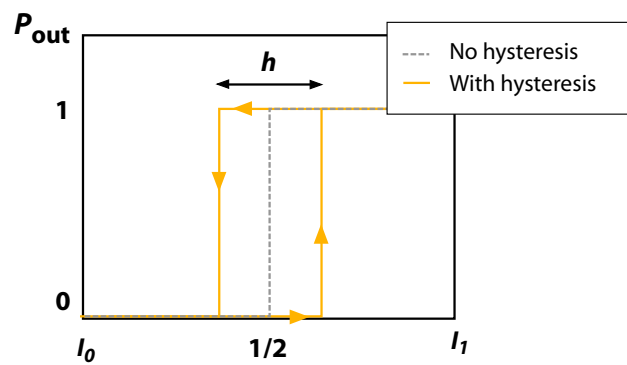
To calculate error probabilities, we can make use of probability density functions of the noise on the zero ( $\text{pdf}_0$ ) and one ( $\text{pdf}_1$ ) levels. The error probability is then determined by the overlap of the two curves as illustrated in Figure 7.4c. For this analysis, we will assume a Gaussian distribution for the probability density functions with an equal noise distribution on the ones and zeros. This assumption is made for the clarity of the theoretical analysis and however it covers a specific case and might not be verified by all types of impairments that result in the broadening of the one and zero levels, it allows us to obtain insight in the regeneration mechanism. The optimal point for the decision level ( $I_D$ ) is in that case in the middle where the two Gaussians cross. The shaded area below the decision level corresponds to  $P(0|1)$  while the area above corresponds to  $P(1|0)$ . In order to avoid confusion with probabilities  $P$ , we express the optical power as a normalized optical intensity  $I$  where  $I = 1$  corresponds to the logical one level and  $I = 0$  with the logical zero level. When expressed in a mathematical form, we can write:

$$\text{BER} = \frac{1}{2} \int_{-\infty}^{I_D} \text{pdf}_1(I) dI + \frac{1}{2} \int_{I_D}^{\infty} \text{pdf}_0(I) dI \quad (7.2)$$

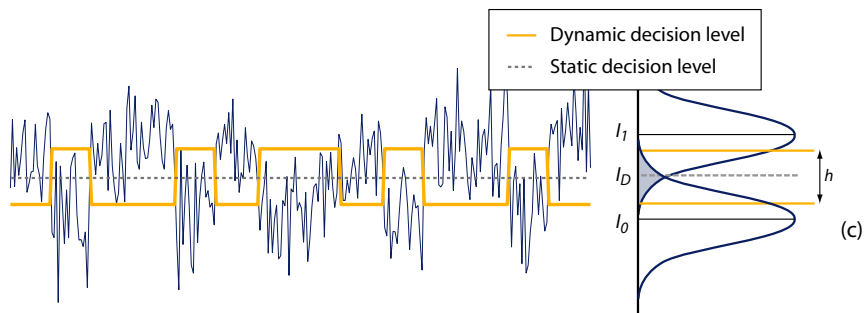
In case of standard Gaussian noise, the bit error rate can be derived as a function of the  $Q$  parameter. The  $Q$ -parameter is defined as the ratio between signal power and the sum of the standard deviations of the Gaussian noise distribution on the ones  $\sigma_1$  and zeros  $\sigma_0$  [37]. We can make use of the definition of the complementary error function (erfc) to express the above bit error rate for



(a)



(b)



(c)



(d)

**Figure 7.4:** (a) Schematic of the DFB laser based 2R regeneration; (b) Ideal hysteresis curve of the transmission characteristic; (c) Bit pattern with noise and the dynamically moving decision level (orange, with hysteresis) and static decision level (grey dashed, without hysteresis); (d) Correctly reconstructed bit-pattern by the 2R regenerator with hysteresis.

Gaussian noise distributions as [37]:

$$\text{BER} = \frac{1}{2} \operatorname{erfc} \left( \frac{Q}{\sqrt{2}} \right) \quad (7.3)$$

For simplicity, we assume that the noise distributions on the ones and zeros is equal ( $\sigma_1 = \sigma_0$ ). In that case, the decision is located exactly in the middle  $I_D = 1/2$ .

A decision characteristic with a hysteresis will require a more complex analysis because the output depends on the state at a previous time step. This means that the above reasoning needs to be reconstructed to include how the device will switch its state during a single bit period. We assume a regenerator with a hysteresis that has a relative width  $h$  with  $h < 1$  for realistic situations. The intensity noise on these signals is mainly coming from amplified spontaneous emission noise of the amplifiers and therefore fluctuating very fast. If we assume that the device has a reaction time that is significantly shorter than the duration of a single bit, we can look at it from the point of view of the threshold level which will change at the beginning of a bit period following a transition in the bit sequence while the noise is changing throughout the bit period. We will therefore follow a similar procedure as in [39, 40] where a mathematical analysis for hysteresis based detectors is given and divide the time window of one bit in  $N$  different time steps. This approach is only valid if the time required to change the state of the regenerator is comparable to this discretized time step. The error probability when there is no state difference will be lower than considered with a standard fixed decision characteristic due to the shifted decision level. There is however also an adverse effect because of the higher threshold of changing from a zero bit to a one bit and vice versa. We will show that this adverse effect can be overcome when the regenerator acts faster than the duration of individual bits and in case the hysteresis is not very wide.

Using the above analysis, we can write the probability  $p_{x|y|z}$  to change from state  $x$  to  $y$  while  $z$  is given, as follows:

$$p_{00|1} = \int_{-\infty}^{(1+h)/2} \text{pdf}_1(I) dI = \frac{1}{2} \operatorname{erfc} \left( (1-h) \frac{Q}{\sqrt{2}} \right) \quad (7.4)$$

$$p_{10|1} = \int_{-\infty}^{(1-h)/2} \text{pdf}_1(I) dI = \frac{1}{2} \operatorname{erfc} \left( (1+h) \frac{Q}{\sqrt{2}} \right) \quad (7.5)$$

$$p_{01|0} = \int_{(1+h)/2}^{\infty} \text{pdf}_0(I) dI = \frac{1}{2} \operatorname{erfc} \left( (1+h) \frac{Q}{\sqrt{2}} \right) \quad (7.6)$$

$$p_{11|0} = \int_{(1-h)/2}^{\infty} \text{pdf}_0(I) dI = \frac{1}{2} \operatorname{erfc} \left( (1-h) \frac{Q}{\sqrt{2}} \right) \quad (7.7)$$

When using a hysteresis, the previous state is used to determine the next state and a recursive expression for  $P_n(0|1)$  (being the probability on time step

$n$  to decide zero when a one is expected) can be written as:

$$P_{n+1}(0|1) = P_n(0|1) p_{00|1} + P_n(1|1) p_{10|1} \quad (7.8)$$

$$P_1(0|1) = \frac{1}{2} p_{00|1} + \frac{1}{2} p_{10|1} \quad (7.9)$$

and a similar equation holds for for  $P_n(1|0)$ :

$$P_{n+1}(1|0) = P_n(1|0) p_{11|0} + P_n(0|0) p_{01|0} \quad (7.10)$$

$$P_1(1|0) = \frac{1}{2} p_{11|0} + \frac{1}{2} p_{01|0} \quad (7.11)$$

To simplify the calculations, we assume that the noise distribution on the ones is similar to the noise distribution on the zeros and we can write down the following equations:

$$p_{00|1} = p_{11|0} \quad (7.12)$$

$$p_{10|1} = p_{01|0} \quad (7.13)$$

Because of the above equalities and  $P(1|1) = 1 - P(0|1)$ , we can reduce equations 7.10-7.11 to equations 7.8-7.9. The time discretized BER( $n$ ) can then be written as follows (using Equation 7.1):

$$\text{BER}(n) = \frac{1}{2} (P_n(0|1) + P_n(1|0)) \quad (7.14)$$

$$= P_n(0|1) \quad (7.15)$$

Using equations 7.8-7.9, the recursive equation for the BER is:

$$\text{BER}(n+1) = \text{BER}(n) p_{00|1} + [1 - \text{BER}(n)] p_{10|1} \quad (7.16)$$

$$\text{BER}(1) = \frac{1}{2} p_{00|1} + \frac{1}{2} p_{10|1} \quad (7.17)$$

The second term of Equation 7.16 appears to be dominant for realistic values of the hysteresis ( $h < 1$ ) and the bit error rate asymptotically becomes equal to  $p_{10|1}$  after a sufficient amount of time steps. This asymptotical bit error rate is depicted in Figure 7.5 for different values of the normalized hysteresis width  $h$ . However, this figure does not take into account the adverse effect of the higher threshold for switching between two different states. As discussed above, the bit error rate will improve during the time window of a single bit. For high values of the hysteresis width, it will take more time steps to achieve an improvement. The time evolution of the BER is depicted in Figure 7.6 for different time steps  $n$  using a hysteresis with a width of  $h = 0.4$ . We can observe an improvement in bit error rate after 3 time steps and it saturates thereafter for  $n > 3$ . This means that - according to this model - the reaction time of the device should be 4 or 5 times

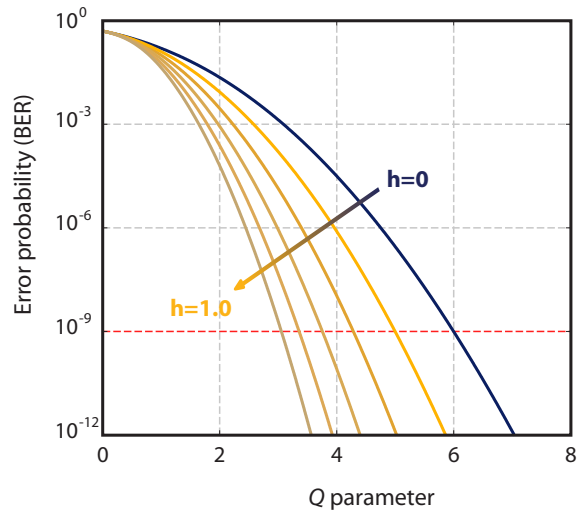


**Figure 7.5:** Asymptotical behaviour of BER as a function of the  $Q$  parameter for different values of the hysteresis width  $h$  (and  $n \rightarrow \infty$ ).

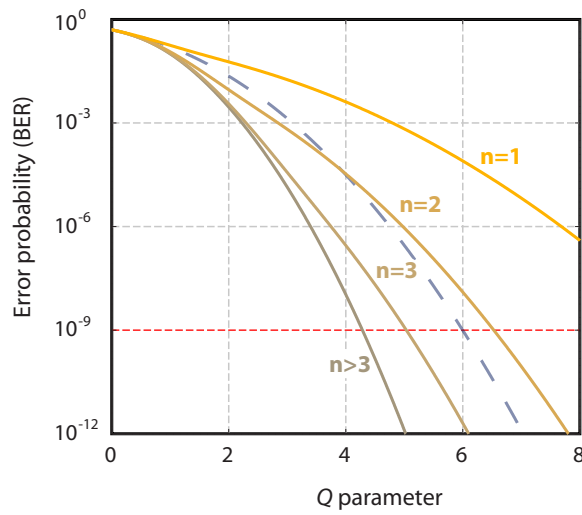


**Figure 7.6:** BER as a function of the  $Q$  parameter at different time steps  $n$  for a hysteresis with width  $h = 0.4$ . The dashed line represents the situation without hysteresis.

faster than the bit duration when  $h = 0.4$ . The number of time steps needed for an improvement in bit error rate increases with the hysteresis width, eg. for a hysteresis of  $h = 0.1$  there is already an improvement in the second time step but it takes 15 time steps for a hysteresis width of  $h = 0.9$ .

To conclude, the theoretical model that is derived above, suggests that the bit error rate of a noisy signal can be improved by using a hysteresis in the decision level. However, to overcome the adverse effect of switching between the two states, it is necessary that the response time of the regenerator is significantly fast relative to the time window of a single bit. The hysteresis width has a large impact on the amount of time steps needed to obtain BER improvement but wider hystereses allow for a larger improvement.

### 7.3 Experiment

The experiments were attained in two different labs. The first experimental results were accomplished using bitrates of 10 Gbit/s signals in the lab of Prof. Y. Nakano at the University of Tokyo where the wavelength independence of the device was also measured. Later experiments at bitrates of 25 Gbit/s were achieved in cooperation with Prof. C. Peucheret at the high-speed photonics laboratory of the Technical University of Denmark. In the latter, we included also a fiber link experiment to demonstrate the feasibility of the concept in real telecommunication systems.

#### 7.3.1 Results at 10 Gbit/s

For the experiment, we use the set-up as depicted in Figure 7.7. A pulse pattern generator (PPG) generates a pseudo-random bit-sequence (PRBS) of  $2^{31} - 1$  bits. The original signal is being attenuated and amplified to decrease the OSNR. The regenerator is a standard, non-optimized  $\lambda/4$ -shifted DFB laser diode with AR-coated facets from Alcatel-Thales III-V lab. It has a  $\kappa L$  value of 1.6, a bias current of 150 mA and its central wavelength is 1553 nm. Lensed fibers are aligned at both sides of the laser to couple the light. The degenerated signal has an input power of 5-7 dBm (depending on the power injected in the EDFA) and is combined with a holding beam of 5 dBm (both measured in fiber after the coupler). The holding beam is not strictly necessary but allows to adjust the position of the hysteresis to the incoming signal. Its power can be easily adjusted by an attenuator and it has a wavelength of 1546 nm. The width of the hysteresis is approximately 1 dB wide (resulting in a value for  $h$  between 0.1 and 0.2 in the analysis of section II). An optical bandpass filter with a width of 1 nm removes the remaining laser light so that only the signal at the original wavelength is sent to the pre-amplified receiver for a bit error rate (BER) analysis. A variable atten-

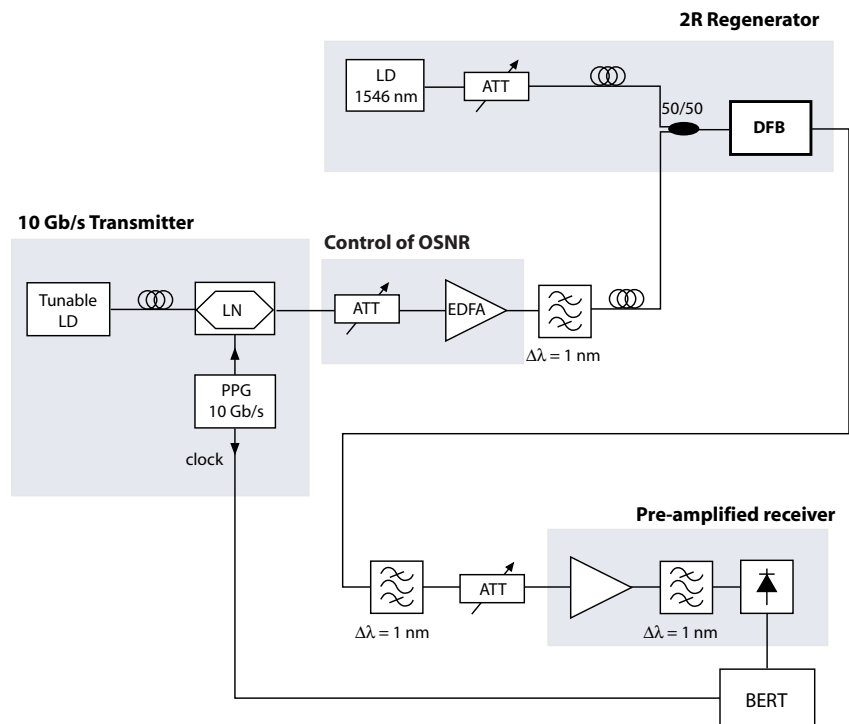


**Figure 7.7:** Schematic of the set-up. (LD: laser diode; LN: lithium-niobate modulator; PPG: pulse pattern generator; ATT: attenuator; EDFA: erbium-doped fiber-amplifier; BERT: bit error rate tester.)

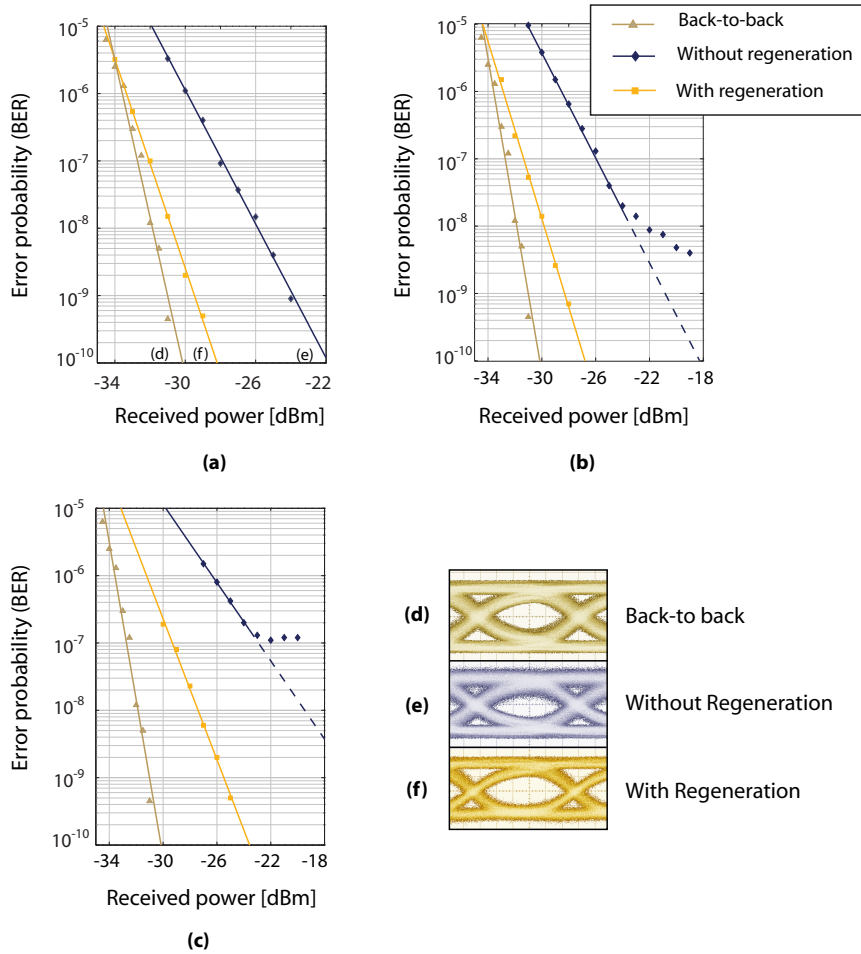


**Figure 7.8:** BER as a function of the received optical power for different values of the OSNR and corresponding eye diagrams. (a) Input OSNR of 19.8 dB; (b) Input OSNR of 18.8 dB; (c) Input OSNR of 17.7 dB; (d) eye diagram of original signal; (e) degraded signal; (f) regenerated signal.

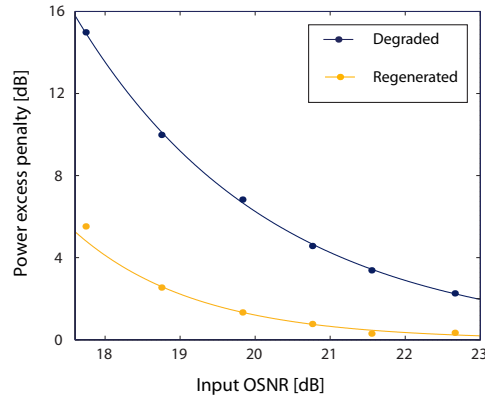


**Figure 7.9:** Excess penalty at  $\text{BER}=10^{-9}$  of the degraded and regenerated signal compared to the original signal as a function of the input OSNR.

uator is used to change the received optical power on the receiver in order to make BER diagrams.

In Figure 7.8a-c, the BER diagrams as a function of the received optical power are shown for different values of the input OSNR. From these diagrams, it is clear that the 2R regenerator is able to improve the degraded signal significantly. The corresponding eye diagrams for the regeneration are depicted in Figure 7.8d-f. Its noise suppression capabilities are demonstrated by Figure 7.9 where the excess power penalty for the regenerated and degraded signal compared to the original signal are depicted as a function of the OSNR. The power penalty is defined as the increase in the received optical power required to obtain error-free operation (at  $10^{-9}$ ). Besides the noise reduction, the noise floor of the signal is also improved with several orders of magnitude. This is beyond the capabilities of regenerators with a single decision level.

The extinction ratio is defined as the ratio between the one and zero level. The improvement in extinction ratio is depicted in Figure 7.10. However, in this diagram, we did not take the influence of the 5 dBm holding beam into account and an amplified signal without holding beam might result in a better extinction ratio improvement. The extinction ratio is however not a good qualitative measure for the noise reduction on a signal because it is difficult to distinguish noise on the zero level from receiver noise. The optical signal-to-noise ratio (OSNR) gives a better figure of merit by measuring the difference between the signal and noise on a spectrum analyzer which is set at a resolution of 0.1 nm. In Figure 7.11, the OSNR at the output of the 2R regenerator is depicted as a function of the OSNR at the input. We can observe an improvement between 2 and

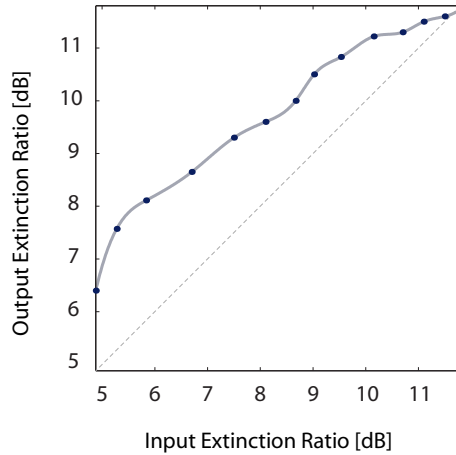


**Figure 7.10:** The extinction ratio improvement.

4 dB. The improvement in extinction ratio and OSNR only account for the noise reduction and are not a measure for the improvement of the BER.

The 2R regenerator can work at any wavelength outside the stopband of the DFB grating as illustrated for three arbitrary wavelengths in Figure 7.12. The BER diagrams for different injected wavelengths are depicted and show broadband operation that is only limited by the spectral width of the gain medium. The gain medium in our device are quantum wells leading to a gain bandwidth of approximately 20 nm. This means that the 2R regenerator works in a colourless mode within that range. Only the wavelengths corresponding with the stopband of the DFB grating are inaccessible which accounts only for a few nanometers in the spectrum. The small differences between the graphs are mostly due to the spectral variation in gain of the EDFA.

When we set the wavelength of the OBPF at the lasing wavelength instead of the wavelength of the injected signal, we obtain a reversed, wavelength converted signal. The noise floor is much higher and error-free wavelength conversion was only obtained at a smaller bitrate of 3 Gb/s.

### 7.3.2 Results at 25 Gbit/s

The effect of spatial hole burning is based on relatively small changes in carrier density. Therefore, the regeneration can be done at very high speeds despite the typical limited speed of semiconductor components. The effects of chirp that often accompany changes in carrier density are accordingly also limited.

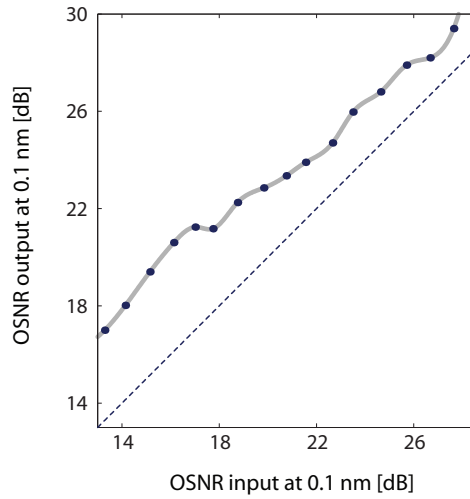


**Figure 7.11:** OSNR in 0.1 nm at the output of the all-optical 2R regenerator as a function of the input OSNR.

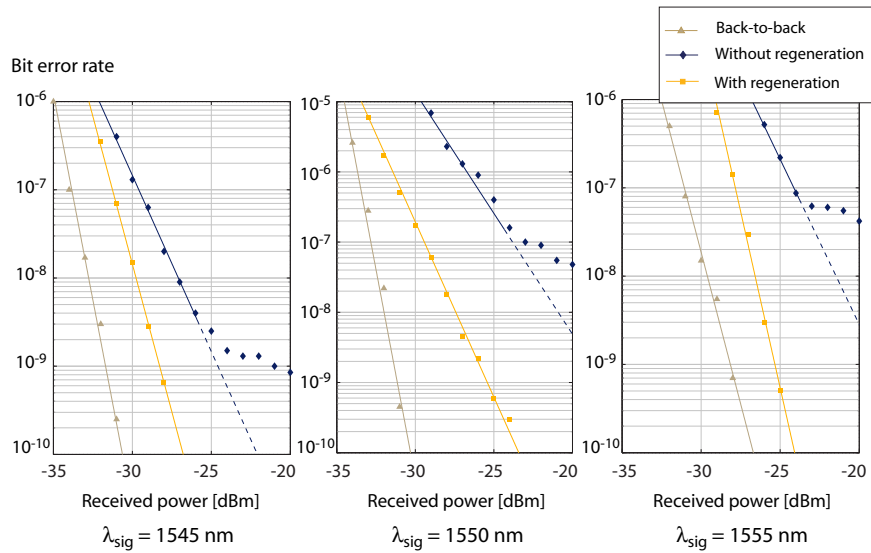


**Figure 7.12:** Wavelength independence: BER as a function of the received optical power for different transmission wavelengths.

To illustrate this, we will do the same experiments at a bit rate of 25 Gb/s and test if the regeneration is still effective after transmission through a fiber link.

The set-up that is used to characterize the regeneration at 25 Gb/s is depicted in Figure 7.13. The measurements at 25 Gbit/s were carried out at a single signal wavelength of 1543 nm with again a PRBS signal of  $2^{31} - 1$  bits. To account for the faster signal, we use wider bandwidths in the optical tunable filters. After controlling the OSNR of the signal by cascading an attenuator with an EDFA, a second EDFA is used to adjust the signal average power to 13.3 dBm (measured in-fiber at the DFB laser input coupling fiber). The holding beam that is combined with the original signal to adjust the position of the hysteresis to the signal power is 14 dBm (measured in-fiber at the DFB laser input coupling fiber). The mentioned power values are higher than the ones reported in previous experiments a.o. due to a different type of coupling between the fiber and DFB laser (tapered fiber instead of lensed fiber) which introduced an additional loss. One can expect much lower power levels when working with a packaged device. However, even with these restrictions, the power levels are still much lower than the ones needed for 2R regeneration using self-phase modulation in optical fibers [33]. The DFB laser has the same specifications as before and a Peltier element is used to keep its temperature stable.

After the DFB laser, we use again an optical band-pass filter (OBPF) tuned to 1543 nm in order to suppress the laser light and select the amplified signal. The regenerated signal is then sent to a preamplified receiver set-up that has been standardized at DTU for these measurements. It consists of an EDFA, an OBPF with 1.95 nm bandwidth, a second EDFA and an OBPF with 0.9 nm bandwidth. The signal is then detected in a PIN photodiode before being sent to the bit error rate tester. Using a variable optical attenuator, the received optical power at the preamplified receiver can be varied. In the transmission experiment, the regenerated signal is sent through a 160 km long link made of two spans of 80 km standard single-mode fiber and matching lengths of dispersion compensating fiber.

The results obtained for the 2R regeneration at 25 Gb/s NRZ signals are depicted in Figure 7.14. BER improvement is achieved with a factor of 20 to 50 times compared to the degraded input signal, depending on the value of the input OSNR. The corresponding improvement in OSNR is over 2 dB. The eye diagrams are shown in Figure 7.15. The device under test only supports one polarization, but the principle should be also applicable for polarization independent laser diodes.

Because semiconductor devices can introduce chirp to the signal, we also transmitted the regenerated signal over a dispersion managed link of 160 km fiber. The result of the regeneration is shown in Figure 7.16. The OSNR of the signal at the regenerator input is 18.3 dB. The set-up did not support clock re-

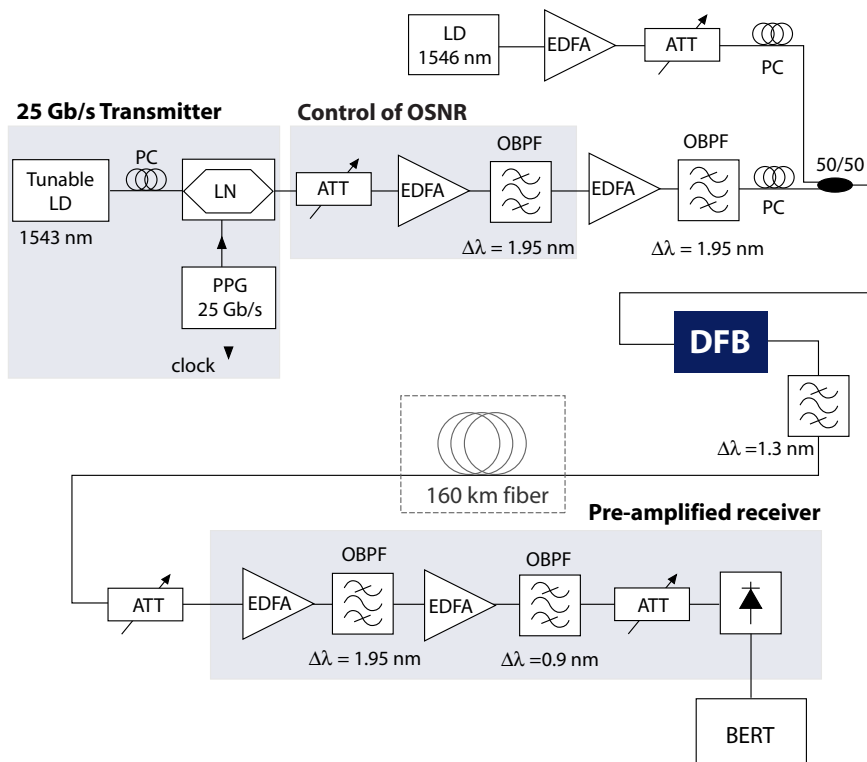


**Figure 7.13:** Schematic of the set-up used to measure the regeneration. (LD: laser diode; ATT: attenuator; PC: polarization controlling wheels; EDFA: erbium-doped fiber amplifier; OBPF: optical band-pass filter; BERT: bit error rate tester; PPG: pulse pattern generator)

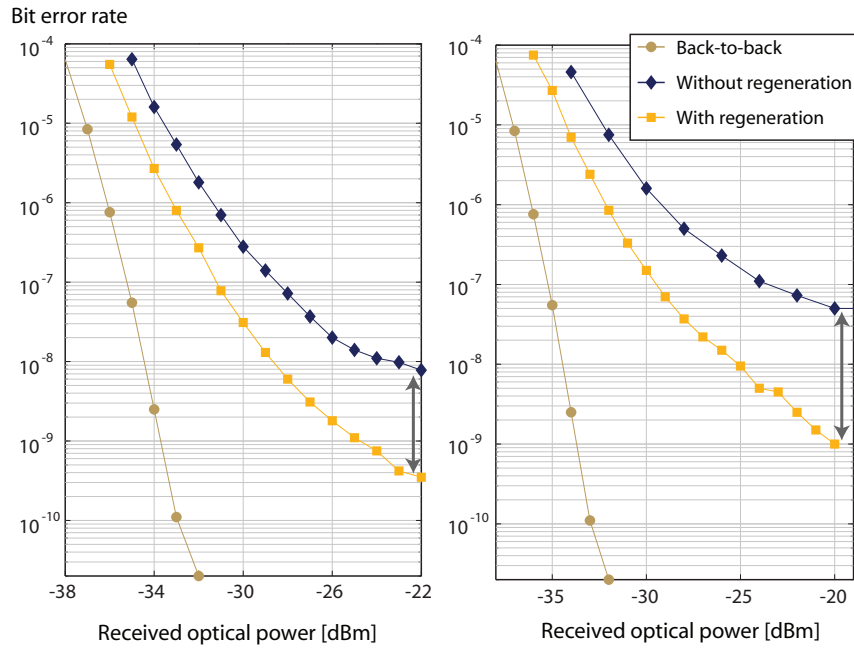


**Figure 7.14:** Bit error rate improvement for NRZ signals at 25 Gb/s. The input OSNR for the left BER diagram is 17.6 dB (output of 19.8 dB) and the right BER diagram has an OSNR of 16.9 dB (output of 19.2 dB).

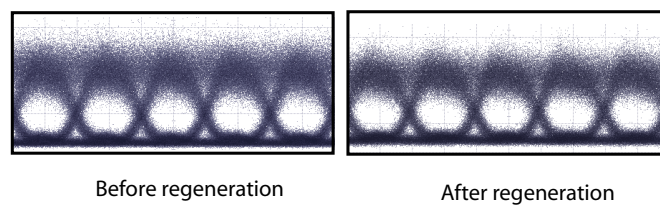


**Figure 7.15:** Eye diagrams for a 25Gb/s input signal with input OSNR of 17.6 dB.

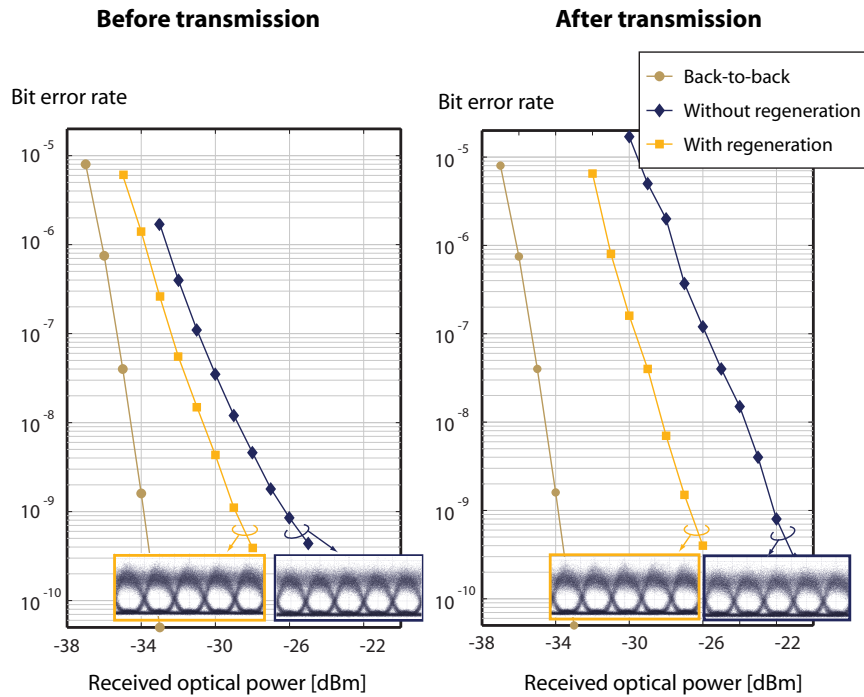


**Figure 7.16:** The 2R regeneration is still effective after transmission through a fiber of 160 km length.

covery at 25 Gb/s, limiting the possibility of using a highly degraded signal. We can clearly observe that the regenerated signal results in a much better transmission with a sensitivity improvement of 4.8 dB (at a BER of  $10^{-9}$ ) compared to the non-regenerated signal that is sent through the fiber. The lack of chirp is probably due to the rather small changes in carrier density in the DFB laser diode. We can conclude from this experiment that chirp has no dominant influence in the present case and that the proposed technique is feasible for practical applications.

The experiment has been carried out also at a bitrate of 40 Gb/s but there was found no significant improvement nor degradation of the signal. The devices under test were, however, not optimized for the specific application of regeneration and on this ground, operation at higher bitrates seems feasible.

## 7.4 Conclusion

A new concept for 2R regeneration is proposed using hysteresis in the transmission characteristic of a single distributed feedback laser diode. The concept is verified experimentally showing bit error rate improvement at 10 Gb/s and 25 Gb/s NRZ signals. Besides noise reduction, the regenerator is also able to improve the bit error rate at much lower power levels than concepts based on self-phase modulation in fibers. It preserves the original wavelength of the signal and broadband operation is possible. The use of a single active device and the absence of wavelength control results in low power consumption (0.6 W), while the simplicity of the concept makes the regenerator suitable for direct application in optical access or metro networks at different bitrates. The device under test supported only a single polarization mode, but the principle should be also applicable for polarization independent devices. An array of DFB lasers in combination with an arrayed waveguide grating on both sides could result in a suitable regeneration technique for 100 Gb ethernet applications as the recent standard proposed by the IEEE 802.3ba 100 Gb ethernet task force has the objective of a 4x25 Gb/s WDM signal for transmission over 10 and 40 km (100GBASE-LR4 and 100GBASE-ER4) [41]. Because direct modulation of DFB lasers has been demonstrated at bitrates up to 40 Gb/s, the regenerator might be also employed at these speeds by using optimized designs.

## References

- [1] J. Leuthold, G. Raybon, Y. Su, R. Essiambre, S. Cabot, J. Jaques, and M. Kauer. *40 Gbit/s transmission and cascaded all-optical wavelength conversion over 1 000 000 km*. *Electronics Letters*, 38(16):890–892, 2002.
- [2] G. Puerto, B. Ortega, M. D. Manzanedo, A. Martínez, D. Pastor, J. Capmany, and G. Kovacs. *Dimensioning of 10 Gbit/s all-optical packet switched networks based on optical label swapping routers with multistage 2R regeneration*. *Optics Express*, 14(22):10298–10306, 2006.
- [3] M. Yong-Jeon, Z. Pan, J. Cao, Y. Bansal, J. Taylor, Z. Wang, V. Akella, K. Okamoto, S. Kamei, J. Pan, and S.J.B. Yoo. *Demonstration of all-optical packet switching routers with optical label swapping and 2R regeneration for scalable optical label switching network applications*. *Journal of Light-wave Technology*, 21(11):2723 – 2733, Nov 2003.
- [4] P. Zakyntinos, G. T. Kanellos, D. Klondis, D. Apostolopoulos, N. Pleros, A. Poustie, G. Maxwell, I. Tomkos, and H. Avramopoulos. *Cascaded operation of a 2R burst-mode regenerator for optical burst switching network transmission*. *IEEE Photonics Technology Letters*, 19(21-24):1834–1836, 2007.
- [5] Z. J. Huang, A. Gray, I. Khrushchev, and I. Bennion. *10-Gb/s transmission over 100 Mm of standard fiber using 2R regeneration in an optical loop mirror*. *IEEE Photonics Technology Letters*, 16(11):2526–2528, 2004.
- [6] J. Mork, F. Ohman, and S. Bischoff. *Analytical expression for the bit error rate of cascaded all-optical regenerators*. *IEEE Photonics Technology Letters*, 15(10):1479–1481, Oct 2003.
- [7] T. Durhuus, C. Joergensen, B. Mikkelsen, R. J. S. Pedersen, and K. E. Stubkjaer. *All-optical wavelength conversion by SOAs in a Mach-Zehnder configuration*. *IEEE Photonics Technology Letters*, 6(1):53–55, 1994.
- [8] G. Morthier, J. Sun, T. Gyselings, and R. Baets. *A novel optical decision circuit based on a Mach-Zehnder or Michelson interferometer and gain-clamped semiconductor optical amplifiers*. *IEEE Photonics Technology Letters*, 10(8):1162–1164, Aug 1998.
- [9] G. Morthier, M. Zhao, B. Vanderhaegen, and R. Baets. *Experimental demonstration of an all-optical 2R regenerator with adjustable decision threshold and "true" regeneration characteristics*. *IEEE Photonics Technology Letters*, 12(11):1516 – 1518, Nov 2000.

- [10] D. Wolfson, P.B. Hansen, A. Kioch, and K.E. Stubkjaer. *All-optical 2R regeneration based on interferometric structure incorporating semiconductor optical amplifiers*. Electronics Letters, 35(1):59–60, Jan 1999.
- [11] M. Zhao, G. Morthier, and R. Baets. *Demonstration of extinction ratio improvement from 2 to 9 dB and intensity noise reduction with the MZI-GCSOA all-optical 2R regenerator*. IEEE Photonics Technology Letters, 14(7):992–994, Jul 2002.
- [12] D. Wolfson, A. Kioch, T. Fjelde, C. Janz, B. Dagens, and M. Renaud. *40-Gb/s all-optical wavelength conversion, regeneration, and demultiplexing in an SOA-based all-active Mach-Zehnder interferometer*. IEEE Photonics Technology Letters, 12(3):332–334, 2000.
- [13] G. Contestabile, R. Proietti, M. Presi, and E. Ciaramella. *40 Gb/s Wavelength Preserving 2R Regeneration for both RZ and NRZ Signals*. In Conference on Optical Fiber communication (OFC/NFOEC 2008), February 2008.
- [14] G. Contestabile, M. Presi, R. Proietti, and E. Ciaramella. *Optical Reshaping of 40-Gb/s NRZ and RZ Signals Without Wavelength Conversion*. IEEE Photonics Technology Letters, 20(13):1133–1135, July 2008.
- [15] J. De Merlier, G. Morthier, P. Van Daele, I. Moerman, and R. Baets. *All-optical 2R regeneration based on integrated asymmetric Mach-Zehnder interferometer incorporating MMI-SOA*. Electronics Letters, 38(5):238–239, Feb 2002.
- [16] J. De Merlier, G. Morthier, S. Verstuyft, T. Van Caenegem, I. Moerman, P. Van Daele, and R. Baets. *Experimental demonstration of all-optical regeneration using an MMI-SOA*. IEEE Photonics Technology Letters, 14(5):660–662, May 2002.
- [17] J. De Merlier. *Optical signal regeneration based on integrated amplifying interferometers*. PhD thesis, Ghent University, 2003.
- [18] A. Kuramoto and S. Yamashita. *All-optical regeneration using a side-mode injection-locked semiconductor laser*. IEEE Journal of Selected Topics in Quantum Electronics, 9(5):1283–1287, 2003.
- [19] S. Yamashita and J. Suzuki. *All-optical 2R regeneration using a two-mode injection-locked Fabry-Perot laser diode*. IEEE Photonics Technology Letters, 16(4):1176–1178, 2004.
- [20] O. Brox, S. Bauer, C. Bornholdt, D. Hoffmann, M. Mohrle, G. Sahin, and B. Sartorius. *Optical 3R regenerator based on Q-switched laser*. In Optical Fiber Communication Conference (OFC'01), volume 1, page MG6, 2001.

- [21] W. Franz. *Einfluss eines elektrischen feldes auf eine optische absorption-skante*. Zeitschrift Fur Naturforschung Part a-Astrophysik Physik Und Physikalische Chemie, 13(6):484–489, 1958.
- [22] L. V. Keldysh. *The effect of a strong electric field on the optical properties of insulating crystals*. Soviet Physics JETP-USSR, 7(5):788–790, 1958.
- [23] L. V. Keldysh. *Behaviour of non-metallic crystals in strong electric fields*. Soviet Physics JETP-USSR, 6(4):763–770, 1958.
- [24] M. Suzuki, H. Tanaka, N. Edagawa, and Y. Matsushima. *New applications of a sinusoidally driven InGaAsP electroabsorption modulator to in-line optical gates with ASE noise reduction effect*. Journal of Lightwave Technology, 10(12):1912–1918, 1992.
- [25] T. Miyazaki, N. Edagawa, M. Suzuki, and S. Yamamoto. *Novel optical-regenerator using electroabsorption modulators*. In Optical Fiber Communication Conference, 1999, and the International Conference on Integrated Optics and Optical Fiber Communication. OFC/IOOC '99. Technical Digest, volume 2, pages 350–352, 1999.
- [26] P.S. Cho, D. Mahgerefteh, and J. Coldhar. *All-optical 2R regeneration and wavelength conversion at 20 Gb/s using an electroabsorption modulator*. IEEE Photonics Technology Letters, 11(12):1662–1664, dec 1999.
- [27] T. Otani, T. Miyazaki, and S. Yamamoto. *Optical 3R regenerator using wavelength converters based on electroabsorption modulator for all-optical network applications*. IEEE Photonics Technology Letters, 12(4):431–433, apr 2000.
- [28] S. Hojfeldt, S. Bischoff, and J. Mork. *All-optical wavelength conversion and signal regeneration using an electroabsorption modulator*. Journal of Lightwave Technology, 18(8):1121–1127, 2000.
- [29] Bei Li, M.I. Memon, G. Mezosi, Zhuoran Wang, M. Sorel, and Siyuan Yu. *Characterization of All-Optical Regeneration Potentials of a Bistable Semiconductor Ring Laser*. Journal of Lightwave Technology, 27(19):4233–4240, Oct 2009.
- [30] B. Li, M.I. Memon, G. Mezosi, G. Yuan, Z. Wang, M. Sorel, and S. Yu. *All-Optical Response of Semiconductor Ring Laser to Dual-Optical Injections*. Photonics Technology Letters, IEEE, 20(10):770–772, May 2008.
- [31] P. V. Mamyshev. *All-optical data regeneration based on self-phase modulation effect*. In 24th European Conference on Optical Communications, pages 475–476, Madrid, Spain, 1998.

- [32] T. Her, T. Leng, G. Raybon, J.-C. Bouteiller, C. Jorgensen, K. Feder, K. Brar, P. Steinvurzel, D. Patel, N.M. Litchinitser, P.S. Westbrook, L.E. Nelson, C. Headley, and B.J. Eggleton. *Enhanced 40-Gbit/s receiver sensitivity with all-fiber optical 2R regenerator*. In Conference on Lasers and Electro-Optics (CLEO '02), volume 1, pages 534 – 535, 2002.
- [33] M. Rochette, L. B. Fu, V. Ta'eed, D. J. Moss, and B. J. Eggleton. *2R optical regeneration: An all-optical solution for BER improvement*. IEEE Journal of Selected Topics in Quantum Electronics, 12(4):736–744, 2006.
- [34] M. Jinno and M. Abe. *All-optical regenerator based on nonlinear fiber Sagnac interferometer*. Electronics Letters, 28(14):1350–1352, 1992.
- [35] J. J. Yu, X. Y. Zheng, F. H. Liu, A. Buxens, and P. Jeppesen. *Simultaneous realization wavelength conversion and signal regeneration using a nonlinear optical loop mirror*. Optics Communications, 175(1-3):173–177, 2000.
- [36] M. Rochette, J. N. Kutz, J. L. Blows, D. Moss, J. T. Mok, and B. J. Eggleton. *Bit-error-ratio improvement with 2R optical regenerators*. IEEE Photonics Technology Letters, 17(4):908–910, 2005.
- [37] G.P. Agrawal. *Fiber-optic communication systems*. John Wiley and sons, pp. 162-164, 2002.
- [38] A. Yariv and P. Yeh. *Photonics - Optical electronics in modern communications*. Oxford University Press, sixth edition, 2007.
- [39] C. E. Korman. *A discrete-time model for binary detection with rectangular hysteresis operators*. In 5th International Symposium on Hysteresis and Micromagnetic Modeling (HMM 2005), pages 17–20, Budapest (Hungary), 2005. Elsevier Science Bv.
- [40] C. E. Korman, R. Barry, and U. C. Kozat. *On binary detection with hysteresis*. Siam Journal on Applied Mathematics, 62(5):1794–1809, 2002.
- [41] *IEEE 802.3ba 40 Gb/s and 100 Gb/s ethernet task force*. <http://www.ieee802.org/3/ba/index.html>.

# 8

## Conclusions and perspectives

### 8.1 Conclusions

We demonstrated novel concepts to realize some of the main building blocks for all-optical signal processing in network nodes. The enormous bandwidth capacity of optical fibers has led to their world-wide implementation in telecommunication systems. The electronics to process high-speed signals in the network nodes is, however, expensive and power consuming. Performing all the processing within the optical domain is a possible solution. In this work we presented new implementations with a focus on simplicity: the all-optical flip-flops and regenerators that are proposed consist of single standard laser diodes. The performance of these laser diodes as all-optical signal processing devices does not only surpass most of the existing (complex) schemes, but their already widespread use as transmitters in current optical communication systems allows for a mature technology which facilitates their short-term implementation.

#### **All-optical flip-flops**

All-optical flip-flops are essential in optical network nodes as they allow to store the header information in an optical packet switch while the data is routed to the desired output port. Such memory elements are typically based on hystere-

sis effects because they exhibit different states under the same input conditions.

It was demonstrated that distributed feedback (DFB) laser diodes can exhibit such a hysteresis under the injection of a holding beam. The underlying physical effect is based on a non-uniformity in the longitudinal carrier density distribution which affects the effectiveness of the Bragg reflections. The obtained bistability was successfully applied to realize flip-flop operation: it was shown that the DFB laser could be switched on and off by injecting light pulses alternately on each side of the cavity. The effect allows for very fast flip-flop operation: switching times as low as 45 ps were demonstrated. Further on, the impact of structural parameters on the bistability was studied with numerical simulations.

Distributed Bragg reflector (DBR) lasers have a hysteresis in their tuning characteristic. When applying a current corresponding to the hysteresis, it is possible to switch between two different wavelengths by injecting optical pulses. This was demonstrated by injection-locking the laser on its two different wavelengths resulting in switching speeds around 50 ps. An alternative approach using a combination of injection-locking and carrier depletion was also studied by applying pulses with a different duration.

Microdisk lasers have a circular cavity structure where the mode is confined at the edge of the disk in the 'whispering gallery mode'. Lasing is possible in the clockwise and counterclockwise direction. Due to a non-linear gain suppression effect, one of the lasing directions can dominate which results in a unidirectional regime. By injecting light pulses, the lasing direction can be altered in order to realize flip-flop operation. We demonstrated this effect in an ultra-small microdisk laser (7.5  $\mu\text{m}$  diameter) and flip-flop operation was possible with very low pulse energies (1.8 fJ). The disk was bonded on a silicon chip which is the standard material to manufacture electronic chips and a promising material for (passive) photonics.

We also performed a theoretical study on the symmetry breaking in small network motifs of three and four coupled cavities. Due to the Kerr non-linearity in (passive) resonators, we can achieve asymmetric states in such structures. We derived a theoretical condition to achieve symmetry breaking and demonstrated with numerical simulations that it is possible to switch between the asymmetric states by injecting light pulses.

### **All-optical packet switching**

The use of DFB lasers as all-optical flip-flops was also demonstrated in a system-oriented experiment. The DFB lasers can store the header information of the packets while the payload is directed to their desired output port. This was shown for packets with bitrates up to 40 Gb/s and color-coded la-

bels. Very fast packet switching is possible with this technique due to the fast response of the DFB flip-flops.

### **All-optical regeneration**

Cascading multiple optical network nodes can result in an accumulation of noise on the signal. Traditional network nodes act as repeaters because the signal is redigitalized during the electronic processing in the routers. Therefore, there is a need for devices that can increase the signal-to-noise ratio within the optical domain. In this work, we presented a novel concept to realize all-optical regeneration by using a single DFB laser diode. We show that the hysteresis allows to improve the bit error rate with several orders of magnitude as it offers a decision level that moves dynamically with the signal. The results were demonstrated at bitrates up to 25 Gb/s.

## **8.2 Perspectives**

As mentioned already in the introductory chapter, the power consumption of devices is nowadays the dominant parameter for evaluating information processing devices. We can not reasonably propose (all-)optical solutions as alternatives to electronics without making an in-depth study of their power consumption. However, very few researchers tackle the question to define the requirements photonic components should actually fulfill in order to make a difference with electronics. The lack of a well-defined and motivated study on the actual requirements for e.g. all-optical flip-flops prohibits us to evaluate their performance with respect to electronic solutions. Moreover, the switch towards a new technology requires significant investments while the telecommunication industry is relatively small compared to the consumer electronics market. Therefore, any optical alternative will need to prove being profitable. It can be expected that when the need for on-chip interconnects rises, the technology for optical signal processing will acquire a new momentum as larger research budgets come into play.

Besides these general remarks, there are still some improvements that could be done on the work presented here:

- The devices used in this work are not packaged. Therefore, the coupling losses to the components were significant and differ in subsequent measurements. This means that the measured values of the pulse energies and optical input powers can be much lower because the coupling losses are estimated to be around 3 dB to 5 dB.

- 
- Devices for use in telecommunication should work in a polarization independent mode because the polarization of the incoming signals can not be specified. Optimized designs of the laser diodes could allow polarization independent operation because the underlying physical effects are not based on the light polarization.
  - The integration of multiple devices on the same chip should be an important next step. Multiple microdisks could represent a shift register and also the all-optical packet switch can be promising when fabricated as an integrated device.
  - Experimental demonstration of the asymmetric states in structures with coupled cavities could be interesting but rather difficult to achieve. As research on strong non-linear materials progresses, this might offer a potentially important research result.
  - The flip-flop operation in DFB lasers could be studied further by comparing devices with different  $\kappa L$ -values as this was shown to be the most influential parameter.
  - Further experiments could be done on the optical regenerator to determine the influence of different parameters (hysteresis width, optical input power, current, ...) on its performance.

# List of Figures

1	De DFB laser als optisch geheugenelement: (a) Illustratie van de component; (b) Hysteresis in het uitgangsvermogen van de laser bij externe lichtinjectie; (c) Experimenteel bekomen resultaat van het schakelgedrag. . . . .	xv
2	Flip-flopwerking in schijflasers. . . . .	xvi
3	Optische pakketschakelaar met DFB lasers als geheugenelementen. xvii	
1	Distributed feedback laser as all-optical flip-flop: (a) Schematic of the device; (b) Hysteresis in laser output power under injection of light; (c) experimental demonstration of flip-flop operation. . . .	xxiii
2	Flip-flop operation in disk lasers. . . . .	xxiv
3	All-optical packet switching scheme using DFB lasers as all-optical flip-flop. . . . .	xxv
1.1	The state of the submarine optical fiber network in 2007. (Source: Alcatel-Lucent ©) . . . . .	4
1.2	The number of internet users has drastically increased in the past decade. (Source: www.internetworldstats.com) . . . . .	5
1.3	A schematic illustration of flip-flop operation: the output switches when the set and reset pulses are injected. . . . .	7
1.4	Schematic of an all-optical packet switch: the all-optical flip-flop is necessary to store the processed header information while the signal is routed to the output. [21, 22] . . . . .	8
1.5	A bistability originating from a coupled laser structure where one laser quenches lasing in the other. [25] . . . . .	9
1.6	Two separate states in an active multi-mode interference coupler (Courtesy of K. Takeda). . . . .	10
2.1	Schematic representation of a Fabry-Pérot laser cavity and a distributed feedback laser cavity with their respective lasing spectra. . . . .	23

2.2	The solutions of the coupled mode equations for a grating without $\lambda/4$ -shift have a stop band around $\Delta\beta = 0$ . The values of the normalized coupling constant $\kappa L$ range from 0.1 to 5 in steps of 0.1.	28
2.3	Physical explanation of the insertion of a $\lambda/4$ -shift in the middle of the grating [15].	28
2.4	The insertion of a $\lambda/4$ -shift results in single mode operation at $\Delta\beta = 0$ . The values of the normalized coupling constant $\kappa L$ range from 0.1 to 5 in steps of 0.1.	29
2.5	The distribution of carriers along the laser section with and without external light injection for a DFB laser with $\kappa L=1.2$ and length $L=400 \mu\text{m}$ . The holding beam is injected from the left side of the laser.	31
2.6	The bistability in the laser output power (up) and the transmitted power of the holding beam (down) for a DFB laser with length $L=400 \mu\text{m}$ , normalized coupling constant $\kappa L=1.2$ and current injection of $4I_{th}$ .	33
2.7	Schematic representation of the flip-flop operation in a single DFB laser.	34
2.8	(a) The transmission-line laser modes divides the laser section into multiple segments. (b) Each segment contains a node where the rate equations are calculated and the fields are transferred to the next node by transmission-lines. (c) To include the feedback from the Bragg grating subsequent high and low impedance lines are placed along the laser section.	36
2.9	The influence of the injected current on the bistable characteristic for a DFB laser with length $L = 600 \mu\text{m}$ , $\kappa L = 1.8$ and $I_{th} = 26.5 \text{ mA}$ .	37
2.10	The influence of the wavelength of the injected light for a DFB laser with length $L = 400 \mu\text{m}$ , $\kappa L = 1.2$ and $I_{bias} = 4I_{th}$ .	38
2.11	The influence of the coupling coefficient on the bistable characteristic for a DFB laser with length $L = 400 \mu\text{m}$ and $I_{bias} = 4I_{th}$ .	39
2.12	The bistable characteristics are very similar for fixed values of $\kappa L$ .	40
2.13	The influence of the carrier lifetime on the bistable characteristic for a DFB laser with length $L = 400 \mu\text{m}$ , $\kappa L = 1.2$ .	41
2.14	The influence of the quality of the anti-reflection coating for a DFB laser with length $L = 400 \mu\text{m}$ , $\kappa L = 1.2$ .	41
2.15	The simulated switching times for a DFB laser with length $L = 400 \mu\text{m}$ , $\kappa L=1.2$ and differential gain $g_0 = 3 \cdot 10^{-16} \text{ cm}^2$ . The rectangular pulses have durations of 200 ps for reset and 125 ps for set. (Courtesy of [28])	42
2.16	A photograph of the measurement stage (left) and the device under test (right).	43

2.17 Schematic of the measurement set-up for the bistability. . . . .	44
2.18 Experimental result for the bistability in the laser diodes. . . . .	45
2.19 Schematic of the measurement set-up for the flip-flop operation. . . . .	46
2.20 Experimental demonstration of fast flip-flop operation in a single DFB laser diode under injection of a holding beam. (a) Output of the DFB laser at 1553 nm when subjected to 100 ps long set and reset pulses separated by 1.65 ns. (b) Details of the leading and trailing edges of the laser output enabling the determination of the rise and fall times. . . . .	47
2.21 Experimentally measured rise and fall times for flip-flop operation as a function of pulse energies. . . . .	48
2.22 Experimental demonstration of flip-flop operation in a DFB laser diode with pulse durations of 7 ps. . . . .	49
2.23 Changes in the holding beam power have no significant influence on the switching times. The error bars indicate the standard deviation on the averaged switching times. . . . .	50
3.1 Illustration of a DBR laser diode with a grating and gain section. . . . .	58
3.2 The wavelength-dependent loss of the DBR grating allows the selection of a specific longitudinal mode. . . . .	58
3.3 The asymmetric gain will cause mode hopping at different tuning currents. This results in a hysteresis in the tuning characteristic. (Courtesy of [8]). . . . .	61
3.4 Simulation of the multiple bistabilities in the tuning characteristic of the lasing wavelength. . . . .	63
3.5 Simulation of the time-resolved frequency which demonstrates the flip-flop operation. . . . .	64
3.6 (a) Bistability in the operating wavelength as a function of the tuning current; (b) Optical spectrum of the two states with side-mode suppression ratio of 44 dB. . . . .	65
3.7 Schematic of the measurement set-up. . . . .	66
3.8 Flip-flop operation by injection locking at the two separate wavelengths using pulses with a duration of 100 ps. The upper graph presents the output at the two operating wavelengths $\lambda_1$ and $\lambda_2$ . Below, details of the leading and trailing edges of the flip-flop output enabling the determination of rise and fall time. . . . .	67
3.9 Flip-flop operation by a combination of injection locking and carrier depletion in a DBR laser. (a) Injected pulses at 1561.3 nm; (b) output at 1561.3 nm; (c) flip-flop operation at 1560.7 nm; (d) switch-on; (e) switch-off. . . . .	69

4.1	(a) FDTD simulation of a whispering gallery mode in a disk laser (top view) and (b) the optical mode depicted after a conformal transformation to an asymmetric, straight slab waveguide. It can be seen that the light is located near the edge of the disk. (Courtesy of [5, 32]) . . . . .	76
4.2	A simulation of the L-I graph with the different regimes. (Courtesy of [32]). . . . .	78
4.3	A schematic of the entire circuit and bonded microdisk. (Courtesy of L. Liu) . . . . .	80
4.4	The measured L-I characteristic of the microdisk indicates that unidirectional operation starts at 1.7 mA. . . . .	81
4.5	The spectrum of the clockwise mode of the microdisk at a bias of 3.8 mA indicates unimodal operation with a free spectral range of 30.4 nm. . . . .	82
4.6	Schematic of the measurement set-up. . . . .	83
4.7	Measurement result for flip-flop operation in a microdisk laser integrated on silicon. . . . .	84
5.1	A schematic representation of a symmetric structure of three coupled cavities. . . . .	93
5.2	The states of the output power as a function of the input power for a structure with (a) $\Delta = 0.1$ and $\phi = -0.5$ and (b) $\Delta = 0.1$ and $\phi = 2.0$ . The unstable states are shaded. . . . .	97
5.3	The stable states of the cavity energies as a function of the input power for a structure with $\tau(\omega - \omega_0) = 0.1$ and $\phi = -0.5$ . The unstable states of the symmetric solutions are shaded. . . . .	98
5.4	The different working regimes for different parameters of $\Delta$ and $\phi$ with a constant input power of $P_{in}/P_0 = 3.0$ . I: two equal solutions in the upper branch and one in the lower branch (bounded by orange line); II: three different outputs (bounded by blue line); III: two equal solutions in the lower branch and one in the higher branch (bounded by brown line). The cross indicates the working point of Figure 2a. . . . .	99
5.5	Switching between the three different states of region III. . . . .	100
5.6	Two possible implementations of the proposed scheme using (a) photonic crystal cavities and (b) ring resonators. . . . .	101
5.7	Schematic representation of a symmetric structure of 4 cavities coupled by waveguides. . . . .	102
5.8	Schematic representation of the symmetry breaking condition for three and four coupled cavities. In the dark regions, the symmetry breaking condition holds. . . . .	103

5.9	Stable states of the output power as a function of the input power for a structure consisting of four cavities with $\Delta = -0.35$ and $\phi = 0.6$ . The unstable states are plotted with a thin line. . . . .	104
5.10	Switching between different states in a configuration of 4 cavities. . . . .	105
6.1	Packet switch based on a network of optical switches driven by optical flip-flops. . . . .	111
6.2	Alternative approach using in-band address labels [5]. . . . .	111
6.3	Concept for all-optical packet switching based on an array of DFB lasers with different wavelengths. The two arrayed waveguide gratings (AWG's) can be identical. . . . .	113
6.4	Schematic of the measurement set-up for all-optical switching of packets with a fixed duration using a DFB AOFF. (LD: Laser Diode, ATT: attenuator, FDL: fiber delay line, PPG: pulse pattern generator, LN: lithium niobate modulator) . . . . .	115
6.5	Results for all-optical switching of packets with a fixed duration. (a) Payload with labels; (b) output of DFB all-optical flip-flop; (c) optically switched packets . . . . .	116
6.6	Schematic of the wavelength conversion in the optical packet switch. . . . .	117
6.7	Transient behaviour at the start and end of the switched packets. . . . .	118
6.8	Bit-error rate measurements for the back-to-back and output. . . . .	118
6.9	Schematic of the measurement set-up for optical packet switching with a DFB AOFF. (LD: Laser Diode, ATT: attenuator, FDL: fiber delay line, PPG: pulse pattern generator, LN: lithium niobate modulator) . . . . .	119
6.10	Results for all-optical packet-switching with a DFB AOFF. (a) set-pulses; (b) reset-pulses; (c) output of DFB all-optical flip-flop; (d) optically switched packets . . . . .	121
7.1	Schematic representation of the different types of regeneration. . . . .	127
7.2	Principle of 2R regeneration using a static decision level. . . . .	128
7.3	Schematic of the difference between noise reduction (class I regenerators) and BER improvement (class II regenerators). . . . .	131
7.4	(a) Schematic of the DFB laser based 2R regeneration; (b) Ideal hysteresis curve of the transmission characteristic; (c) Bit pattern with noise and the dynamically moving decision level (orange, with hysteresis) and static decision level (grey dashed, without hysteresis); (d) Correctly reconstructed bit-pattern by the 2R regenerator with hysteresis. . . . .	132
7.5	Asymptotical behaviour of BER as a function of the $Q$ parameter for different values of the hysteresis width $h$ (and $n \rightarrow \infty$ ). . . . .	135

7.6	BER as a function of the $Q$ parameter at different time steps $n$ for a hysteresis with width $h = 0.4$ . The dashed line represents the situation without hysteresis. . . . .	135
7.7	Schematic of the set-up. (LD: laser diode; LN: lithium-niobate modulator; PPG: pulse pattern generator; ATT: attenuator; EDFA: erbium-doped fiber-amplifier; BERT: bit error rate tester.) . . . .	137
7.8	BER as a function of the received optical power for different values of the OSNR and corresponding eye diagrams. (a) Input OSNR of 19.8 dB; (b) Input OSNR of 18.8 dB; (c) Input OSNR of 17.7 dB; (d) eye diagram of original signal; (e) degraded signal; (f) regenerated signal. . . . .	138
7.9	Excess penalty at $\text{BER}=10^{-9}$ of the degraded and regenerated signal compared to the original signal as a function of the input OSNR. . . . .	139
7.10	The extinction ratio improvement. . . . .	140
7.11	OSNR in 0.1 nm at the output of the all-optical 2R regenerator as a function of the input OSNR. . . . .	141
7.12	Wavelength independence: BER as a function of the received optical power for different transmission wavelengths. . . . .	141
7.13	Schematic of the set-up used to measure the regeneration. (LD: laser diode; ATT: attenuator; PC: polarization controlling wheels; EDFA: erbium-doped fiber amplifier; OBPF: optical band-pass filter; BERT: bit error rate tester; PPG: pulse pattern generator) . . .	143
7.14	Bit error rate improvement for NRZ signals at 25 Gb/s. The input OSNR for the left BER diagram is 17.6 dB (output of 19.8 dB) and the right BER diagram has an OSNR of 16.9 dB (output of 19.2 dB). . . . .	144
7.15	Eye diagrams for a 25Gb/s input signal with input OSNR of 17.6 dB. . . . .	144
7.16	The 2R regeneration is still effective after transmission through a fiber of 160 km length. . . . .	145